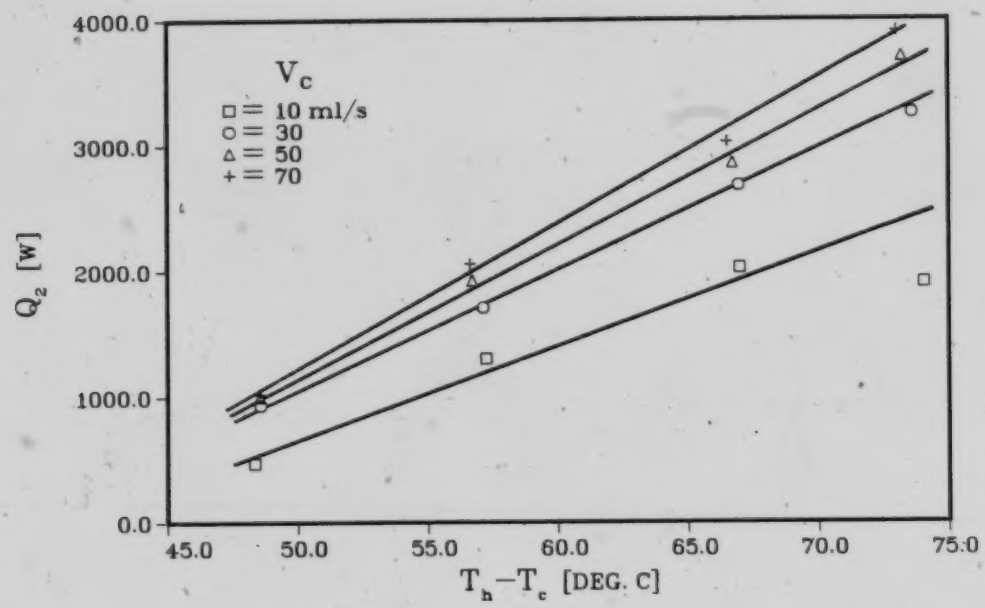

Fig. 3.1 Effect of cooling water flow rate on Q_2 vs. T_h-T_c with 70% charge level and downcomer closed

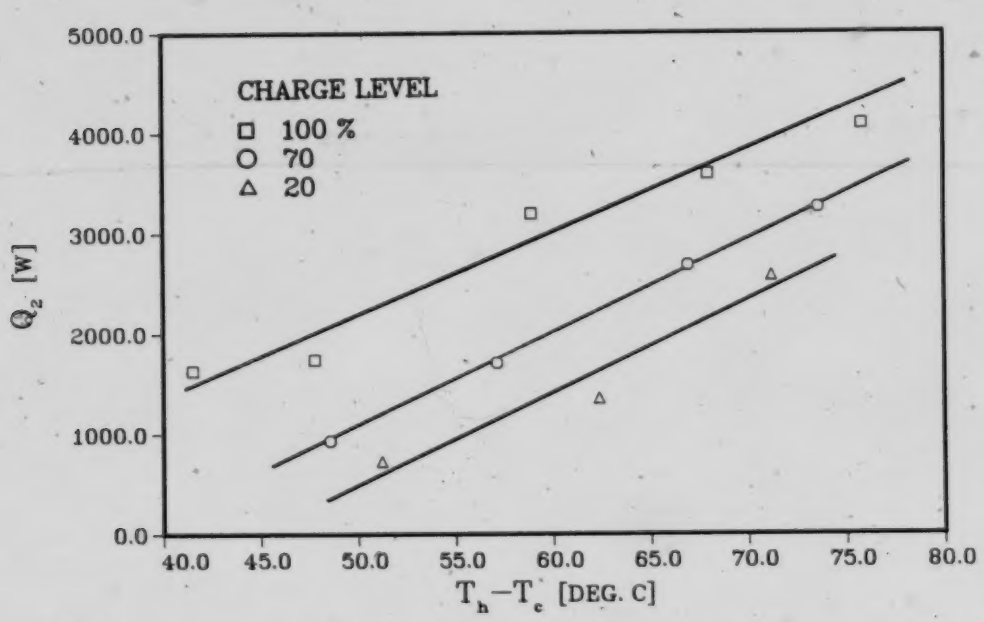

Fig. 3.2 Effect of charge level on Q_2 vs. T_h-T_c with V_C=30 ml/s and downcomer closed

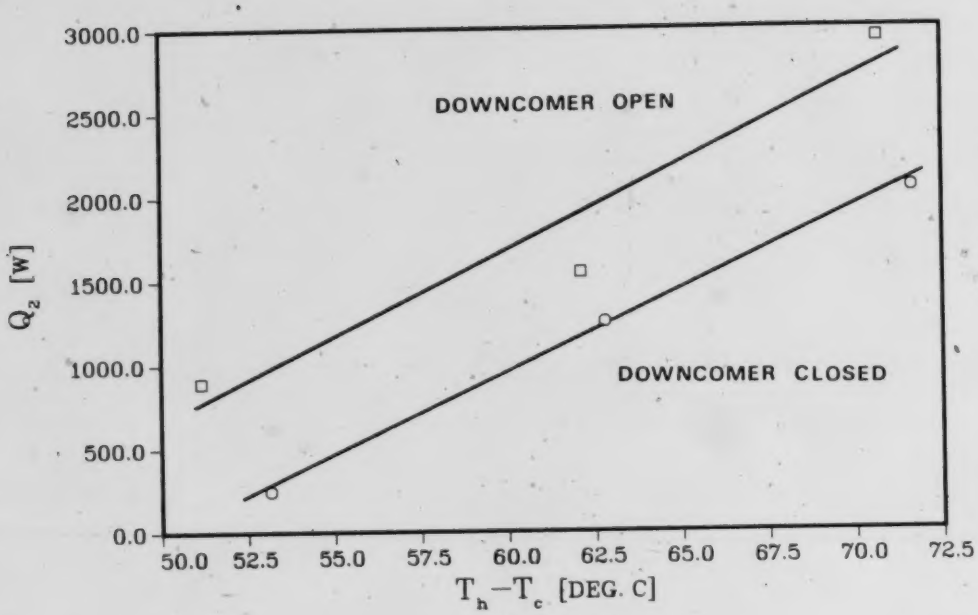

Fig. 3.3 Effect of downcomer on Q_2 vs. $T_h - T_c$ with 20% charge level and V_C=70 ml/s

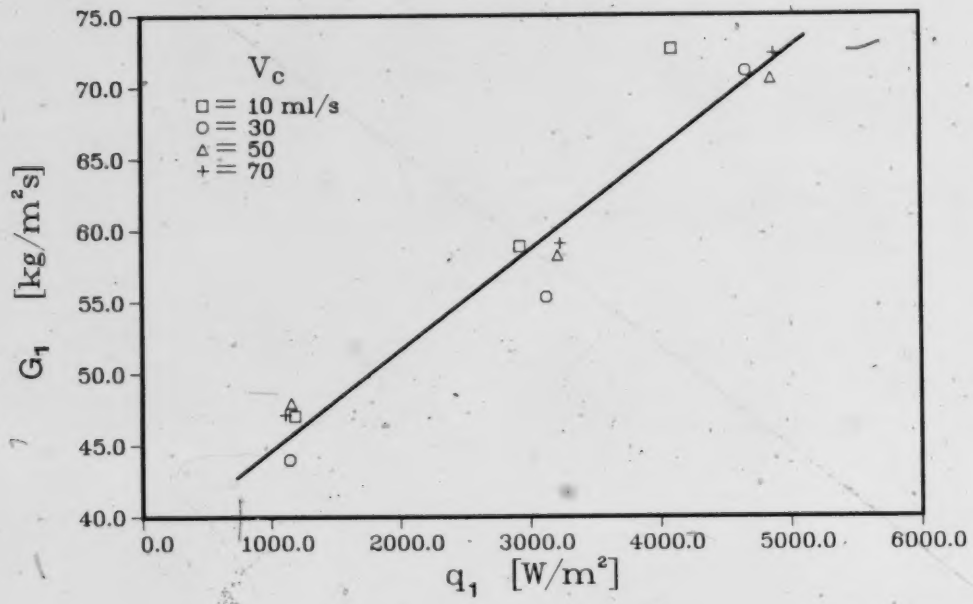

Fig. 3.4 Evaporator tube inlet mass flux vs. wall heat flux with 20% charge level and open downcomer

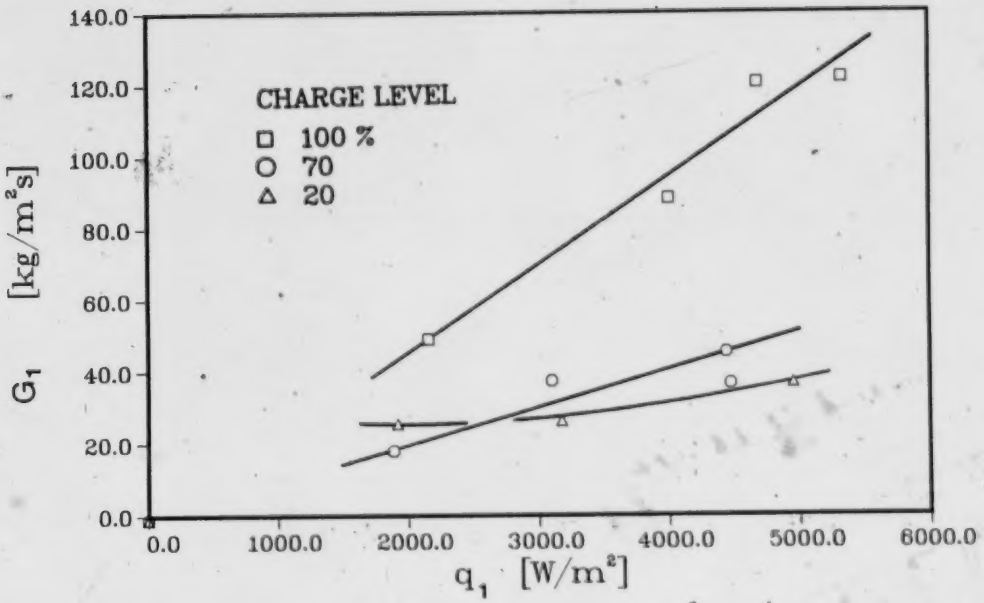

Fig. 3.5 Effect of charge level on G_1 vs. q_1 with V_C=10 ml/s and closed downcomer

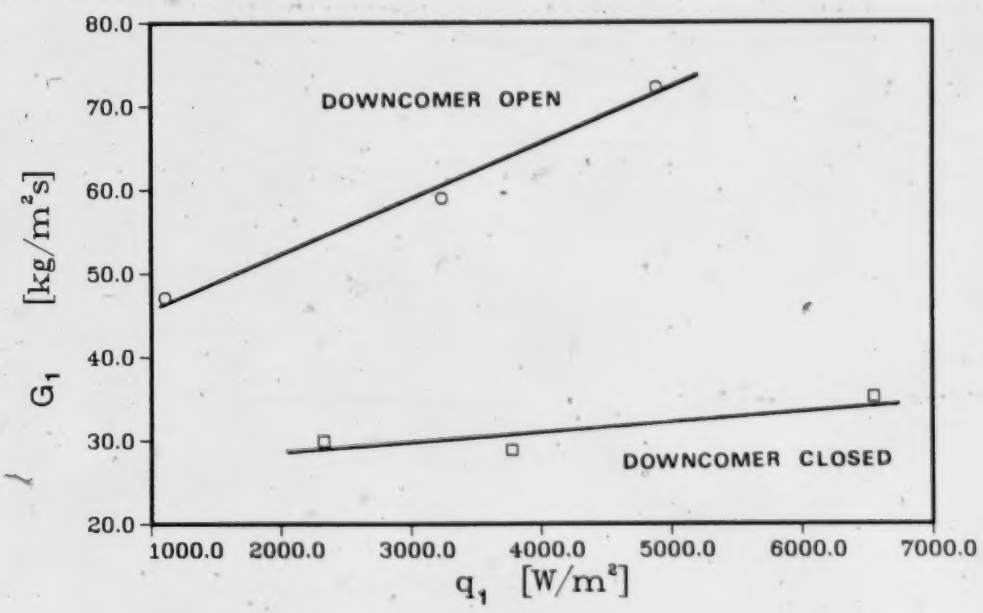

Fig. 3.6 Effect of downcomer on G_1 vs. q_1 with 20% charge level and V_C=70 ml/s

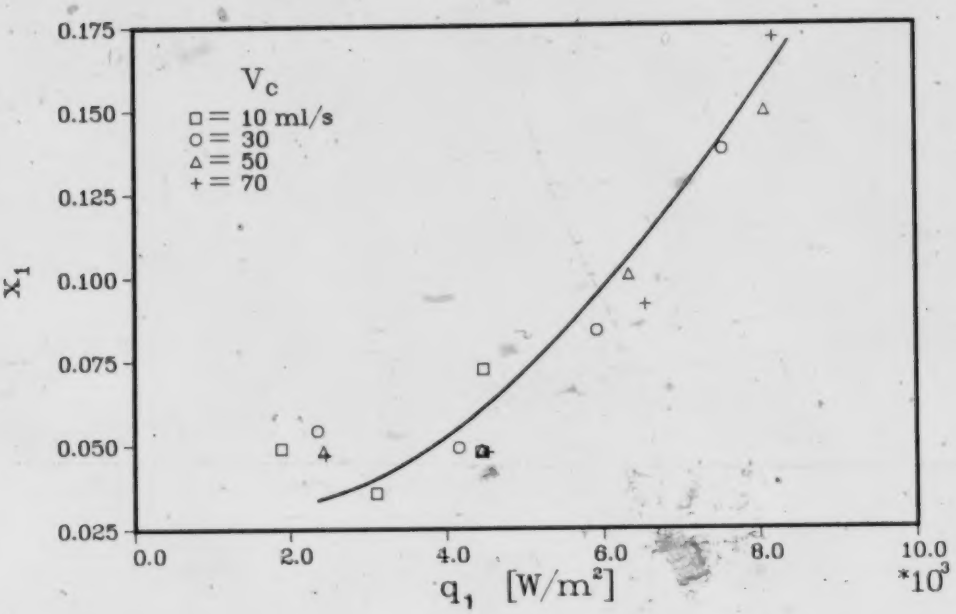

Fig. 3.7 Evaporator exit vapor quality vs. heat flux with 70% charge level and closed downcomer

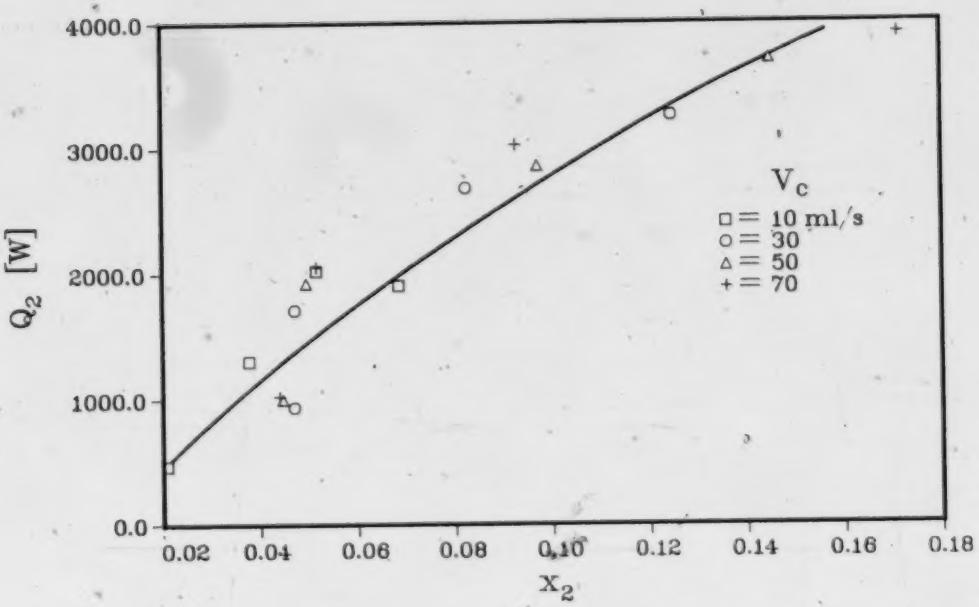

Fig. 3.8 Heat recovered vs. condenser shell side vapor quality with 70% charge level and closed downcomer

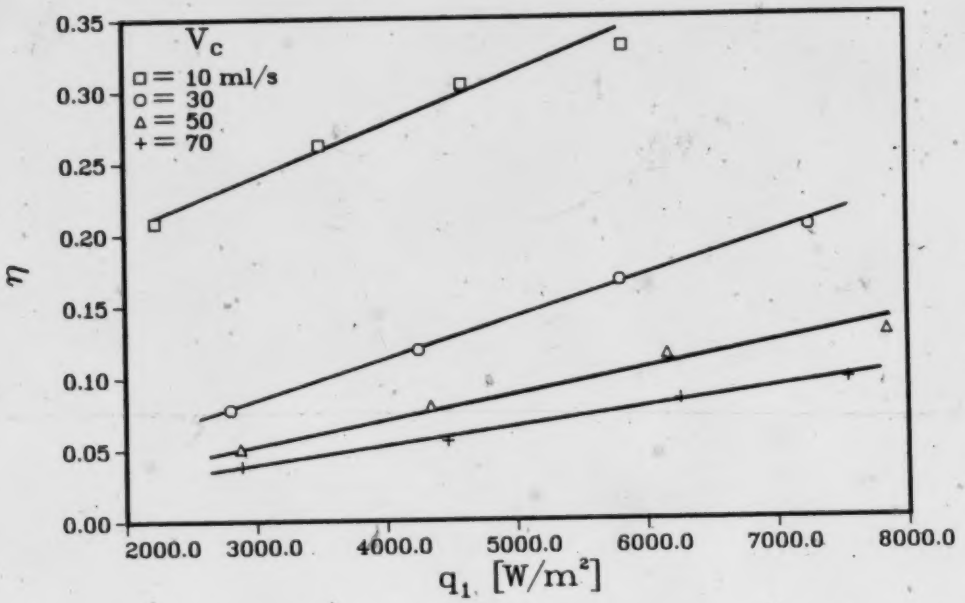

Fig. 3.9 System efficiency vs. input heat flux with 70% charge level and open downcomer

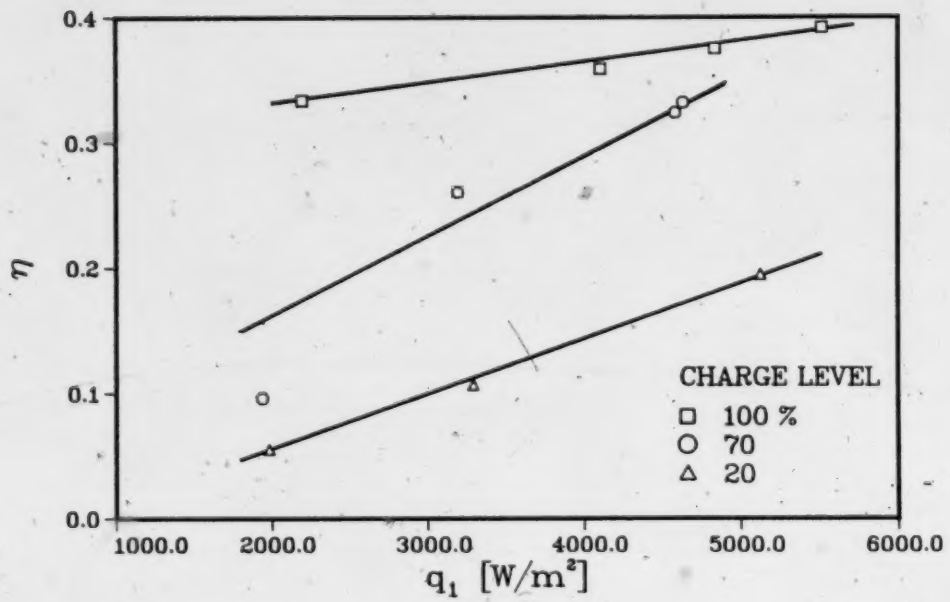

Fig. 3.10 Effect of charge level on η vs. q_1 with V_c = 10 ml/s and closed downcomer

flow restrictions in the working fluid loop caused by the measuring instruments, with the primary losses due to the small orifices in the turbine flow meters and the wire meshes.

The fluctuating phenomena of thermosyphon flow rates, system pressure, and evaporator exit temperature are inherent to a two phase thermosyphon system and typical chart records are shown in Fig. 3.11. The analog records provide a good visual indication of the type of oscillations involved, but beyond that are not particularly useful. Of interest are the frequency of the oscillations and the variance of the amplitudes which are difficult to accurately extract from a record of this nature. For this reason, digital methods of processing these signals is pursued in the next chapter for the two-phase refrigerant R-113 tests.

3.5.2 Upper and Lower Heat Exchangers

The effects of wall heat flux q_1, charge level and liquid-vapor separator on the overall heat transfer coefficient U_1 of the evaporator can be seen in Figs. 3.12 and 3.13. The performance of the evaporator improved considerably over the single phase case with the maximum value of U_1=1370 W/m²°C being approximately double that previously obtained.

The performance of the condenser under the conditions of low quality flow and high liquid entrainment and flooding is of interest. The effects of inlet quality x_2, cooling

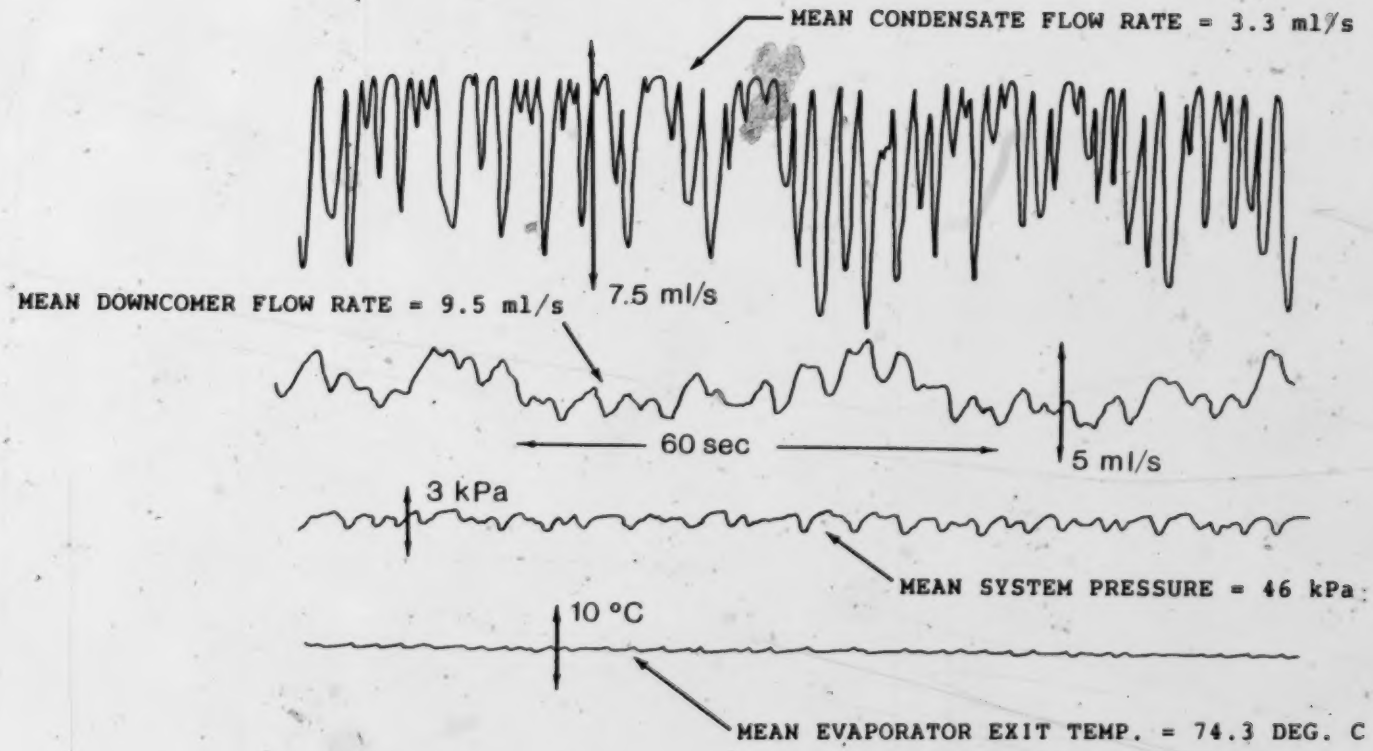
MEAN CONDENSATE FLOW RATE = 3.3 ml/s
7.5 ml/s
MEAN DOWNCOMER FLOW RATE = 9.5 ml/s
60 sec
5 ml/s
3 kPa
MEAN SYSTEM PRESSURE = 46 kPa
10 °C
MEAN EVAPORATOR EXIT TEMP. = 74.3 DEG. C

Fig. 3.11 Examples of fluctuating phenomena for 20% charge level, T_h=75°C, V_C=30 ml/s, and downcomer open

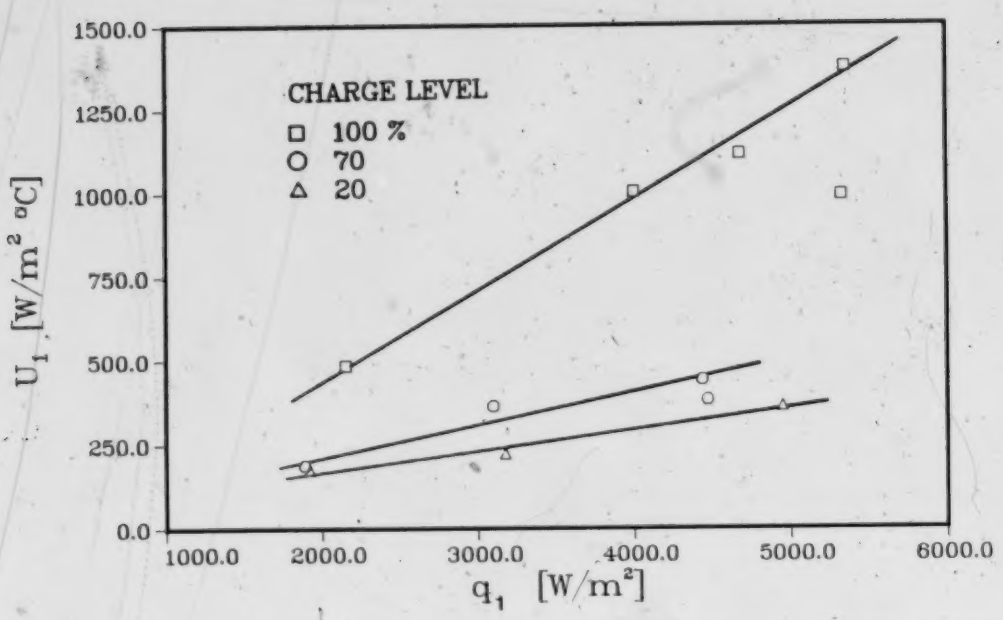

Fig. 3.12 Effect of charge level on U_1 vs. q_1 with closed downcomer and V_C=10 ml/s

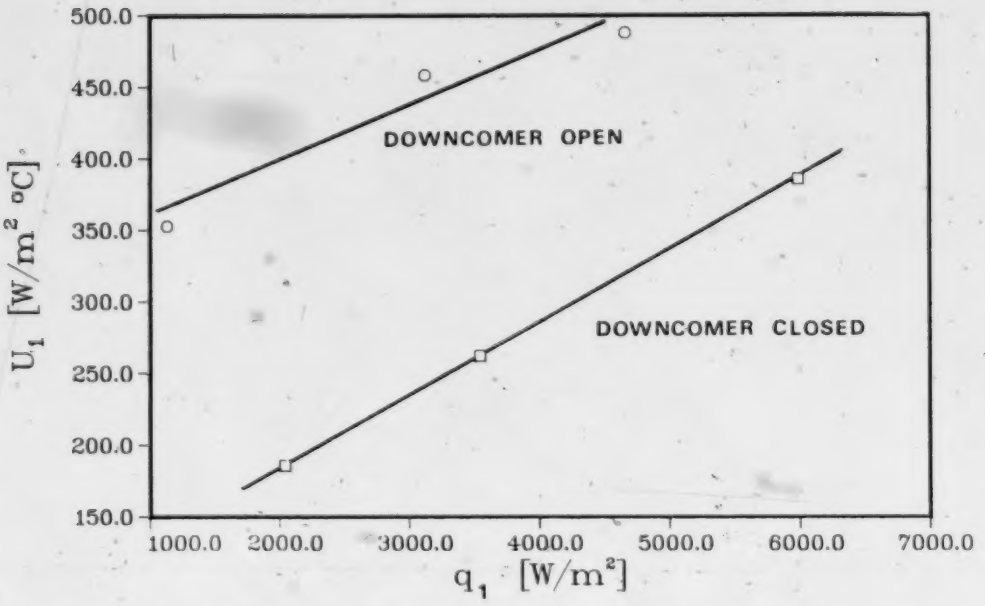

Fig. 3.13 Effect of downcomer on U_1 vs. q_1 with 20% charge level and and V_C=30 ml/s

water flow rate, charge level and downcomer on the overall heat transfer coefficient U_2 are shown in Figs. 3.14, 3.15, and 3.16. As is expected, increasing the cooling water flow rate causes a significant rise in the value of heat transfer coefficient. Higher charge levels result in increased working fluid flow rates and again help to improve performance. The effect of opening the downcomer is to raise the vapor quality in the condenser, which increases the latent component of the heat transfer. The condenser overall heat transfer coefficients for low quality two-phase flow are about 3 times those obtained in single phase for similar operating parameters.

3.5.3 Evaporator Convective Boiling

It is useful to compare the experimental values for the two-phase water heat transfer coefficient h_{exp} with those of the modified Dittus-Boelter equation h_s for single phase turbulent heat transfer, Eq.(3.9), and the results are shown in Fig. 3.17 using the inverse Martinelli parameter for flow in the evaporator tube. The ratio h_{exp}/h_s is lower than would be expected for a high vapor quality situation, however the trend to increase with higher flow quality and larger $1/X_{tt}$ does exist. The high data points near the origin of the horizontal coordinate on the plot are no doubt caused by low quality high speed flow at high charge levels yielding a large amount of sensible heat transfer.

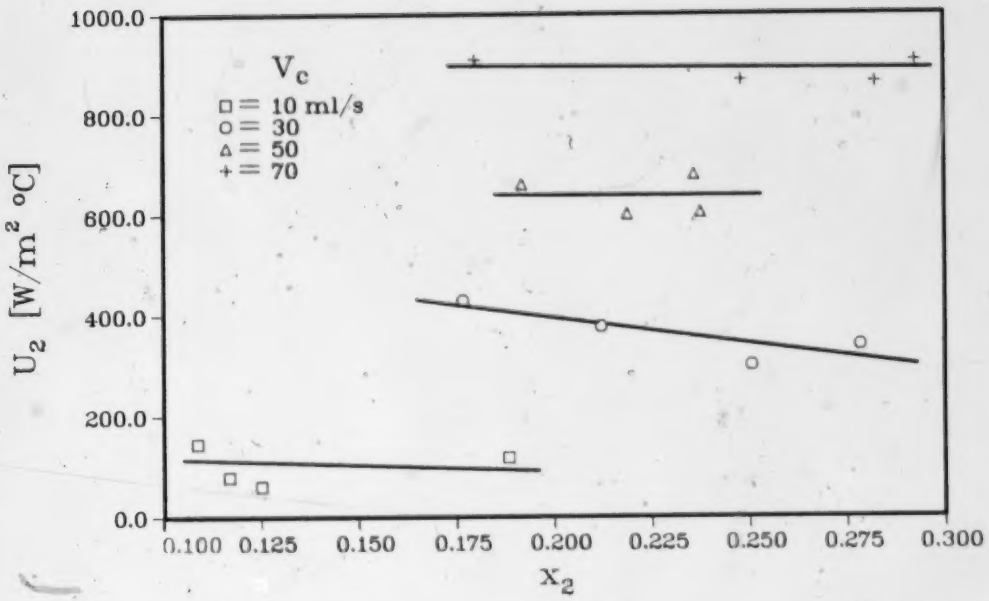

Fig. 3.14 Effect of cooling water flow rate on U_2 vs. x_2 with 70% charge level and open downcomer

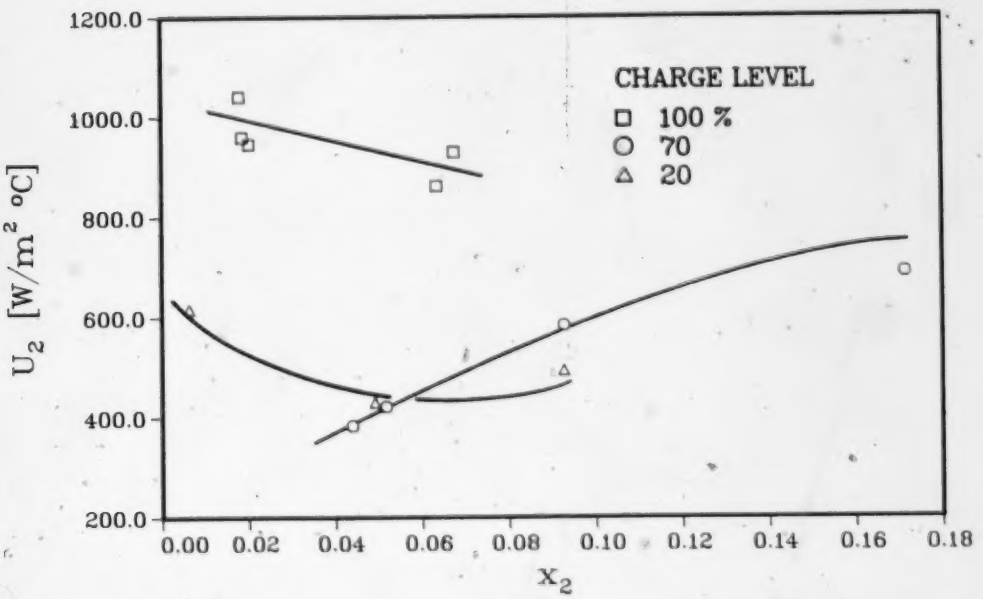

Fig. 3.15 Effect of charge level on U_2 vs. x_2 with closed downcomer and V_c=70 ml/s

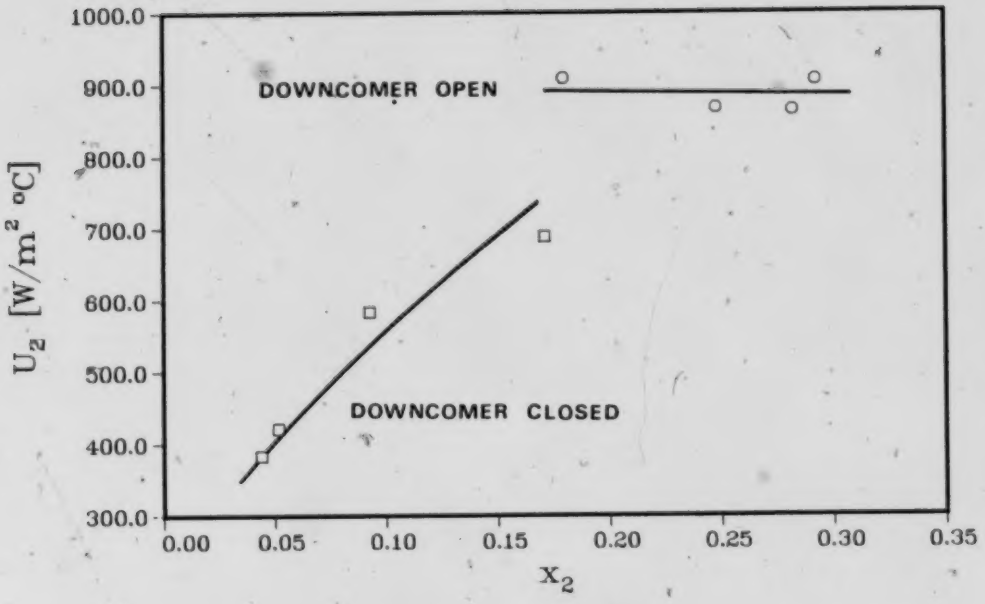

Fig. 3.16 Effect of downcomer on U_2 vs. x_2 with 70% charge level and V_C=70 ml/s

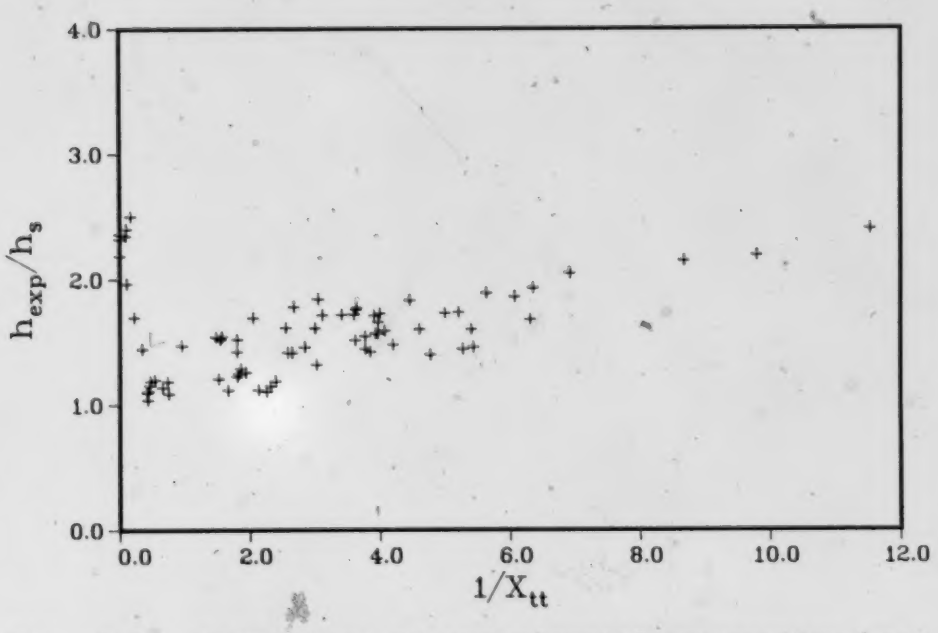

Fig. 3.17 Comparison of experimental evaporator heat transfer coefficient with single phase component correlation

The experimental results are also compared with the predictions of Shah, and Shrock and Grossman, and are shown in Figs. 3.18 and 3.19 using the parameter Boiling number. The trend in the experimental data is to agree with the simple Shah correlation when Bo > $3x10^{-5}$. As can be seen in Fig. 3.19, the Shrock-Grossman correlation seems to overpredict in the range of boiling number greater than $1.0x10^{-5}$.

The single phase tests indicated that the Nusselt number for flow in the inner tube of the lower heat exchanger correlated well with the Graetz parameter. Because the flow quality is low, the same correlation equation is shown in Fig. 3.20 with the two-phase data and the dotted line indicates an extrapolation. In view of the different flow regimes involved, this simple correlation does provide a reasonable estimate of the value of the Nusselt number for the low quality two-phase flow in the evaporator tube. This may be geometry dependent however, and further work must be done to determine the effect of other flow conditions and tube geometries on this simple correlation.

The condensation heat transfer outside the low integral fins of the coiled circular condenser tube is rather complicated. The values of the fin side heat transfer coefficients calculated using Eq.(2.22) are shown in Fig. 3.21 with shell side vapor quality as the major parameter. Comparison with the ideal case predicted by the Beatty-Katz correlation reveals that the experimental heat

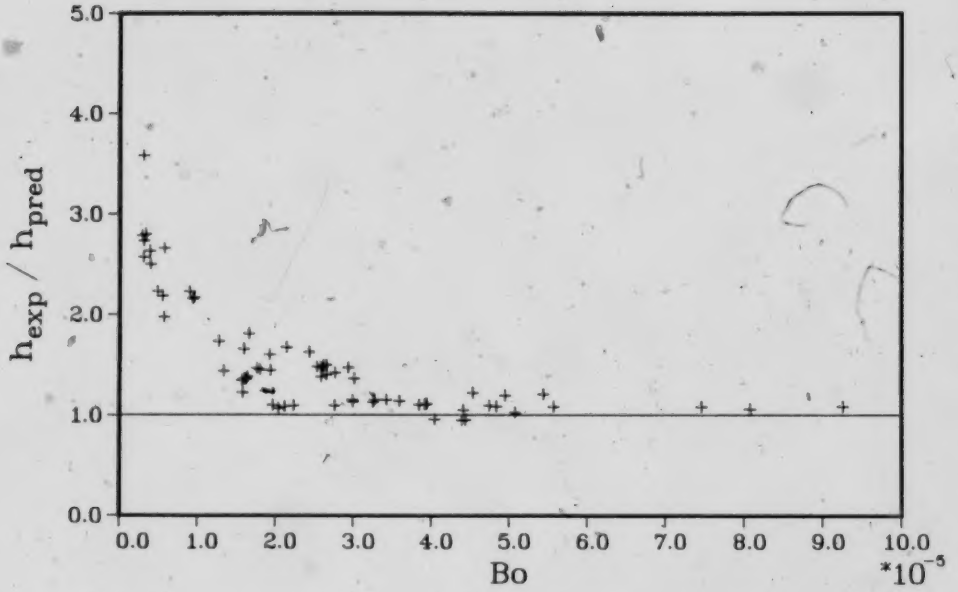

Fig. 3.18 Comparison of experimental evaporator heat transfer coefficient with Shah correlation

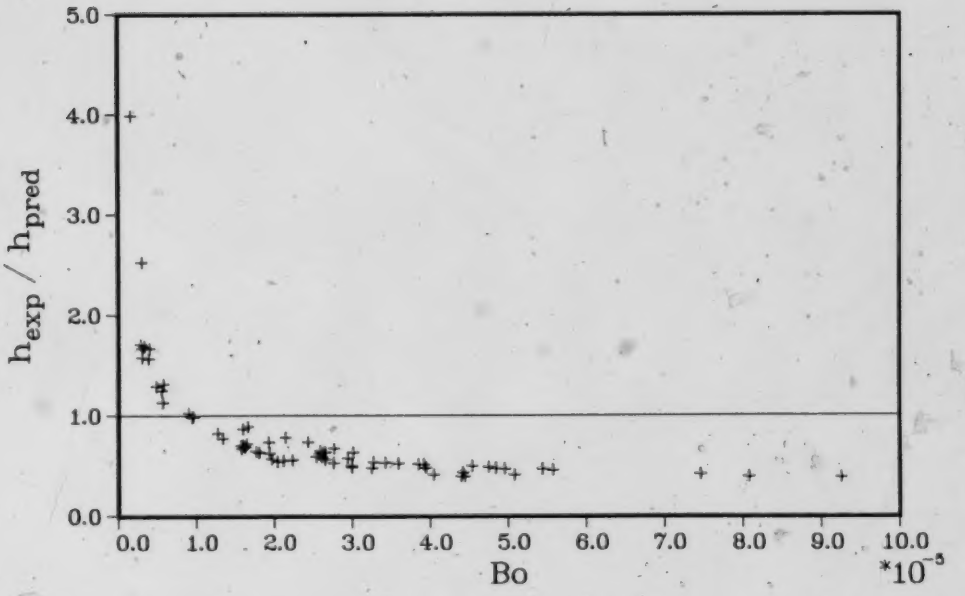

Fig. 3.19 Comparison of experimental evaporator heat transfer coefficient with Shrock-Grossman correlation

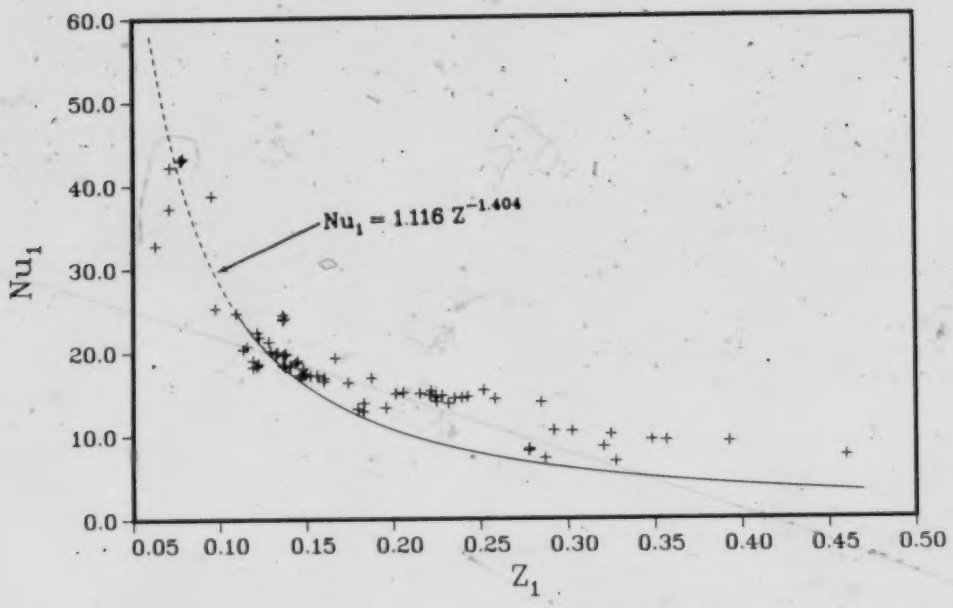

Fig. 3.20 Two-phase water Nu_1 vs. Z_1 with all data and comparison with single phase results

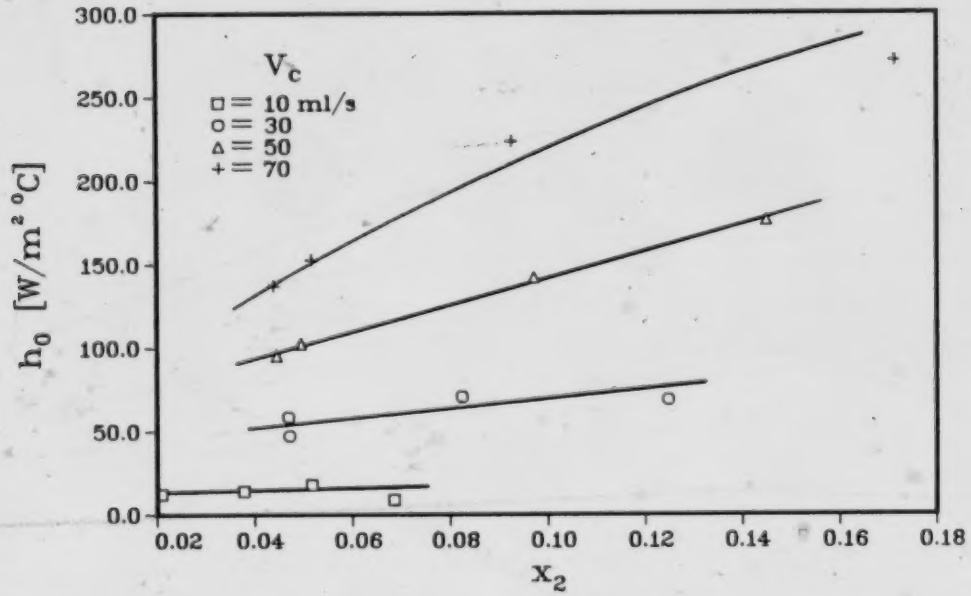

Fig. 3.21 Effect of cooling water flow rate on condenser shell side heat transfer coefficient vs. quality with 70% charge level and closed downcomer

transfer was several orders of magnitude lower than expected. In subsequent Freon tests, the steel shell of the condenser was replaced with a Pyrex glass tube for flow visualization purposes. It was revealed that even for low initial liquid charge levels in the system, vapor generation in the evaporator displaces liquid into the condenser shell and floods the coil, thus reducing condensation area. Liquid entrainment into an empty condenser shell is also serious for high surface tension liquids such as water, where the normally vacant space between the fins may be constantly occupied by stagnant liquid. Thus the tube condensation area takes on a modified cylindrical shape with only small rings of copper exposed for direct condensation.

3.6 Conclusion

The low quality flow closed loop two-phase thermosyphon system tested performed well and increased the level of heat extraction by 15% over its single phase counterpart. Natural circulation was for the most part self initiating, and occurred within minutes after heating and cooling was applied to the primary loop.

The greatest advantage over the single phase system is the large increase in working fluid flow rate under similar operating conditions, which has positive effects on performance in other areas. No doubt agitation caused by the phase change process in both the evaporator and condenser were additional factors in improving performance through

better heat transfer coefficients.

The primary loop mass flow rate was found to increase for higher values of input heat flux, as increased vapor generation caused higher flow velocities with liquid entrainment. This is also reflected in better performance with higher vapor quality flow. The open downcomer and 100% charge level parameters also contributed to greater mass transport, and thus enhanced the overall performance.

The simple Shah correlation valid for low quality flow agreed with the experimental determination of the evaporator tube heat transfer coefficient for Boiling numbers greater than 3, although limited data is available in this region. A simple power correlation between Nusselt number and inverse Graetz number obtained for the evaporator with single phase flow was compared to the low quality convective boiling data encountered here, and the favourable results indicate that further study is warranted.

The condenser fin side heat transfer coefficients were considerably lower than predicted by Nusselt theory, and it is most likely that condenser flooding and liquid entrainment have reduced the heat transfer to an enhanced sensible form.

4. Closed Loop Two-Phase Refrigerant R-113 Thermosyphon Tests

4.1 Introduction

Many flourocarbon refrigerants are ideal for low temperature energy recovery because they have low saturation pressures at low temperatures, and low liquid phase heat capacitance. This enables two phase flow to be achieved easily, and allows for better efficiency due to higher heat transfer coefficients and flow rates. Additionally, they have low freezing points and do not cause scaling and fouling, which makes for long maintenance free life of the thermosyphon loop. Such refrigerants normally have low toxicity, and have been used in the food industry for years.

A condensed pamphlet is available from Dupont [34] which contains a summary of common refrigerants and their properties. Refrigerant R-113 was chosen for these tests as it has a suitable saturation temperature for the range of test parameters desired. Some important physical properties of R-113 [34,35,36] are shown in Table 4.1.

The present experimental closed loop thermosyphon was charged with this refrigerant to determine the optimum operating parameters for the low grade energy recovery situation. The range of operation is from mid vapor quality flow to superheated vapor in the riser line. In addition to the heat transfer analysis of the system, flow visualization photographs are presented in this chapter to give a better

Table 4.1 Properties of Refrigerant R-113

Chemical Name	TRICHLOROTRIFLUOROETHANE
Chemical Formula	$CCl_2F\text{-}CClF_2$
Molecular Weight	187.39 g/mol
Boiling Point at 1 atm	47.47°C
Freezing Point	-35°C
Critical Pressure	33.7 atm
Critical Temperature	214.1°C
Saturated Liquid Density	1569 kg/m³
Latent Heat of Vaporization	152 kJ/kg
Saturated Liquid Specific Heat	0.953 kJ/kg K

understanding of the flow regimes encountered. As well, the pressure and flow rate fluctuations in the primary loop are examined more closely, and the two-phase pressure drop results for flow in the evaporator tube are included.

4.2 Experimental Apparatus and Instrumentation

The fluid in the primary loop was drained down and the tubes flushed with distilled water to remove any debris left over from previous tests. The steel condenser shell was then replaced with a transparent Pyrex glass tube. This was done to enable flow visualization photographs of the condensation process to be taken, as results from the two-phase water tests indicate that the heat transfer mechanism in the heat exchanger is not properly represented by Nusselt theory. An axial dispersal tube was installed in the condenser so that Freon vapor would be better distributed on the finned coil. This was constructed simply of a half inch copper tube with many radial holes located so as to direct the spray onto the coil. The system was then dried by continously passing

compressed air through the primary loop for 72 hours. Before the loop was charged with Freon, the system was evacuated with a vacuum pump for 48 hours to ensure that no air or moisture remained.

Photographs of the flow were also taken at the evaporator exit through the lowermost sight glass, the location of which may be seen in Fig. 2.1. A tripod mounted Nikon FM2 35 mm camera with a 50 mm micro-lens was used with Kodak Tri-X ASA-400 black and white film. The liquid R-113 was dyed red with Trace internal leak detector. As Freon vaporizes, the dye is rejected and remains with the liquid component of the two-phase mixture. When illuminated from behind the sight glass or condenser shell, and photographed with black and white film, the vapor is light in appearance, and the liquid dark.

The analog signals for the fluctuating primary loop flow rates and pressure which were recorded on chart recorders for the two-phase water tests were found to be extremely difficult to quantitatively analyze. For the Freon series of tests, these signals were additionally processed with a fast Fourier transform spectrum analyzer (Nicolet Scientific Corporation 444A Mini-Ubiquitous FFT)[5] to determine their frequency contents. The frequency spectrums were hard copied from the FFT with a Watanabe X-Y recorder. The analog signals were still recorded on Hewlett Packard chart recorders for visual interpretation.

---

[5] henceforth referred to as FFT

When the flow at the evaporator exit is in the two-phase region, the working fluid exit temperature will be the saturation temperature at that point, and this quantity is required in the calculation of the vapor mass quality. However, it was anticipated that the flow at the evaporator exit would enter the superheated vapor region, thus making it difficult to determine the local saturation temperature. For this reason additional static pressure taps and pressure transducers were installed in the working fluid loop at the evaporator exit and condenser inlet to measure the local pressures. With this information, it is possible to compute the saturation temperature from the thermodynamic relationships between pressure and temperature in the saturation region of the refrigerant.

As before, all the instruments were recalibrated before the new series of tests were begun.

4.3 Experimental Procedure

The operating parameters studied with the two-phase refrigerant charged system are heat source temperature (45-85°C), cooling water flow rate (25, 35, 55, and 75 ml/s), and initial liquid Freon charge level (100, 65, and 20%). The downcomer line from the liquid-vapor separator to the evaporator inlet was always open. The heating water flow rate was held between 32 and 36 ml/s, and the cooling water temperature was constant in the range of 10-12°C. The lower limit of the cooling water flow rate range was raised from

10 ml/s to 25 ml/s because wear in the bearings of that particular flow meter were causing some inaccuracies at very low flow rates.

The initial system pressure for all tests was the vapor pressure of R-113 at room temperature (about 40 kPa absolute). This was obtained by drawing a vacuum on the sytem until boiling was achieved, then allowing the system to settle for one hour before a test was begun.

The startup sequence is the same as that for the previous tests, and self-starting two-phase natural flow was always achieved within 20 seconds of the circulation of the secondary loop fluids. Photographs of the transition between flow regimes at the evaporator exit were also taken.

A steady state was judged to exist when the short term time averaged temperatures and system pressure (averaged over about a one minute period) were constant over about a 30 minute time interval. The final computer acquired data were read consecutively 30 times and then averaged. Additionally, the fluctuating flow rates and system pressure voltage signals were sampled consecutively 100 times each at a rate of 10 readings per second. This data was then analyzed to determine the statistical variance of the signals for various operating conditions.

The data was stored in hard copy form on paper, and on Hewlett Packard magnetic tape cassettes, and later transferred to the University computer system for final analysis.

4.4 Data Analysis

The analysis of the experimental data is similar to that done in the previous chapters except that the properties of the working fluid are that of refrigerant R-113. Correlation equations developed for refrigerants by Fujii, Noshu, and Honda [37] are used and the FORTRAN library of R-113 properties may be found in Appendix III. The properties of the cooling and heating water streams are given by the correlations mentioned in Chapter 2, and may be found in Appendix II.

A statistical analysis of the fluctuating signals from the primary loop instrumentation was done to gain further insight into the mechanisms of the instabilities involved in a closed loop two-phase system. The frequency spectrum was obtained by processing the data with an FFT spectrum analyzer. It is also useful to examine the variance of an output signal, which is calculated by [38]

$$s^2 = \frac{\sum_{i=1}^{n} (e_i - E)^2}{n-1} \qquad (4.1)$$

where E is the mean voltage output of the sampled data and e_i is the amplitude of the ith sample. The raw variance of the voltage output may be converted to the true variance in units of flow rate (ml/s) or pressure (kPa) by multiplying by the square of the slope of the linear calibration curve:

$$v = m^2 s^2 \tag{4.2}$$

The experimental heat transfer results for convective boiling in the evaporator were compared with the correlations of Shah, and Shrock and Grossman in Chapter 3. For the Freon tests, a correlation developed by Kandlikar (1982) will also be applied. This empirical equation is an extension of Chen's proposal [39] that the two-phase heat transfer be treated as a result of two separate processes, with a convective component and nucleate boiling component. The total heat transfer is given by

$$h_t = h_{pool} + h_{conv} \tag{4.3}$$

For R-113 in horizontal convective boiling Kandlikar's correlation [40] gives

$$h_t = [D1\ Co^{D2}\ (25Fr)^{D5} + D3\ Bo^{D4}\ (25Fr)^{D6}\ (1.35)]\ h_s \tag{4.4}$$

with the dimensionless parameters Froude number Fr and Convection number Co given by

$$Fr = G^2/(\rho_f^2\ g\ d) \tag{4.5}$$

$$Co = \left(\frac{1-x}{x}\right)^{0.8} (\rho_g/\rho_f)^{0.5} \tag{4.6}$$

The constants required for the correlation are given in

Table 4.2.

The degree of superheating of the vapor at the evaporator exit is of interest and this is simply the difference between the measured temperature and the saturation temperature calculated from the local pressure. In order to check the accuracy of the predicted saturation temperature, the measured and calculated temperatures can be compared while the flow is still in the two-phase regime. When this is done, the degree of superheating is zero, as both values should yield the saturation temperature. The maximum error between the two was found to be 0.9°C over the range of tests conducted in the saturation region, which is considered to be excellent agreement.

4.5 Results and Discussion

4.5.1 Overall System Characteristics

The overall thermal performance of the system, convective boiling heat transfer and pressure drop results, and analysis of the fluctuating phenomena caused by flow instablities in the refrigerant charged thermosyphon are examined graphically in this chapter. Due to the voluminous amount of data gathered during the course of the tests, only representative portions of the results can be shown here, as was indicated in Chapter 3 for the two-phase water tests. Data points which occur for different heat source temperatures will be included in all figures. In this way

Table 4.2 Kandlikar Correlation Coefficients

	Co<0.65	Co>0.65
D1	1.091	0.809
D2	-0.948	-0.891
D3	887.46	387.53
D4	0.726	0.587
D5	0.333	0.096
D6	0.182	0.203

the individual effects of different external operating parameters can be more clearly seen. In cases where these effects are not individually important, all data points will be shown.

The cooling water heat extraction is plotted against the temperature difference between the heat source and heat sink in Figs. 4.1 and 4.2 where the effects of cooling water flow rate and charge level are seen. An interesting phenomenon occurs for a condition of high cooling water flow rate or low liquid charge level. As the temperature difference increases for these situations, the curves begin to flatten out, indicating that the system overall heat transfer coefficient is falling. This was not the case for the liquid-phase or low quality two-phase water thermosyphons, as any increase in overall temperature difference produced higher heat extraction. This will be later shown to be the result of superheated vapor production in the evaporator. Up until the point that the curves begin to flatten, higher cooling water flow rates and a lower charge level result in improved performance.

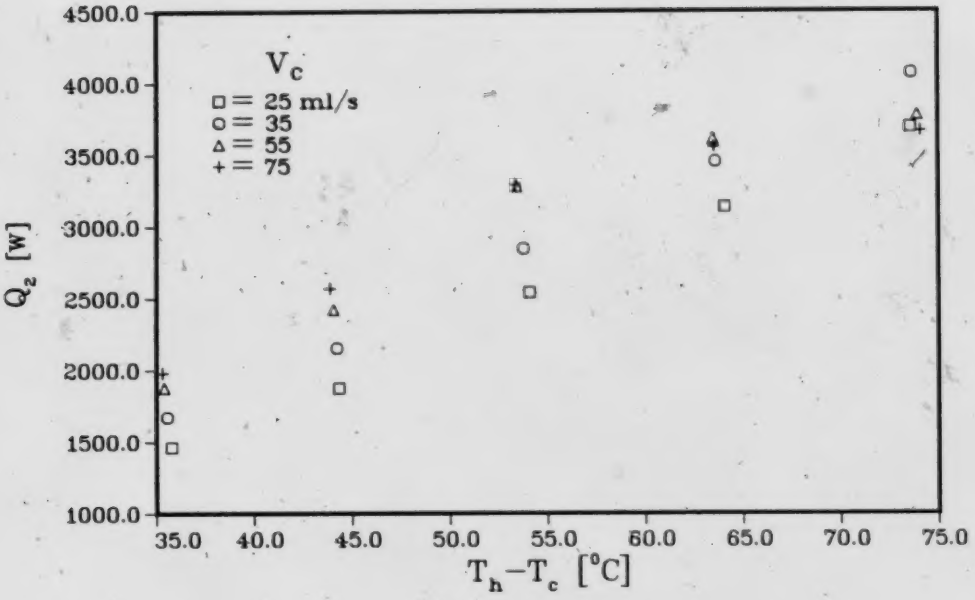

Fig. 4.1 Heat recovery vs. system temperature difference with 20% charge level

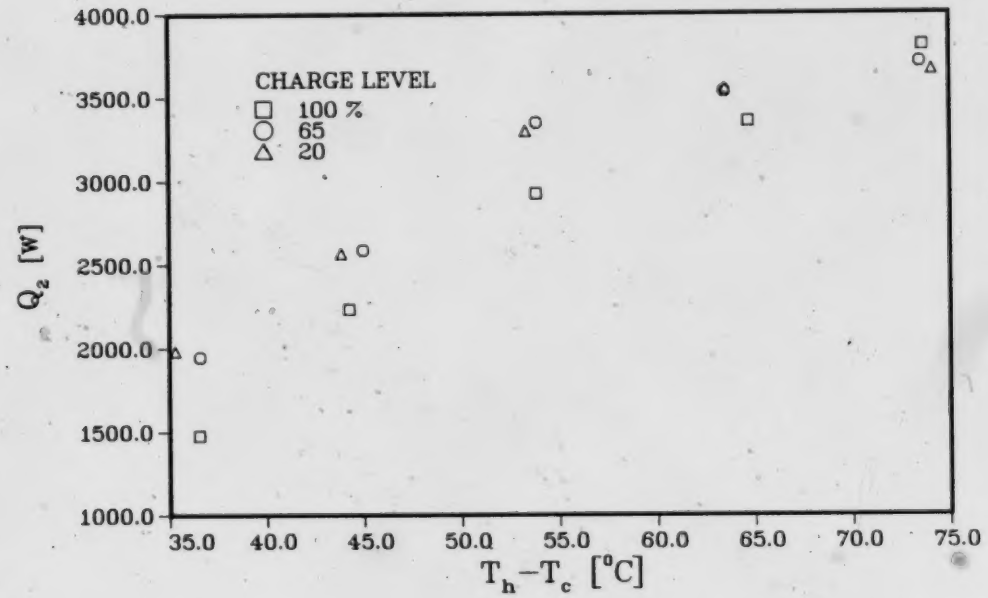

Fig. 4.2 Heat recovery vs. system temperature difference with V_c=75 ml/s

It was noted in previous chapters that the mass flow rate of the working fluid in the primary loop increased for a higher input heat flux, which in turn resulted in increased heat extraction. This is not the case for the high quality flow Freon system as is shown in Fig. 4.3. Note that the total mass flux through the evaporator reaches a somewhat constant level, even though the heat flux is increasing. As the heat input goes up, so does the rate of vapor generation and the vapor mass quality. The final result is that although the mass transport has reached a steady value, the heat input and thus heat extraction is increasing as shown in Fig. 4.4, due to the latent energy content of the flow. Thus a distinguishing feature of this system is that energy transfer occurs through higher latent heat content and lower flow rate, as opposed to the low quality water system which was characterized by high mass flow rates and large sensible heat transfer.

In order to better understand the overall process of heat transport in the system, it is necessary to further examine the properties of the flow in the primary loop at the evaporator, riser line, and condenser. The low saturation temperature, liquid specific heat, and latent heat of vaporization of R-113 allows much greater vapor qualities to be achieved than were possible for the water system. The evaporator exit vapor mass quality is plotted against the average input heat flux in the evaporator tube in Figs. 4.5 and 4.6. A vapor quality of 1.0 indicates that

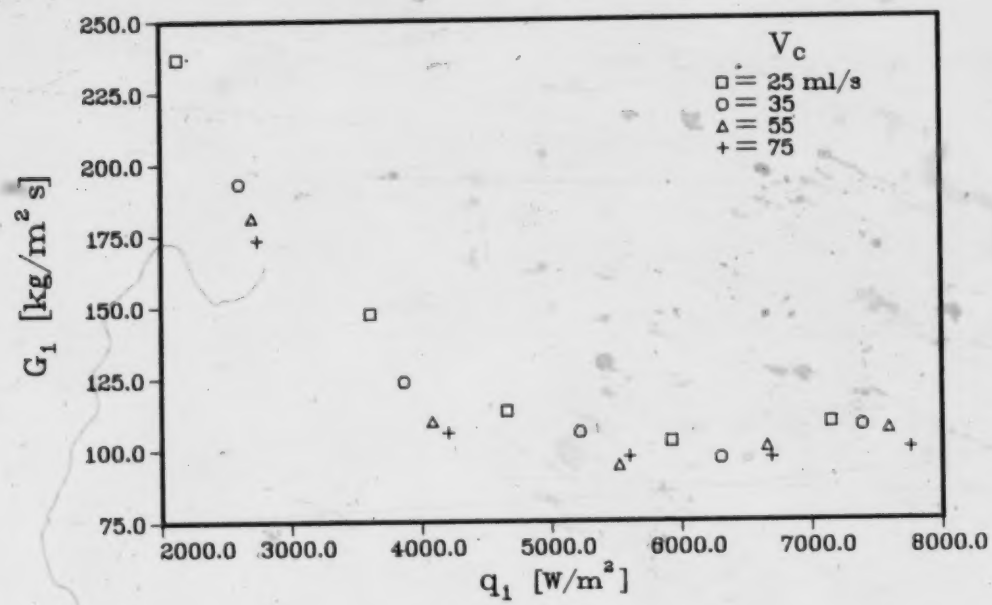

Fig. 4.3 Total working fluid mass flux at evaporator inlet for 100% charge level

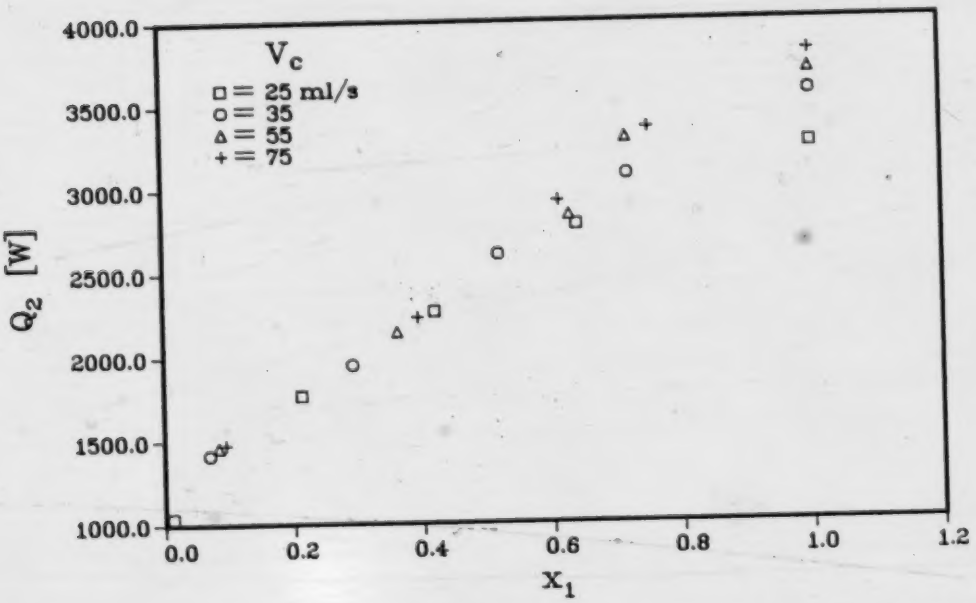

Fig. 4.4 Effect of evaporator exit quality on total heat recovery for 100% charge level

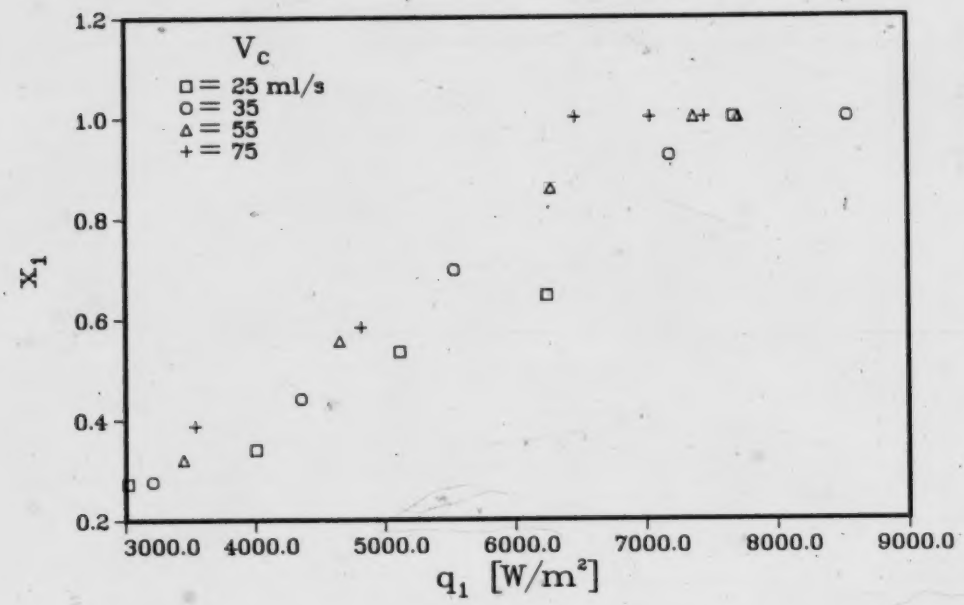

Fig. 4.5 Evaporator exit quality vs. wall heat flux with 65% charge level

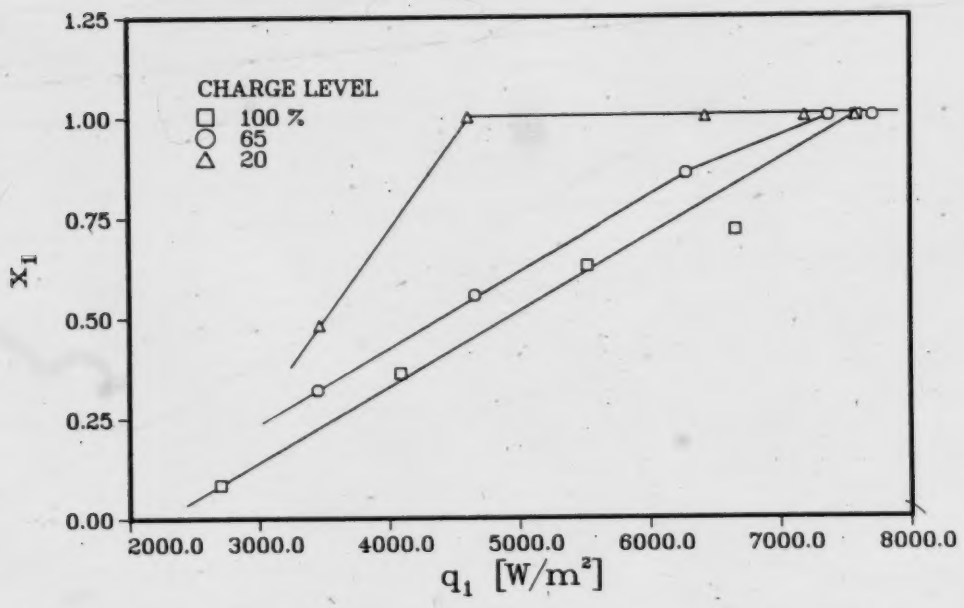

Fig. 4.6 Evaporator exit quality vs. wall heat flux with V_c=55 ml/s

the flow is either saturated or superheated vapor, thus the input heat flux which is required to generate superheated vapor for a particular operating condition may be identified. Note that higher cooling water flow rates produce somewhat higher quality flow, and lower charge levels drastically increase the vapor quality for the same heat flux.

A quality of 1.0 indicates only that superheating is occurring, and it is also useful to have a quantitative indication of superheating. For this reason the degree of superheat (DSH) of the fluid at the evaporator exit is plotted against the input heat flux in Figs. 4.7 and 4.8. DSH is the amount above saturation that the vapor is heated, and is given by the difference between the exit temperature and the saturation temperature at that point. As indicated by Figs. 4.7 and 4.8, higher cooling water flow rates and lower charge levels allow superheating to occur earlier and in larger amounts.

It was found that increasing the cooling water flow rate lowered the pressure in the primary loop, thus lowering the saturation temperature in the evaporator. This enhances vapor generation giving higher quality flow, and a greater possibility of superheating. The lower charge levels promote superheating because there is less liquid in the system, which results in a smaller static head at the evaporator. The absolute pressure is then lower, and this also decreases the saturation temperature. The effect of cooling water flow

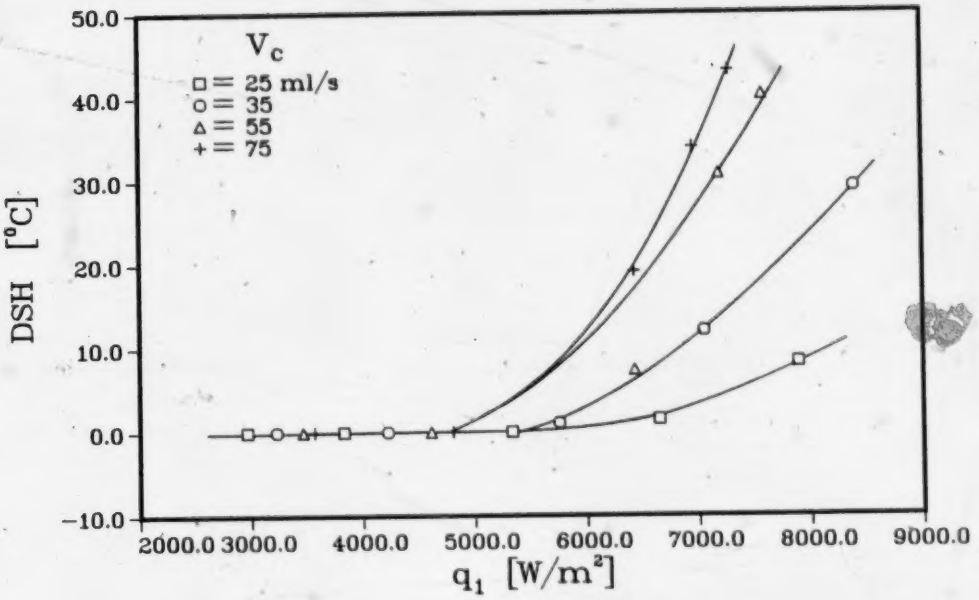

Fig. 4.7 Effect of cooling water flow rate on vapor superheating at evaporator exit with 20% charge level

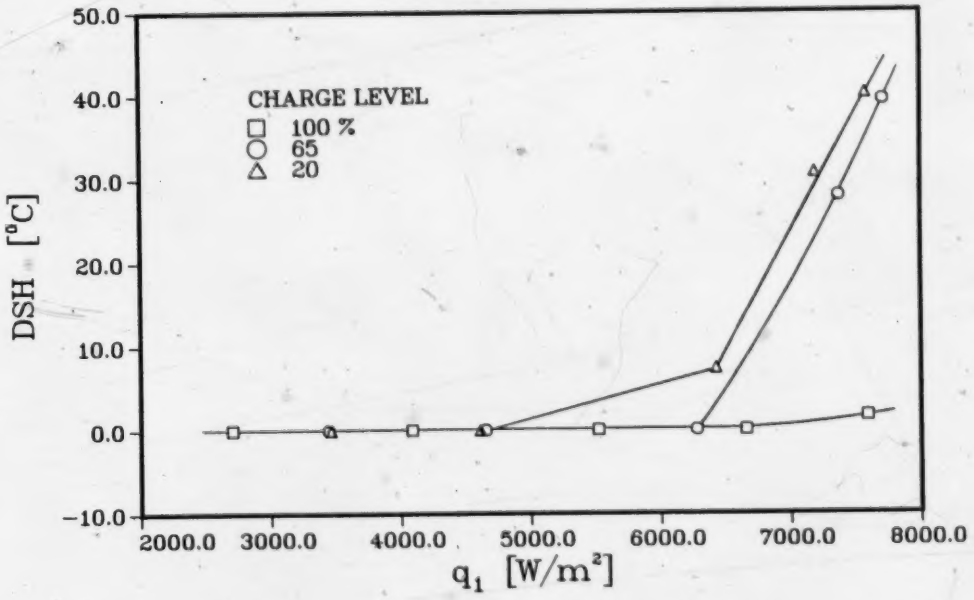

Fig. 4.8 Effect of charge level on vapor superheating at evaporator exit with V_c=55 ml/s

rate is felt strongly at the evaporator, as was found to be the case for the liquid-phase and two-phase water thermosyphons. The indication from these figures is that the vapor enters the superheated regime for an input heat flux around 6000-7000 W/m^2.

Figs. 4.9 and 4.10 show the effect of the difference between the wall temperature and the evaporator saturation temperature on the exit quality and average wall heat flux for the same conditions. The temperature difference required to increase the flow quality to the superheated state is about 15°C. At this point the heat flux flattens off immediately, even though the temperature difference is increasing. This indicates that the internal heat transfer coefficient is dropping, as more of the inner surface area of the evaporator tube becomes dry. This has detrimental effects on the overall performance as is discussed later in this chapter.

The effects of external parameters on the flow in the evaporator tube have been examined, and it is also of interest to see the changes that occur due to the prescence of the riser tube and liquid-vapor separator. Figs. 4.11 and 4.12 show the condenser shell side vapor quality as a function of the evaporator exit quality. Fig. 4.11 illustrates the effect of the liquid-vapor separator on the flow as the condenser quality is roughly 1.5 times that at the evaporator exit. The two-phase mixture has been dried somewhat with a portion of the liquid component separated

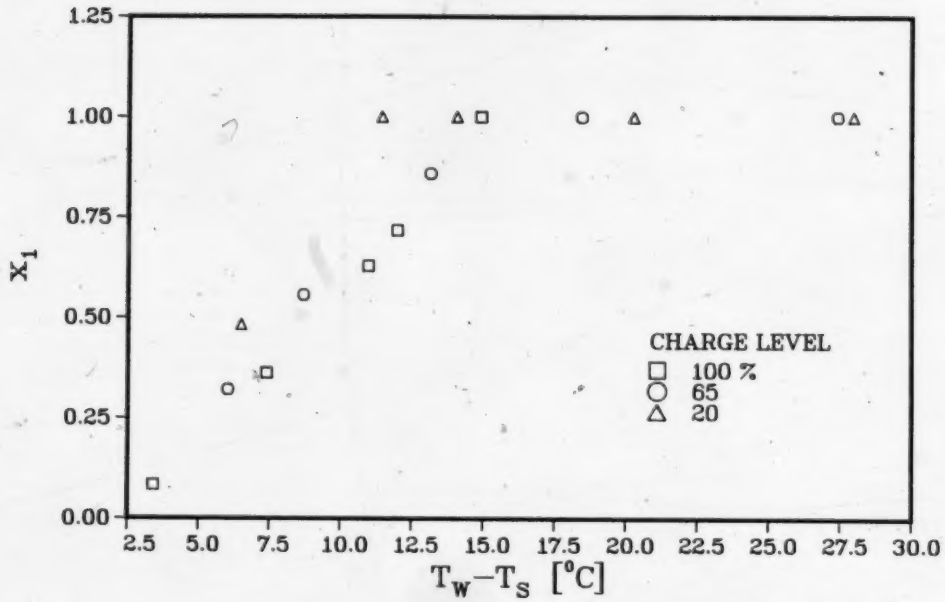

Fig. 4.9 Evaporator exit quality vs. (T_w-T_s) for V_c =55 ml/s

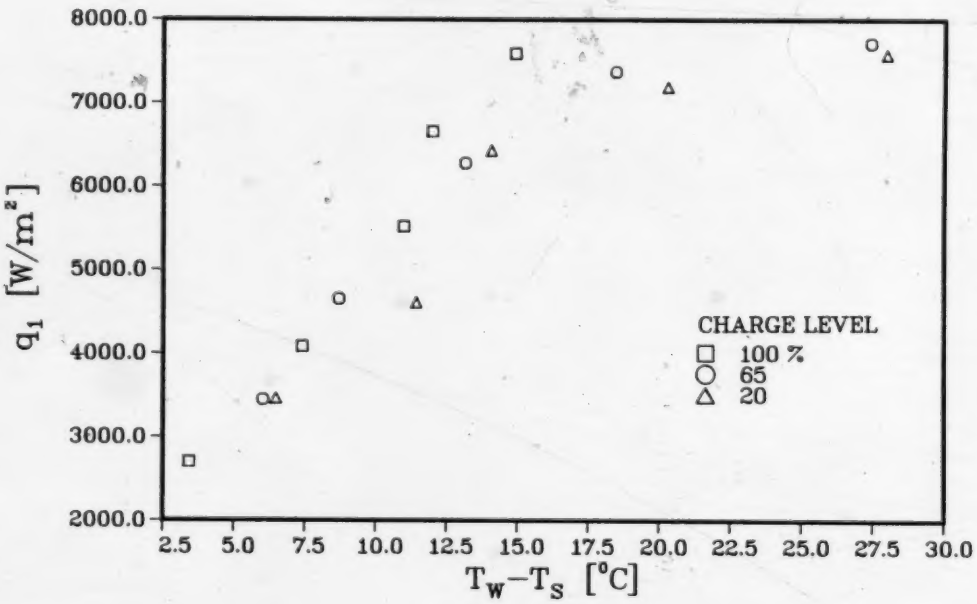

Fig. 4.10 Effect of (T_w-T_s) on wall heat flux with V_c =55 ml/s

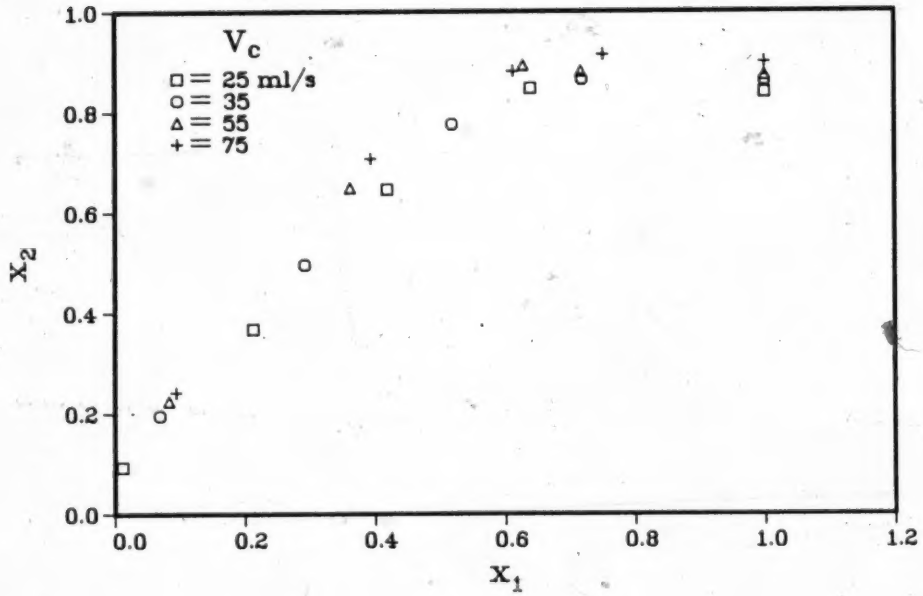

Fig. 4.11 Condenser shell side quality vs. evaporator exit quality for 100% charge level

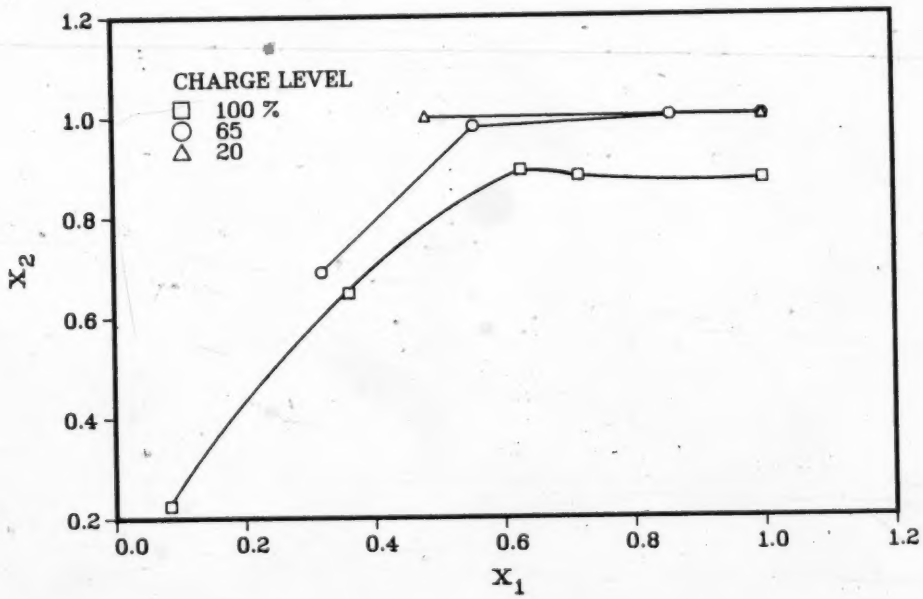

Fig. 4.12 Condenser shell side quality vs evaporator exit quality for V_c=55 ml/s

and returned to the evaporator. The tapering off of the seemingly linear curve is probably a result of liquid entrainment by high speed vapor passing through the separator, as it is likely flooded for the high charge level case. The cooling water flow rate has a minimal effect and Fig. 4.12 indicates the stronger influence of charge level. Note that the 100% charge level curve shows the same drop indicated by Fig. 4.11.

The effect of condenser shell side quality on the cooling water heat extraction is shown in Figs. 4.13 and 4.14. The effect of cooling water flow rate appears to be small compared to that of the quality. The maximum heat extracted is somewhat higher for the lower charge levels, and the 20% charge level data lies entirely in the superheat region.

It is interesting to compare the separate operating systems used; that of liquid-phase thermosyphon and forced flow, two-phase water thermosyphon flow, and the two-phase R-113 system. The maximum heat transport rates for two common operating conditions between these arrangements is shown in Table 4.3.

The best performance of the natural circulation systems is achieved with R-113 as the working fluid, and this is expected for this low temperature range. The best heat extraction is obtained with the single phase forced flow situation, but requires the inclusion of a pump.

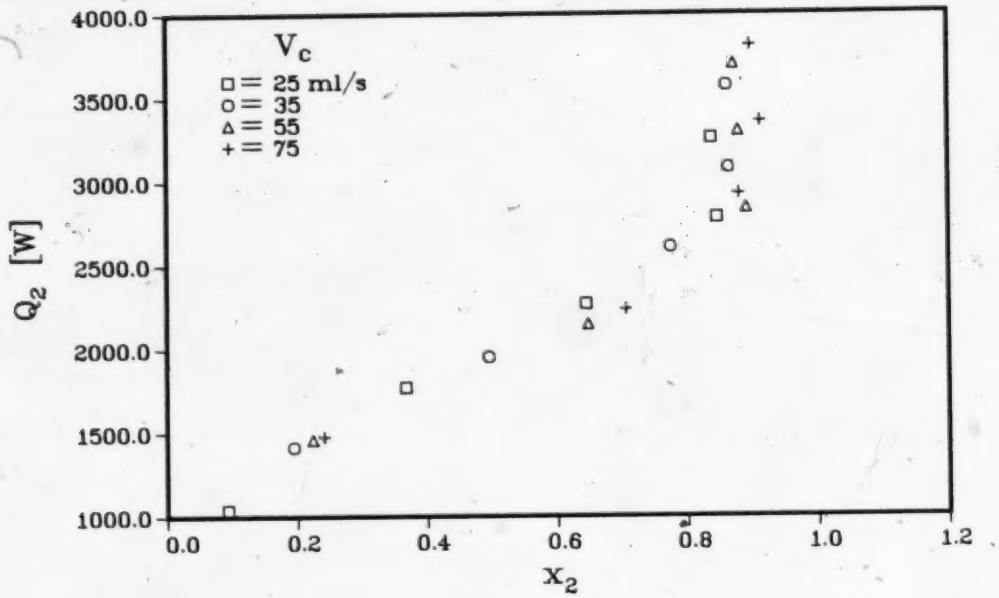

Fig. 4.13 Effect of cooling water flow rate on Q_2 vs. x_2 for 100% charge level

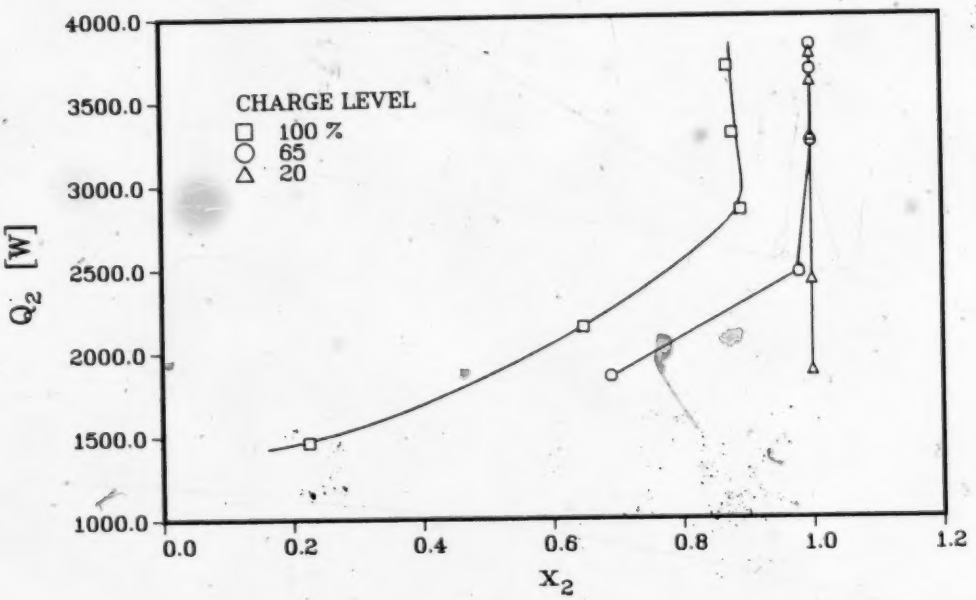

Fig. 4.14 Effect of charge level on Q_2 vs x_2 with V_c=55 ml/s

Table 4.3 Heat Recovery with Different Working Fluids

Working Fluid	T_h=55°C Heat Recovered (Watts)	T_h=85°C Heat Recovered (Watts)
Liquid-Phase Water	1000	3650
Two-Phase Water	1800	3800
Two-Phase Freon R-113	2250	4100
Forced Flow Water	2500	4800

note: cooling water flow rate and temperature are approximately constant for all cases.

4.5.2 System Efficiency

The overall thermodynamic efficiency of the system as calculated by Eq.(2.24) yields some important information. This is plotted against the average input heat flux in Figs. 4.15 and 4.16. Fig. 4.15 reveals that the efficiency actually falls off for high cooling water flow rate and high heat flux, and this begins to occur in a heat flux range of 6000-7000 W/m². This is the same operating region that was earlier shown to characterize superheated vapor production in the evaporator. Fig. 4.16 indicates that the lower charge levels provide better efficiency until superheating begins, but drop off more rapidly beyond that point. This is due to the higher sensitivity of the lower charge levels to superheating as was shown in Fig. 4.8 (both a lower charge level and higher cooling water flow rate increase the possibility of superheating, as discussed earlier). The low quality flow two-phase water tests showed that the efficiency increased for any increase in the input heat flux.

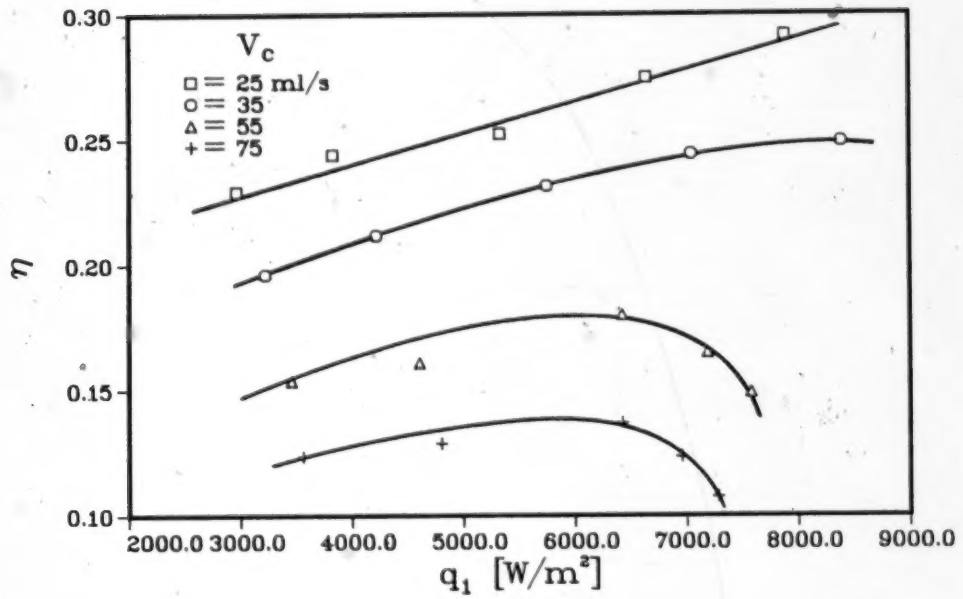

Fig. 4.15 Effect of cooling water flow rate and input heat flux on efficiency for 20% charge level

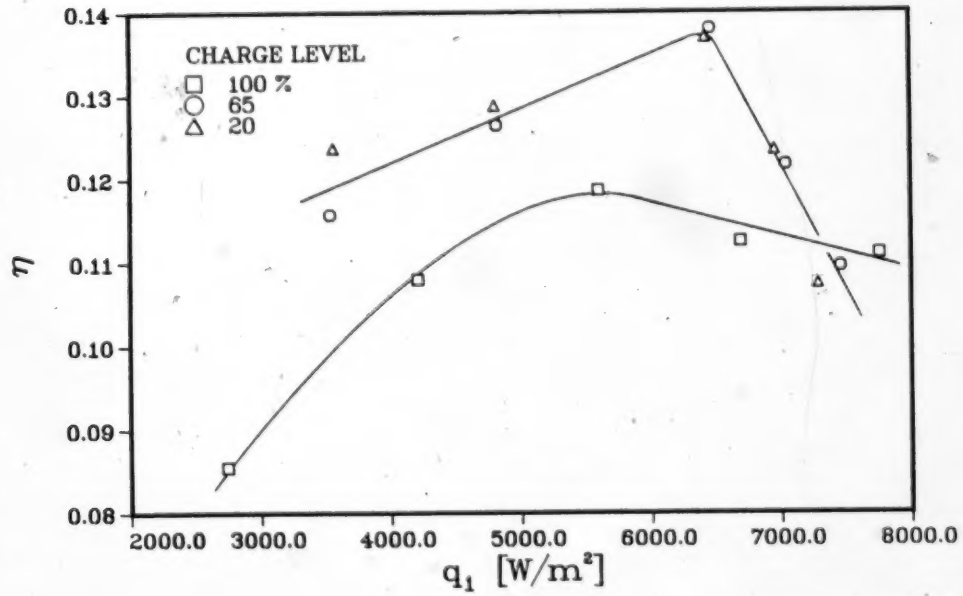

Fig. 4.16 Effect of charge level and input heat flux on efficiency with V_c=75 ml/s

The effect of having superheated vapor flowing in the riser line is further illustrated by plotting the efficiency against the evaporator exit quality, as in Figs. 4.17 and 4.18. It is clear that the optimum system efficiency for a particular charge level or cooling water flow rate occurs as the evaporator exit quality approaches 1.0, or fully saturated vapor flow. Deviation from saturation into the superheated vapor region results in an immediate and rapid reduction in efficiency. This agrees with the work of McDonald, et al [17], who found that for a system with a multiple tube evaporator and condenser, that optimum performance occurred when there was no evaporator dryout.

The experimental data indicates that this system operates most efficiently in the saturation (two-phase) region of the working fluid. This means avoiding excessive subcooling of the working fluid at the condenser, or superheating at the evaporator exit. This is due to higher two-phase heat transfer coefficients, and a lower working fluid temperature which reduces heat losses.

The numerical values obtained for the efficiency of this system are quite low as compared to a single heat exchanger. As mentioned earlier, this might be improved by removing flow restrictions in the primary loop, which in this system are caused by the flow meters, piping, and fittings. An increase in the mass flow rate of the working fluid would decrease the chance of superheated vapor production in the evaporator. An ideal system with no

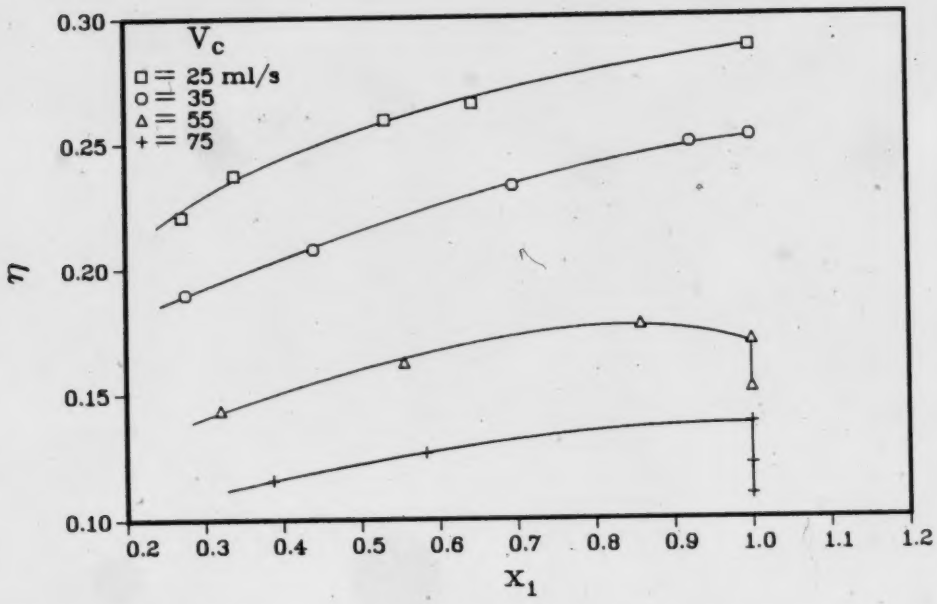

Fig. 4.17 Effect of cooling water flow rate and flow quality on efficiency for 65% charge level

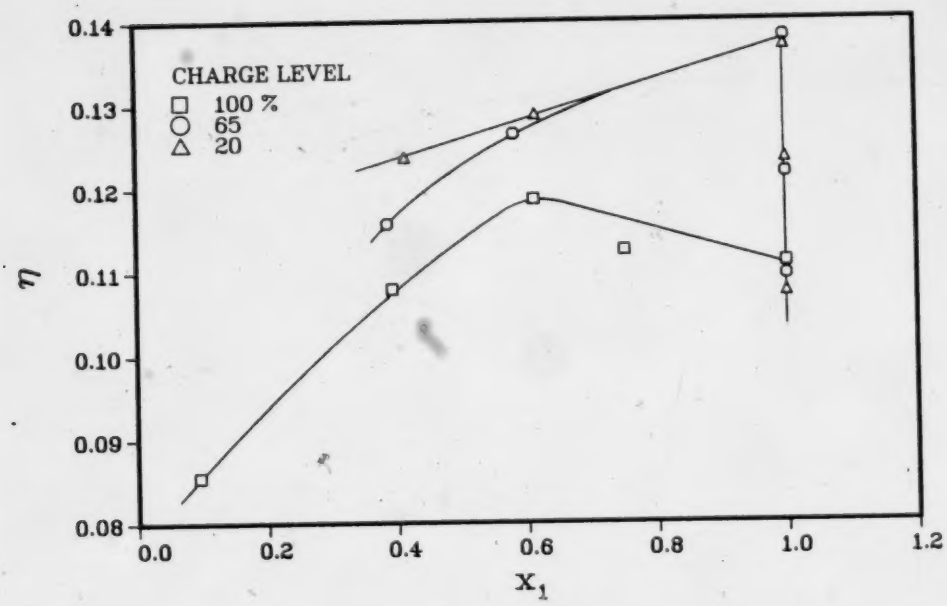

Fig. 4.18 Effect of charge level and flow quality on efficiency with V_c=75 ml/s

pressure drop or heat loss might operate as illustrated on a T-s diagram as in Fig. 4.19. The evaporation process occurs from left to right in the saturation region, and the condensation process on the same line from right to left, returning to the initial point.

4.5.3 Evaporator Convective Boiling

As with the two phase water tests, the experimentally determined convective boiling heat transfer coefficient is compared with that of the turbulent liquid-phase component predicted by Eq.(3.9). The ratio of experimental to single phase coefficient is shown in Figs. 4.20 and 4.21, with inverse Martinelli parameter and Boiling number as the major parameters. The results for data lying in the saturation region only are included, as the equations fail outside the two-phase region. The results follow the expected trend as the latent component of heat transfer is much greater for higher vapor generation rates, while the liquid-phase flow and contribution to heat transfer decreases.

The experimental results for the high quality convective boiling heat transfer coefficients are compared with three separate correlation equations by Shah [31], Shrock and Grossman [32], and a recent one (1982) by Kandlikar [40].

The ratio of experimental to predicted heat transfer coefficient for the Shah correlation is plotted against the correlation's major parameter Boiling number in Fig. 4.22.

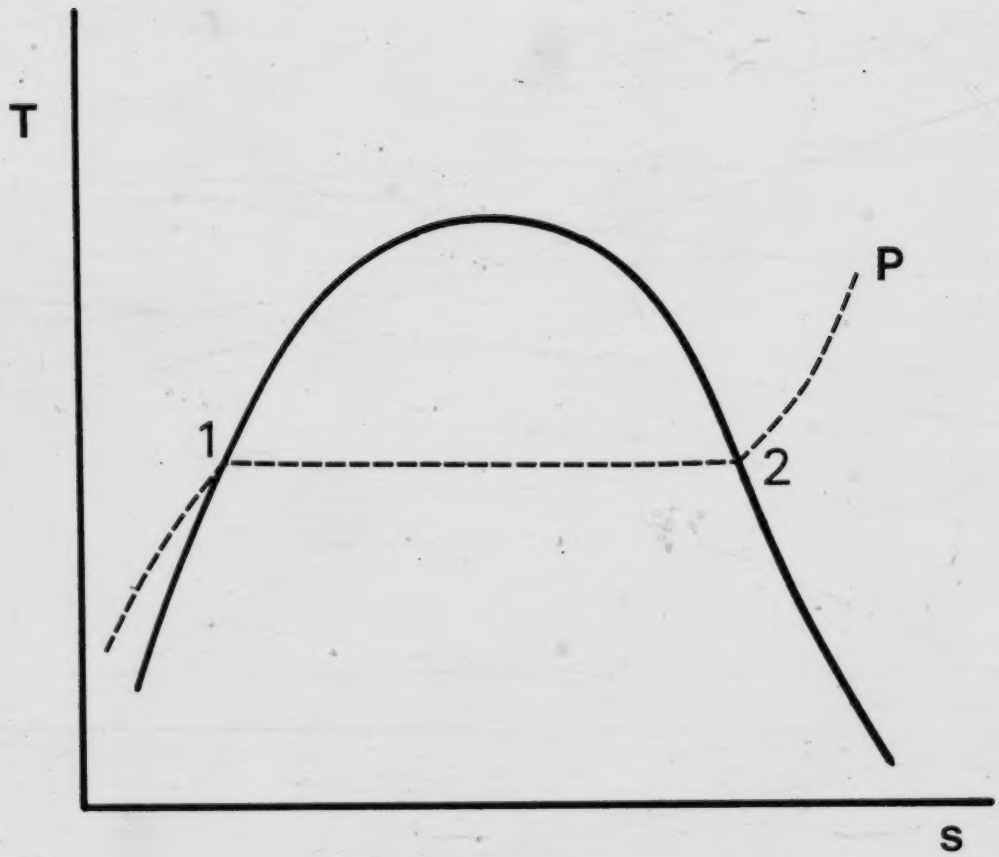

Fig. 4.19 Operating region of thermosyphon for isobaric conditions

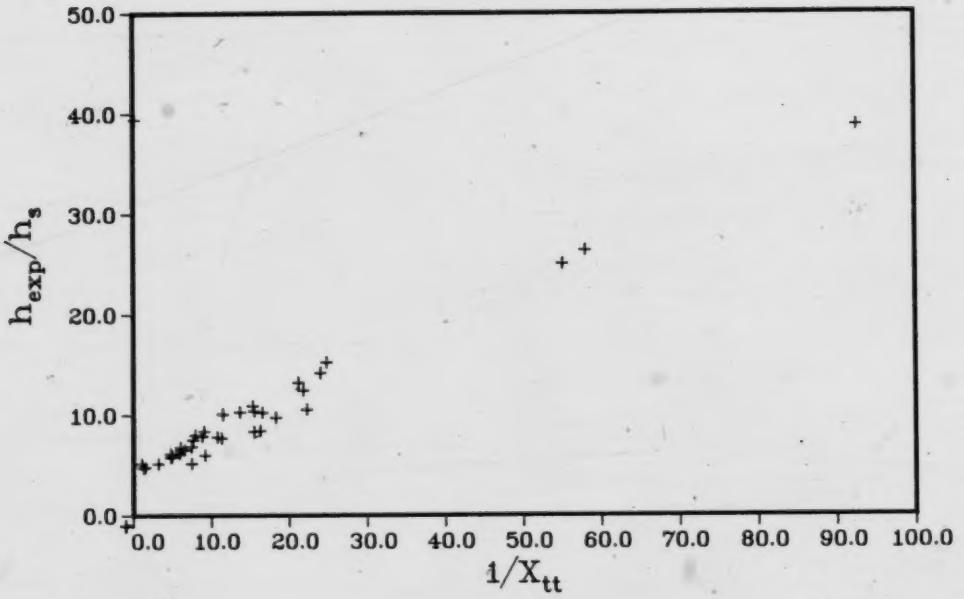

Fig. 4.20 Ratio of experimental to single phase turbulent evaporator tube heat transfer coefficient vs. inverse Martinelli parameter

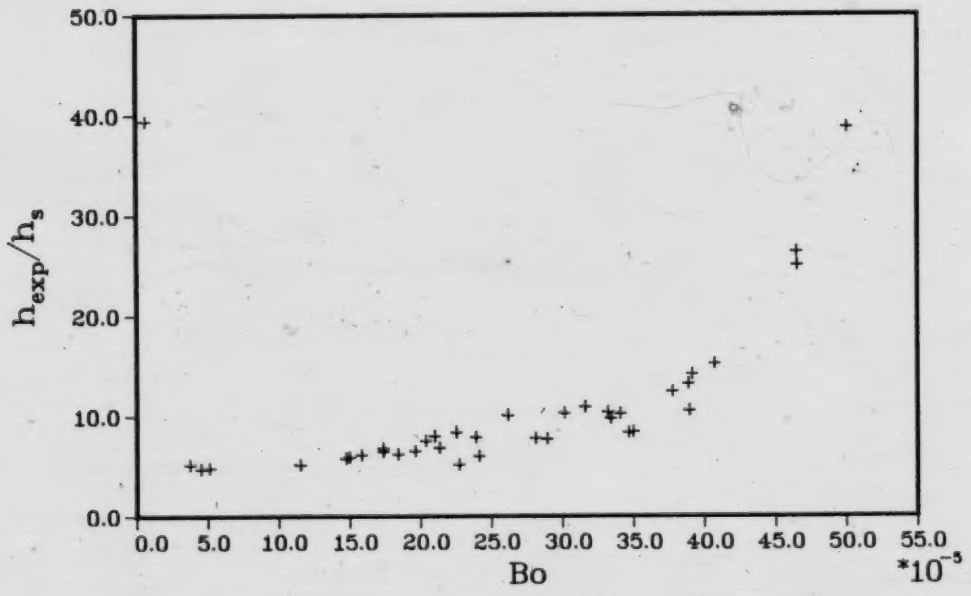

Fig. 4.21 Ratio of experimental to single phase turbulent evaporator heat transfer coefficient vs. Boiling number

Although this correlation was found to predict well for the low quality water tests, it underpredicts as vapor generation increases (increase in Bo). Although the Shrock-Grossman equation was originally specified for flow in vertical tubes, it predicts reasonably well for inverse Martinelli parameters greater than 5, as seen in Fig. 4.23.

Eq.(4.4) describes the correlation equation developed by Kandlikar for boiling flow in horizontal pipes and compares favourably with the experimental results, as show in Fig. 4.24. The Convection number, Co, given by Eq.(4.6) is a major parameter for this correlation, and describes the convective component of the flow.

4.5.4 Primary Loop Flow and Pressure Instabilities

Interest in flow and pressure oscillations in two-phase systems has grown considerably since the 1950's due to the advent of nuclear reactors and their associated cooling problems. However, oscillatory flow instabilities may occur whenever energy is added to a flowing fluid and produces a change in volume [41]. A good review paper by Kakac and Veziroglu [42] explains the different mechanisms of flow and pressure oscillations, and sums the history and present work in this field.

The most common types of dynamic oscillations are pressure-drop oscillations, which are related to the amount of compressible volume in the system and have large time periods, and density wave oscillations, which are related to

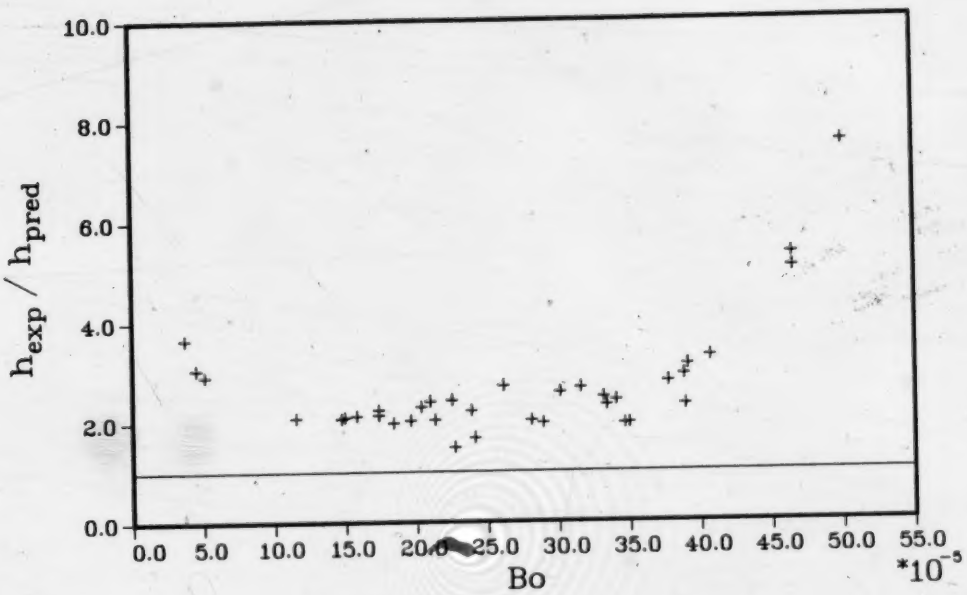

Fig. 4.22 Comparison of experimental evaporator heat transfer coefficient with Shah correlation

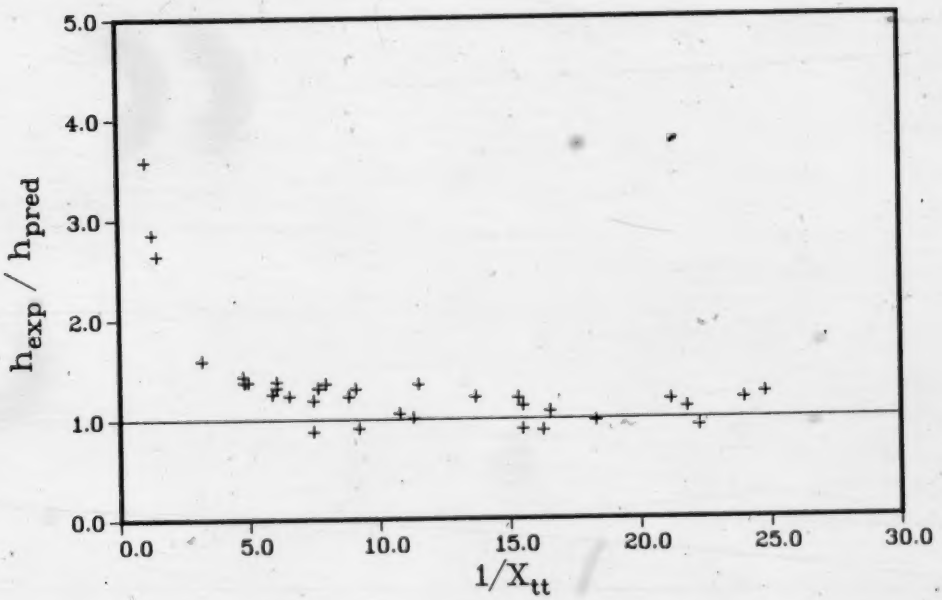

Fig. 4.23 Comparison of experimental evaporator heat transfer coefficient with Shrock-Grossman correlation

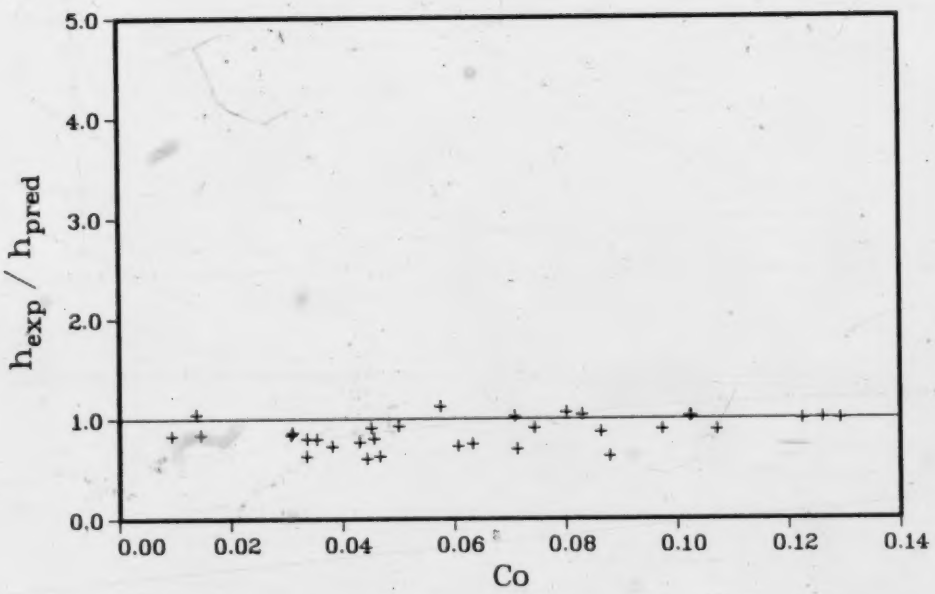

Fig. 4.24 Comparison of experimental evaporator heat transfer coefficient with Kandlikar correlation

the residence time of a fluid particle in the system, and have shorter periods. There are other types also, such as acoustic oscillations and thermal oscillations, the latter of which are related to the instabilities of the liquid film in high vapor quality flow.

These oscillations are particularly important for natural circulation systems as they may be of the same order of magnitude as the mean flow rates and pressures. This can lead to flow reversal, or fatiguing of piping and joints due to fluctuating stresses. Large, regular fluctuations in flow rates and pressure in the primary loop of the two-phase water system were noted, but it was difficult to analyze the data. For this reason, the data from the Freon system was processed with an FFT spectrum analyzer to determine the frequency content of the signals. A typical chart recorder trace of the output signals from the system pressure transducer, downcomer line flow meter, and condensate flow meter are shown in Fig. 4.25. Note that the magnitude of the condensate line fluctuations are much greater than that for the downcomer line, and this was found to always be the case over the range of tests conducted.

When the analog version of this signal is fed through the FFT, the fundamental frequencies may be identified, as in Fig. 4.26. The additional smaller peaks are the harmonics of the 0.35 cycles per second fundamental frequency. This indicates that an additional acoustic wave may be travelling around the system after the initial excitation is provided

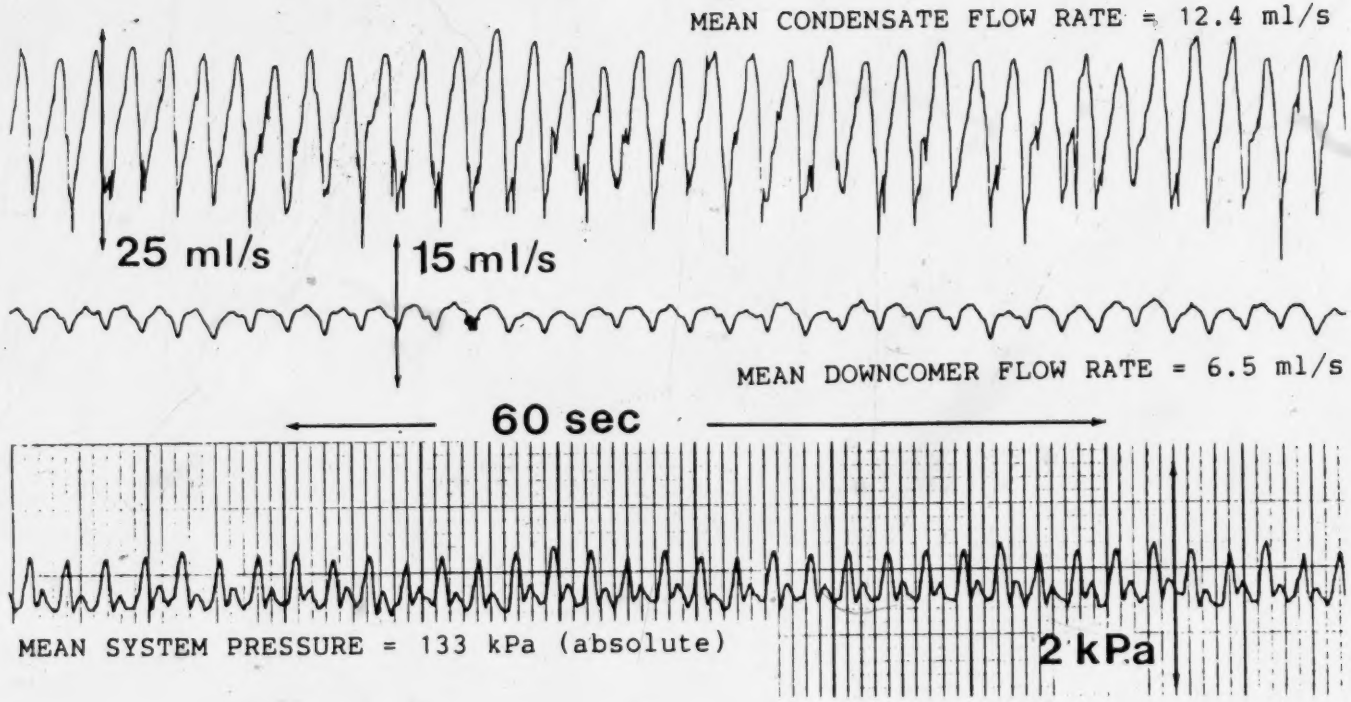
MEAN CONDENSATE FLOW RATE = 12.4 ml/s
25 ml/s
15 ml/s
MEAN DOWNCOMER FLOW RATE = 6.5 ml/s
60 sec
MEAN SYSTEM PRESSURE = 133 kPa (absolute)
2 kPa

Fig. 4.25 Primary loop flow and pressure oscillations for 65% charge level, 65°C heat source temperature, and V_C=25 ml/s

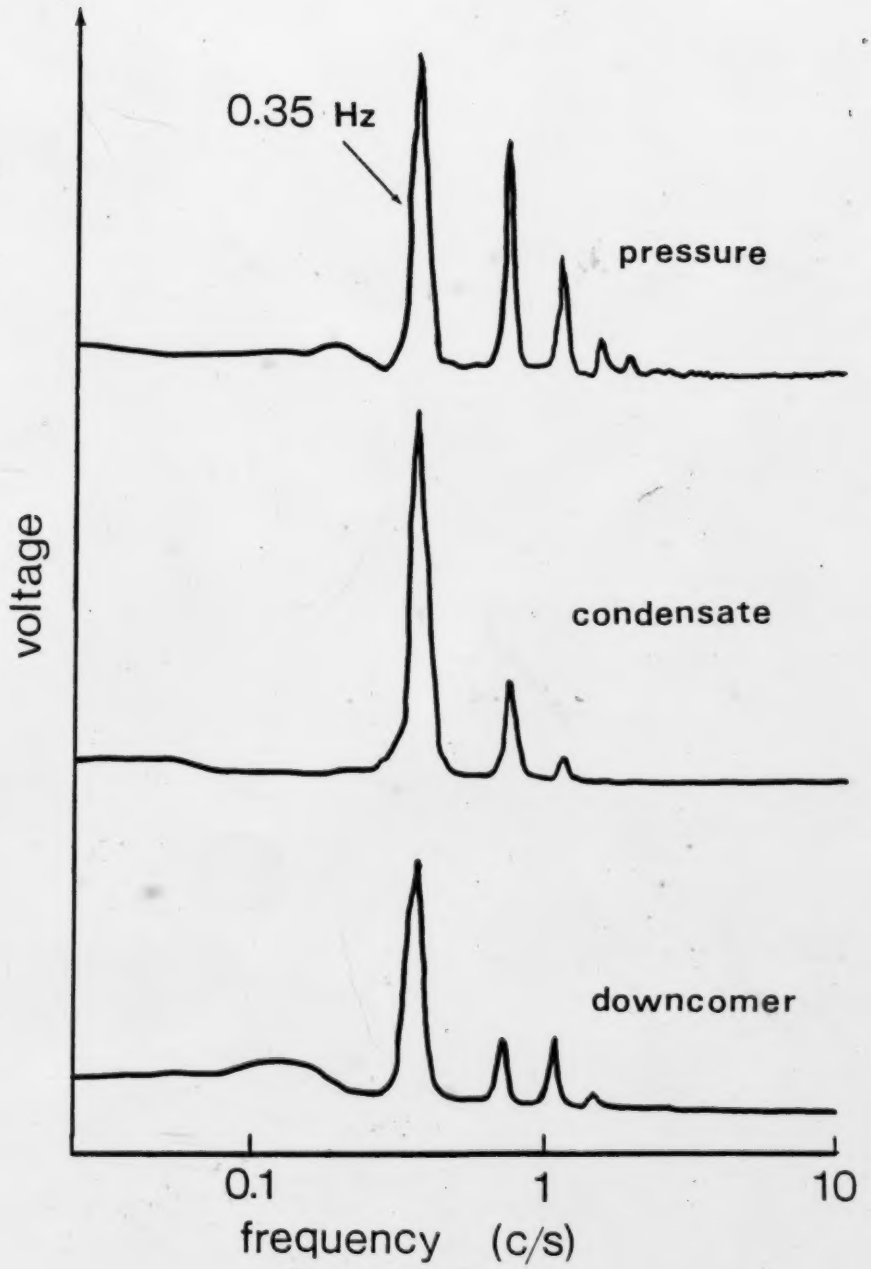

Fig. 4.26 Frequency spectrum of primary loop flow and pressure oscillations for 65% charge level, 65°C heat source temperature, and V_C=25 ml/s

by the fundamental. One important fact to be drawn from this figure is that all three parameters have the same frequency of oscillation, and this was found to be the case for the majority of the tests conducted. In addition, the fundamental frequency was found to be a basically constant value, varying between 0.35 and 0.375 c/s, with some data scatter. The frequencies of oscillation of the flow rates and pressures are plotted against input heat flux in Figs. 4.27, 4.28, and 4.29.

Pressure drop oscillations are of much lower frequency than 0.35 c/s, as reported in [41], and for the most part were not detected. The regularity of the oscillations for changing heat flux (thus changing vapor quality of the riser flow) indicates that they may be dependent on geometry rather than on the state of the flow. Stenning [43] indicated that the time period of density wave oscillations was of the order of the residence time of a fluid particle in the system. For an open system forced flow experiment, Verizoglu and Lee [41] found that the period of density wave oscillations was approximately 2.32 times the residence time of a particle in their heater and exit tubing, and that the frequency was in the range 0.33-0.5 c/s.

For the present closed system, a good linear relationship was not found between the oscillation periods and the time for a particle to travel around the loop. This could be due to the different sizes of tubing and fittings used, and the inability to determine the flow density at

some points. Thus the average velocity of the flow could not be accurately determined. However, the fluctations are of the same order of magnitude as a roughly determined frequency of the flow around the loop. This, and the agreement with [41] for the frequency of density-wave oscillations indicates that this is the mechanism of the observed fluctuations, and the acoustic wave which is generated is the probable cause of the harmonics as it travels around the system and is eventually damped out.

The amplitude of the oscillating signal is important as well as the frequency. The statistical variance of the system pressure fluctuations was computed from Eq.(4.2) and the result is shown in Fig. 4.30 plotted against average evaporator heat flux. This calculation represents the deviations in the system pressure from the mean value of the fluctuations, and the figure shows that the variance increases only slightly with higher heat fluxes until a critical point is reached, at which point a dramatic increase in the variance is seen. This point is once again characterized by entry into the region of superheated vapor production in the evaporator, and this is further exemplified in Fig. 4.31, where the system pressure variance is plotted against evaporator exit quality (all data shown).

This would often cause an audible noise to emanate from the system, as well as some vibration of the primary loop tubes. This drastic effect which occurs for superheated vapor production may be caused by an increasingly unstable

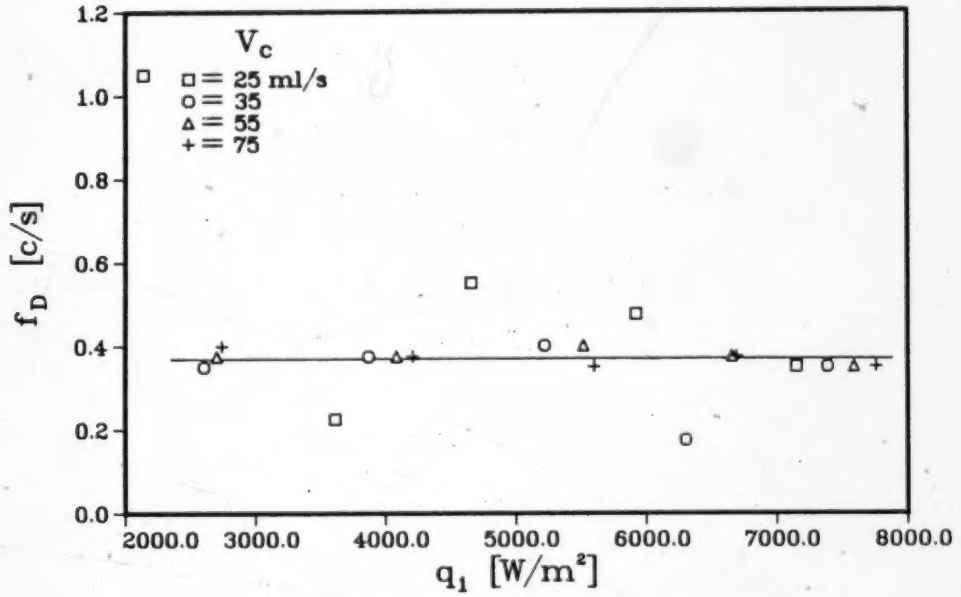

Fig. 4.27 Frequency of downcomer flow fluctuations for 100% charge level

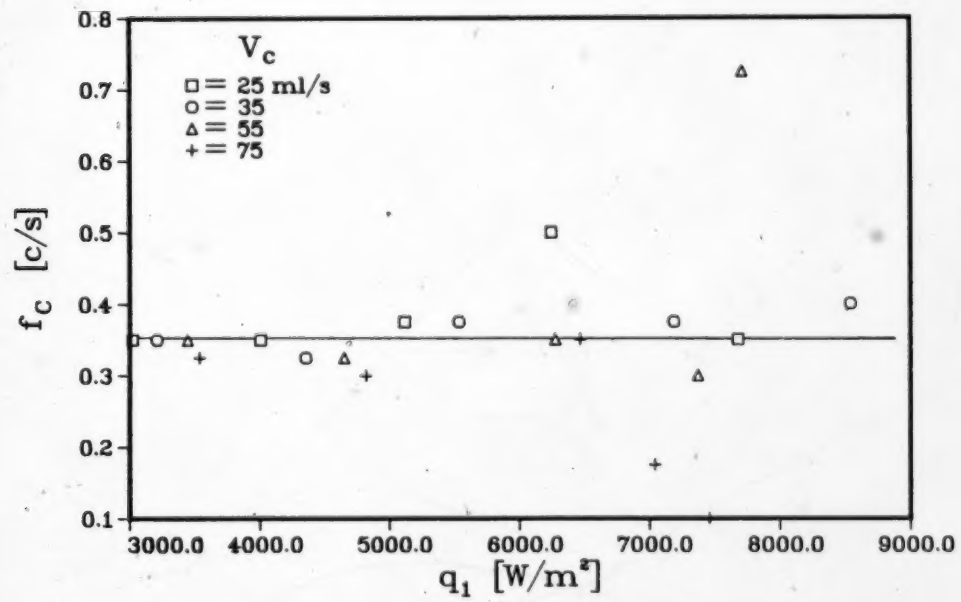

Fig. 4.28 Frequency of condensate flow fluctuations for 65% charge level

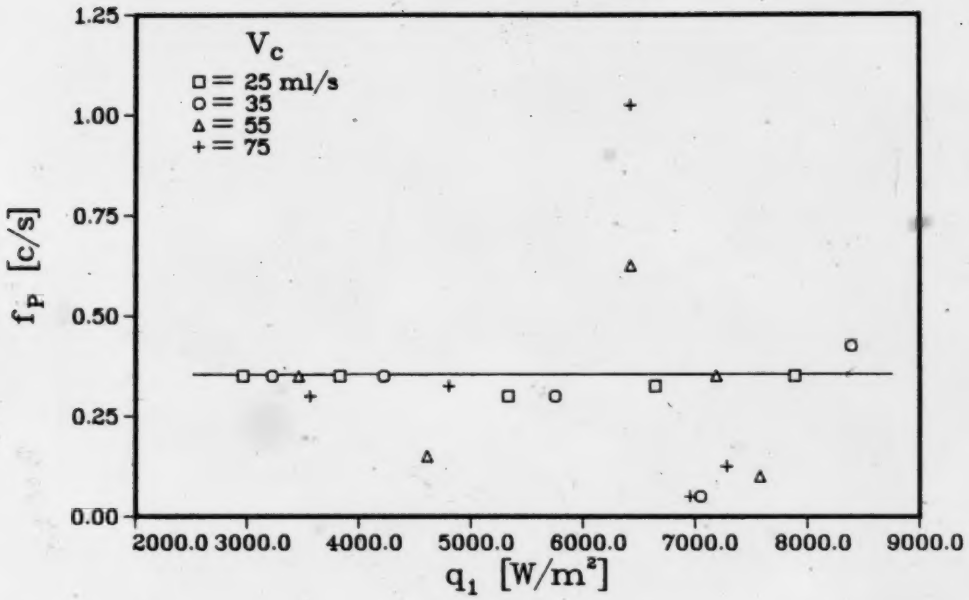

Fig. 4.29 Frequency of system pressure fluctuations for 20% charge level

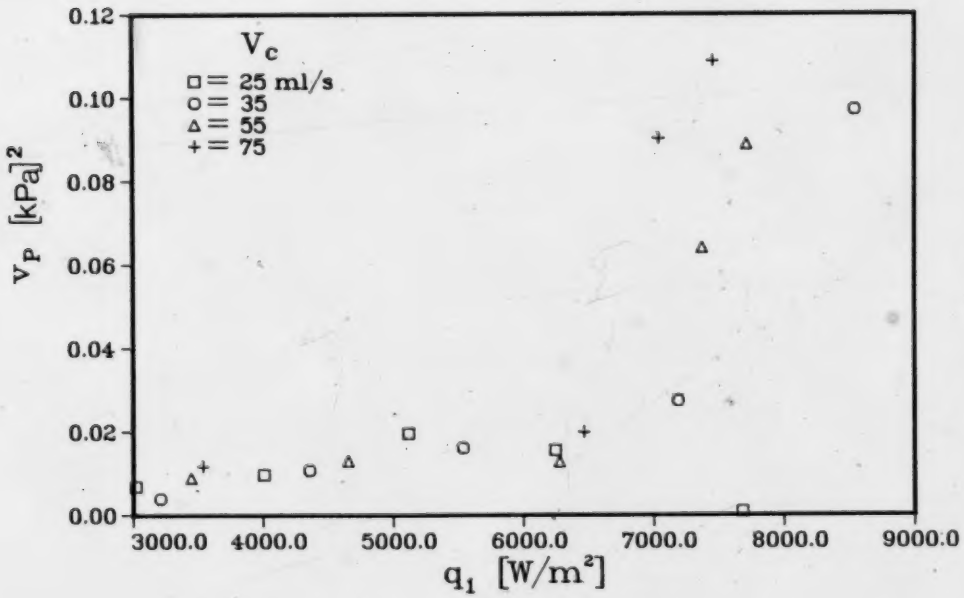

Fig. 4.30 Variance of system pressure signal for 65% charge level

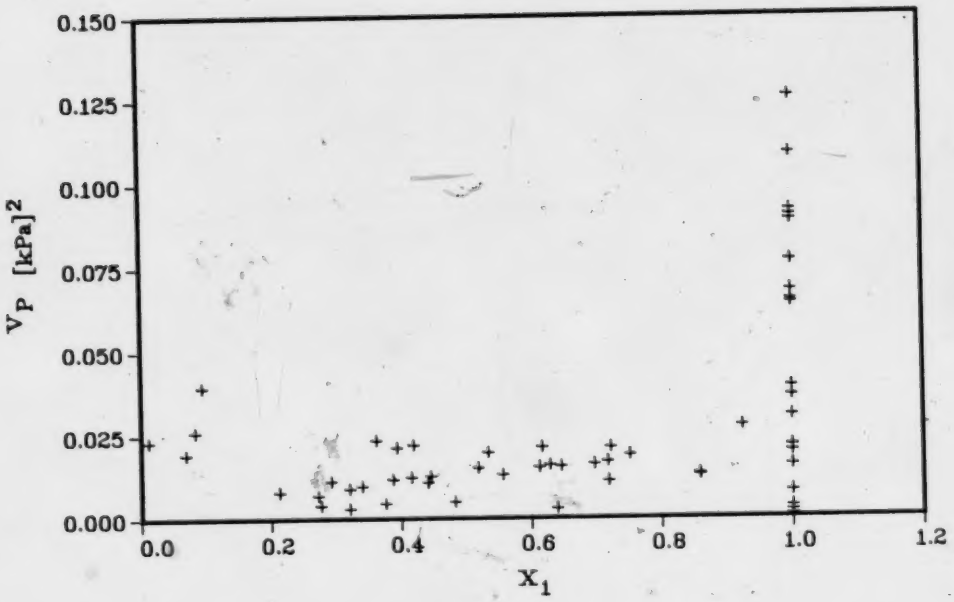

Fig. 4.31 Variance of system pressure signal with evaporator exit quality, all data

liquid film on the evaporator tube surface, or a destructive collapse of hot vapor volume as it encounters the cold surfaces and liquids in the condenser. For the particular arrangement tested, the production of superheated vapor causes mechanical effects which should be avoided.

Experiments performed with forced boiling flow in parallel channels [44] have revealed that introducing a pressure drop at the inlet to the heated section stabilizes pressure-drop and density-wave type oscillations. However, any flow restriction in the natural circulation system hinders performance, so the avoidance of mechanical problems may have to be effected through operation in the two-phase region. The system tested is the most thermodynamically efficient when superheating is avoided, which is additional incentive not to exceed saturated vapor production in the evaporator.

4.5.5 Convective Boiling Pressure Drop

Two different models are widely used to describe pressure gradients in two-phase flow, these being the homogeneous model and the separated flow model. The homogeneous model, which will be used here, assumes good mixing with equal liquid and vapor velocities, thermodynamic equilibrium between phases, and some mean property value between the two phases of the flow. The homogeneous mean absolute viscosity and density may be calculated by

$$\overline{\mu} = \left(x/\mu_g + \frac{1-x}{\mu_f}\right)^{-1} \tag{4.7}$$

$$\overline{\rho} = \left(x/\rho_g + \frac{1-x}{\rho_f}\right)^{-1} \tag{4.8}$$

When measuring the total pressure drop for the working fluid in the evaporator from an inlet static pressure tap to an outlet static pressure tap, three elements are included: the frictional, accelerational, and gravitational components. Following Shrock and Grossman [32], the accelerational pressure drop component is considered negligible. It is of primary interest to extract the frictional part of the pressure drop from the total experimental measurement. Because the heat exchanger has a 0.25 meter height, corrections for the gravity component of the reading caused by the large density change from the inlet (liquid) to the outlet (liquid-vapor) must be considered.

The pressure transducer is located in the same horizontal plane as the upper exit pressure tap, and liquid filled copper tubes connect the transducer with both pressure taps. The required correction for the gravity component is found from the density difference between the liquid filled lower pressure tap line and liquid-vapor filled evaporator tube. The flow in the evaporator tube may change from a liquid at the inlet to vapor at the outlet so

a mean density for the fluid is calculated. This is done by assuming that the flow quality varies linearly from the inlet to the outlet [13]. The density of the inlet fluid is that of liquid Freon R-113, and the density of the exit mixture is calculated from Eq.(4.8). This yields a mean evaporator tube density of

$$\overline{\rho}_m = \frac{1}{2}\left[\rho_{fi} + \left(\frac{x}{\rho_g} + \frac{1-x}{\rho_f}\right)^{-1}\right] \tag{4.9}$$

The liquid filled pressure tap line contains R-113 at room temperature (density=1569 kg/m^3), so the gravitational portion of the total pressure measurement is given as

$$P_{grav} = (\overline{\rho}_m - 1569)\, gh \tag{4.10}$$

Finally, the friction component may be extracted from the measured pressure drop through the following equation with SI units:

$$\Delta P = P_{meas} - (\overline{\rho}_m - 1569)(9.81)(0.25) \tag{4.11}$$

The experimental two-phase frictional pressure drop will also be compared with a homogeneous model correlation. From Collier [45], the frictional pressure gradient is

$$-dp/dz = 2\, f_t\, G^2/\overline{\rho} d \tag{4.12}$$

with f_t given by the Blasius equation assuming the boiling

flow is turbulent:

$$f_t = 0.079 \left(Gd/\overline{\mu}\right)^{-0.25} \qquad (4.13)$$

The total frictional pressure drop through the evaporator may then be written as

$$\Delta P_t = 2 f_t G^2/\overline{\rho} \left(\ell/d\right) \qquad (4.14)$$

The experimentally measured friction component of pressure drop for convective boiling in the evaporator tube is plotted against the input heat flux in Figs. 4.32 and 4.33. Two data points have been eliminated from Fig. 4.32. Earlier, the total mass flow rate through the evaporator was shown to decrease and then level off for increasing heat flux. In a single phase system, this would result in a lower pressure drop over the length of the tube. Here however, the pressure drop increases in a linear fashion with increasing heat flux until a drastic reduction of the pressure loss occurs, as seen in Fig. 4.33. Note that this is for the two lower charge levels, which indicates that the superheated vapor state is being encountered. The high charge level data shown in Fig. 4.32 lie entirely in the saturation region, with a two-phase mixture being present at the evaporator exit.

The trends seen in the experimental data agree with those found in Freon R-11 tests by Kakac and Veziroglu

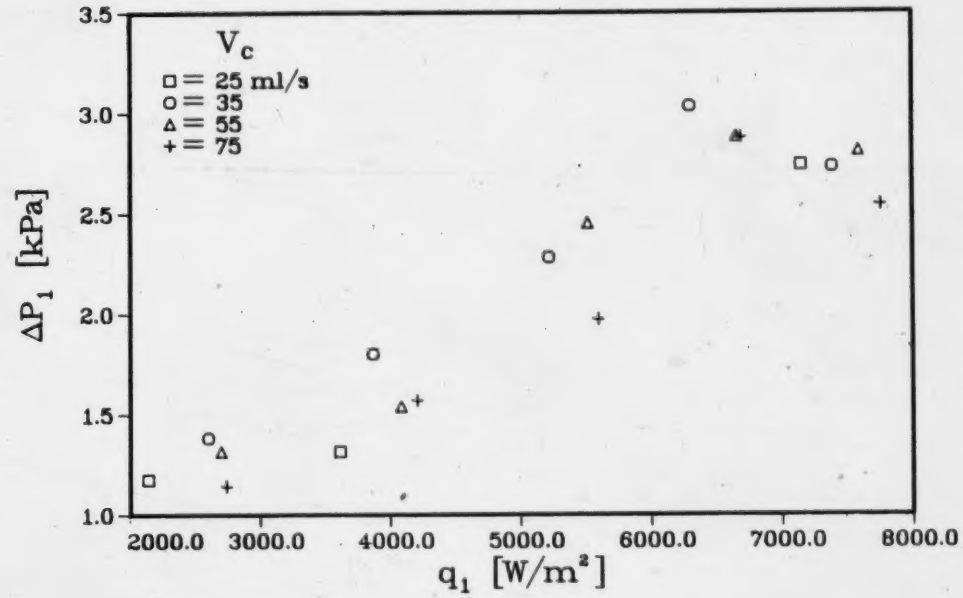

Fig. 4.32 Two-phase friction pressure drop through evaporator vs. heat flux for 100% charge level

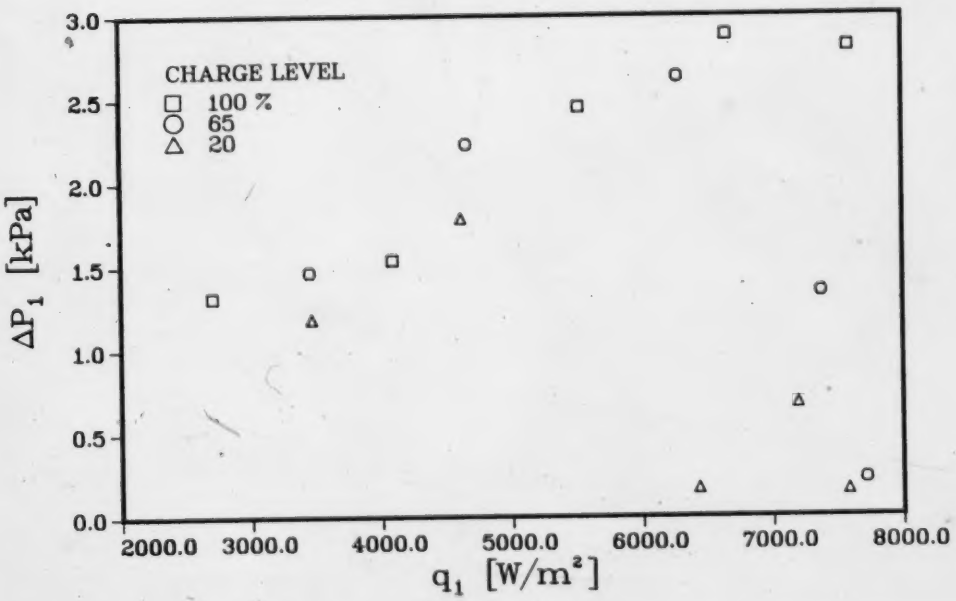

Fig. 4.33 Two-phase friction pressure drop through evaporator vs. heat flux for V_C=55 ml/s

reported in [41,42] for single channel upflow boiling tests. In those experiments, the wall heat flux was held constant, and the mass flow rate varied to produce different fluid states in the boiler. It was found that when the liquid in the evaporator reached saturation, further decreases in the mass flow rate caused an increase in the pressure drop as bulk boiling commenced. Eventually the pressure drop was reduced as the mass flow rate approached zero. This type of result is to be expected, as the pressure drop caused by the turbulent mixing of a boiling fluid may offset the gain produced by lowering the mass flow rate. The volume change created by vapor generation increases the velocity of the flow which also contributes to greater friction losses.

To further illustrate the effect of the state of the fluid on the pressure drop, it is compared with the evaporator exit quality in Figs. 4.34 and 4.35. This data spans the saturation region, as well as superheated vapor production for a vapor quality of 1.0. The pressure drop increases as more of the total flow in the evaporator becomes vapor, and the mean velocity of the two-phase mixture is raised. Upon the generation of superheated vapor, the pressure drop decreases, even though the total mass flow rate does not greatly vary. For the same mass flow rate, the single phase flow exhibits a lower friction pressure drop than a two-phase mixture. Neither cooling water or charge level affect the data other than their influence on the state of the fluid in the evaporator tube.

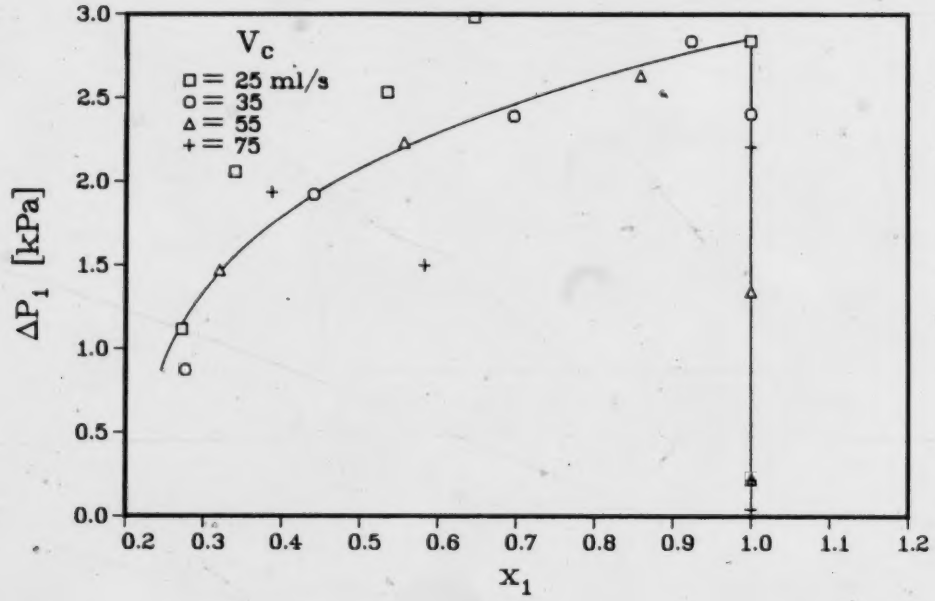

Fig. 4.34 Effect of evaporator exit quality on two-phase frictional pressure drop for 65% charge level

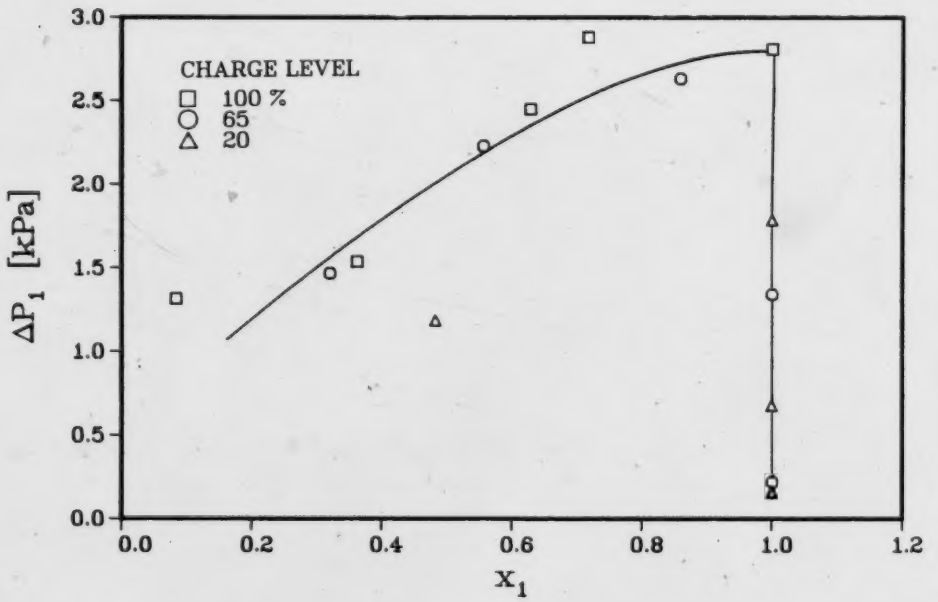

Fig. 4.35 Effect of evaporator exit quality on two-phase frictional pressure drop for V_C=55 ml/s

The frictional component of pressure drop is plotted against the inverse Martinelli parameter in Fig. 4.36. The parameter is valid only for two-phase flow, so superheated data is omitted. The Martinelli parameter is the ratio of the frictional pressure gradients of liquid flowing alone to gas flowing alone and is thus a separated flow parameter. The pressure drop increases as the inverse Martinelli parameter increases, indicating again the additional pressure drop caused by the prescence of vapor in the flow.

The ratio of the experimental pressure drop to that predicted by the homogeneous model of Eq.(4.14) is plotted against evaporator exit quality in Fig. 4.37. The ratio varies from 0.5 to 2 in the saturated flow region. The prediction becomes inaccurate with excessive superheating, as most of the tube length contains single-phase vapor and the correlation does not apply.

In Fig. 4.38, only the results for the two-phase mixture are shown with the ratio of experimental to homogeneous model pressure drop plotted against the inverse Martinelli parameter (two large scatter data points have been ommitted). The effect of the separated flow parameter indicates that modelling of two-phase pressure drop may be better described using a combination of both the homogeneous and separated-flow techniques. Of course, no one mathematical model can be expected to account for all the physical variables encountered in real situations.

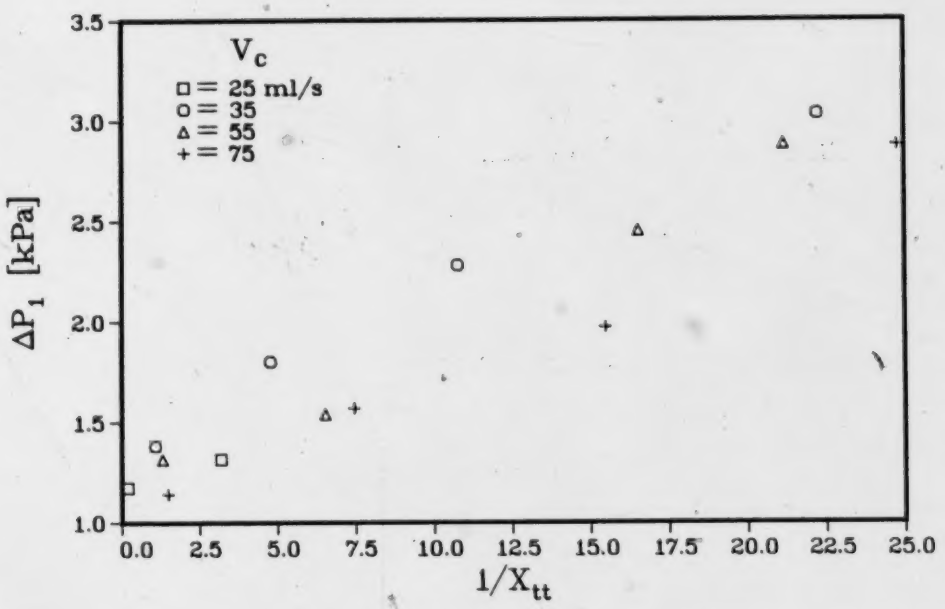

Fig. 4.36 Two-phase pressure drop vs. inverse Martinelli parameter for 100% charge level

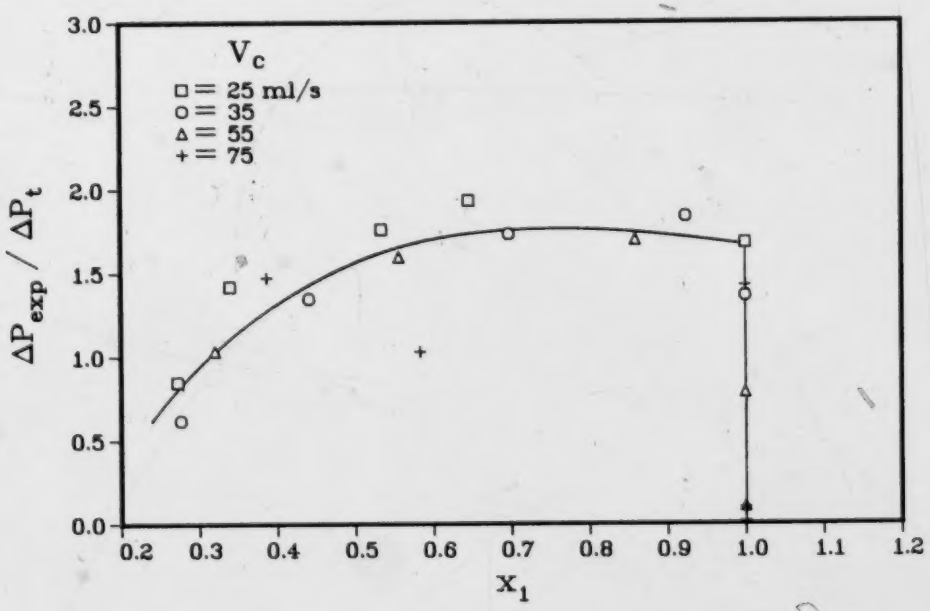

Fig. 4.37 Ratio of measured evaporator pressure drop to homogeneous model prediction vs. x_1 for 65% charge level

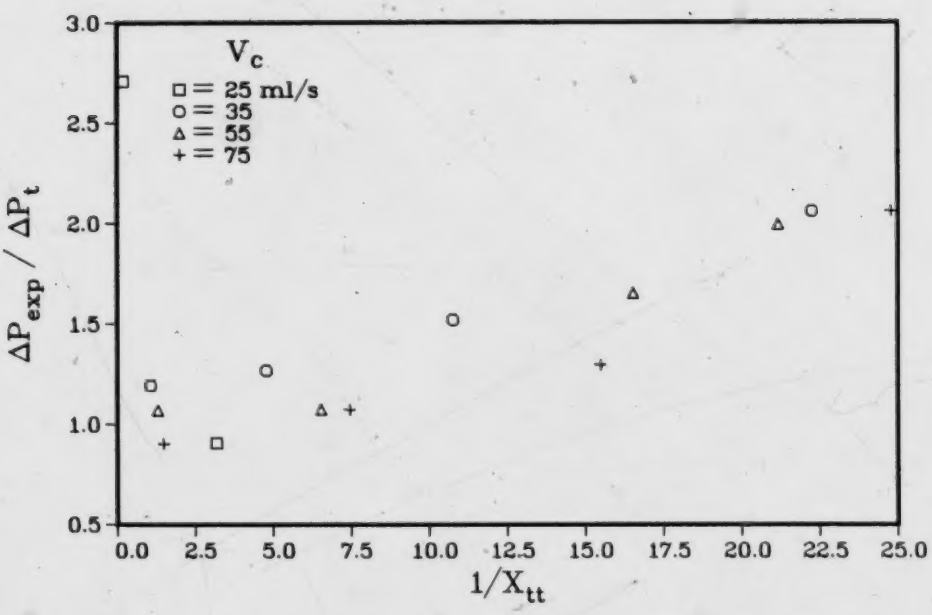

Fig. 4.38 Ratio of measured evaporator pressure drop to homogeneous model prediction vs. inverse Martinelli parameter for 100% charge level

4.5.6 Flow Visualization

The clear condenser shell and sight glass located at the evaporator exit enabled photographs of the flow patterns to be taken at these points. In the photographs, the vapor component of the two-phase mixture appears light and the liquid component somewhat darker in tone. The figures containing the photos are collected at the end of this chapter.

A time series of the flow patterns at the evaporator tube exit for a 20% charge level test are shown in Fig. 4.39. The cooling water flow rate was set at 75 ml/s, and the heating water temperature at 85°C, so that the exit state would progress from saturated liquid to superheated vapor. The first seven shots were taken over a total period of about four minutes, with a progressively longer time interval between each photograph. The liquid level at time zero is shown in (a). With the commencement of circulation of the heating and cooling fluids, low velocity bubbly flow is observed within seconds (b). In (c), the individual bubbles begin to group together, so that alternating slugs of liquid and vapor occur. Well developed slug flow did not exist for this charge level, as the flow rapidly entered the annular regime (d), with vapor flowing in the center of the tube, and a thin annulus of liquid existing around the circumference of the sight glass.

The vapor quality is increasing in (e) and (f), with only a small amount of liquid remaining in the annular

region. Here the slip velocity between the vapor core and the liquid annulus is sufficient to cause waves to appear on the inner surface of the glass. In (g), the fluid enters the superheated vapor region. The streaks which can be seen are caused by small amounts of dye trapped in the heat exchanger during the evaporation process. As the liquid containing length of the tube recedes, the non-evaporating dye is entrained by the high velocity superheated vapor. The secondary flow superimposed by the spiral geometry of the tube causes the vapor to exit the evaporator in a swirling motion, as evidenced by the patterns of the dye. The final photograph (h) is shown for the near steady state operating condition, about 20 minutes after startup.

It was found that charge level, heat source temperature, and cooling water flow rate all affect the state of the working fluid in the evaporator. Fig. 4.40 shows the combined effects of charge level and temperature as (a) occurs for steady state operation with 100% charge and a 55°C source temperature, while (b) is for 65% charge level and 85°C heat source temperature. Both have a cooling water flow rate of 25 ml/s. The effect of cooling water flow rate on the evaporator flow regime can be seen in Fig. 4.41. A change in the coolant flow from 25 ml/s to 35 ml/s for the same operating parameters of 20% charge level and 85°C heat source temperature causes the exit flow to enter the superheated vapor region as the system pressure is lowered.

A geysering phenomenon occurred for a few combinations of operating parameters. This is characterized by alternating pulses of low quality and high quality flow, at about the same frequency (manually counted) as the observed fluctuations in the system pressures and flow rates. Two instances were noticed, both for the case of 55°C heat source temperature, and 75 ml/s cooling water flow rate. Fig. 4.42(a) is for the 65% charge level condition and Fig 4.42(b) is for 100%.

The left photograph for each situation is a high quality pulse with more vapor content than on the right. The blurring of the photos on the right in both sets indicates that the flow velocity has increased, as the camera speed is the same as that for its left counterpart. The shutter speeds were 1/1000 s and 1/500 s for (a) and (b), respectively.

Photographs of the flow in the condenser shell reveal some important characteristics of the system. It was found that the condenser became flooded with liquid Freon, even for a low initial liquid charge level. With the charge level and heat source temperature fixed at 20% and 85°C, the progression of the liquid level in the condenser is seen in Fig 4.43(a-d) for cooling water flow rates of 25, 35, 55 , and 75 ml/s, respectively. The liquid level in each photograph is indicated by an arrow for clarity. Steady state conditions have been achieved in each case.

At first, no flooding is observed, as the vapor generation in the evaporator is low. As the cooling water flow rate is increased, the vapor quality at the evaporator exit rises, thus displacing the liquid volume of the system into the condenser. Not much difference is observed for an increase in cooling water flow rate from 55 to 75 ml/s, as superheating does not have as great of an effect on the volume change of the vapor. Fig. 4.44(a-c) shows the same effect for the highest charge level of 100%. The initial no heating or cooling condition (a), is followed by steady state photographs for cooling water flow rates of 25 and 55 ml/s. The heating water temperature is 85°C. At this point the axial vapor dispersal tube of the condenser is completely submerged in liquid, and the heat transfer process takes on an added complexity.

With an initial liquid charge level of 65%, the condenser is flooded to the mid-plane for a heating fluid temperature of 85°C and cooling water flow rate of 75 ml/s, and the dispersal tube is partially immersed. The injection of the vapor into the liquid causes considerable splashing as seen in Fig. 4.45(a). At the other end of the condenser, an interesting phenomenon occurs at the dispersal tube inlet section. The hot vapor flowing inside the tube raises the external surface temperature to a point where bubble nucleation occurs as seen in Fig. 4.45(b), shot from below the liquid surface.

When the condenser is completely flooded, no fin surface is available for direct condenstion. Rather, the process occurs as in Fig 4.46(a) for the condition of 100% charge, heat source temperature of 85°C, and cooling water flow rate equal to 35 ml/s. In 4.46(b) the cooling water flow rate is increased to 55 ml/s, and the photograph enlarged. Due to the buoyancy of the vapor phase in the liquid, immediate upflow is observed, and the vapor is almost entirely condensed before the upper finned surface is reached. The heat transfer process then relies on natural convection and conduction in the liquid to transport the heat energy to the finned cooling tube. This is no doubt less efficient than direct condensation on the metal surface, and in addition large pressure drops may be incurred by the injection of the vapor jet into the liquid phase.

It was found in [17] that condenser flooding and liquid entrainment had detrimental effects on thermosyphon performance, and the behaviour observed here helps to explain low system efficiencies through poor fin side heat transfer coefficients. Arrangements similar to the present experimental apparatus are used for phase change solar collector systems, and improved condenser design might help to make such systems more efficient by eliminating flooding caused by vapor generation in the evaporator section.

4.6 Conclusion

The refrigerant charged closed loop two-phase thermosyphon system performed well and natural circulation flow was immediately self initiating upon the application of external heating and cooling. The flow regimes in the riser line ranged from a two-phase mixture to superheated vapor. Due to the properties of the R-113 working fluid, heat transfer was found to be primarily latent, with increasing input heat flux generating vapor without raising the mass flow rate.

Optimum thermodynamic efficiency was obtained for operation in the saturation region of the refrigerant. Generation of superheated vapor in the evaporator was found to greatly decrease efficiency, while the best values were found for a flow quality of 1.0 corresponding to saturated vapor production. Both an increase in cooling water flow rate and a lower charge level were found to assist vapor generation by lowering the system pressure, and thus the saturation temperature of the working fluid.

Primary loop flow and pressure fluctuations were found to have a basically constant frequency in the range of 0.35-0.375 cycles/sec. Evidence presented by other investigators indicates that the mechanism of the instablities is the so called density wave oscillation. The variance of the system pressure signal was found to drastically increase for superheated vapor production, which could result in mechanical problems such as fatiguing of the

pipe joints.

The recent correlation equation developed by Kandlikar for the prediction of convective boiling heat transfer coefficient was found to agree with the present experimental data. Convective boiling pressure drop in the evaporator was found to decrease when superheating was encountered. This is probably due to the abscence of turbulent mixing between phases which may occur for lower quality flow.

Flow visualization photographs in the condenser shell revealed that liquid flooding was prevalent over almost the entire range of operation. This either reduced the effective condensation area, or when flooding was complete, reduced the heat transfer to a convection situation. The lower efficiency of this heat transfer process as compared to direct condensation would have detrimental effects on system performance and is an area for improvement.

Fig. 4.39 Transient boiling flow at the evaporator exit for 20% charge level, 85°C heat source, and V_c =75 ml/s

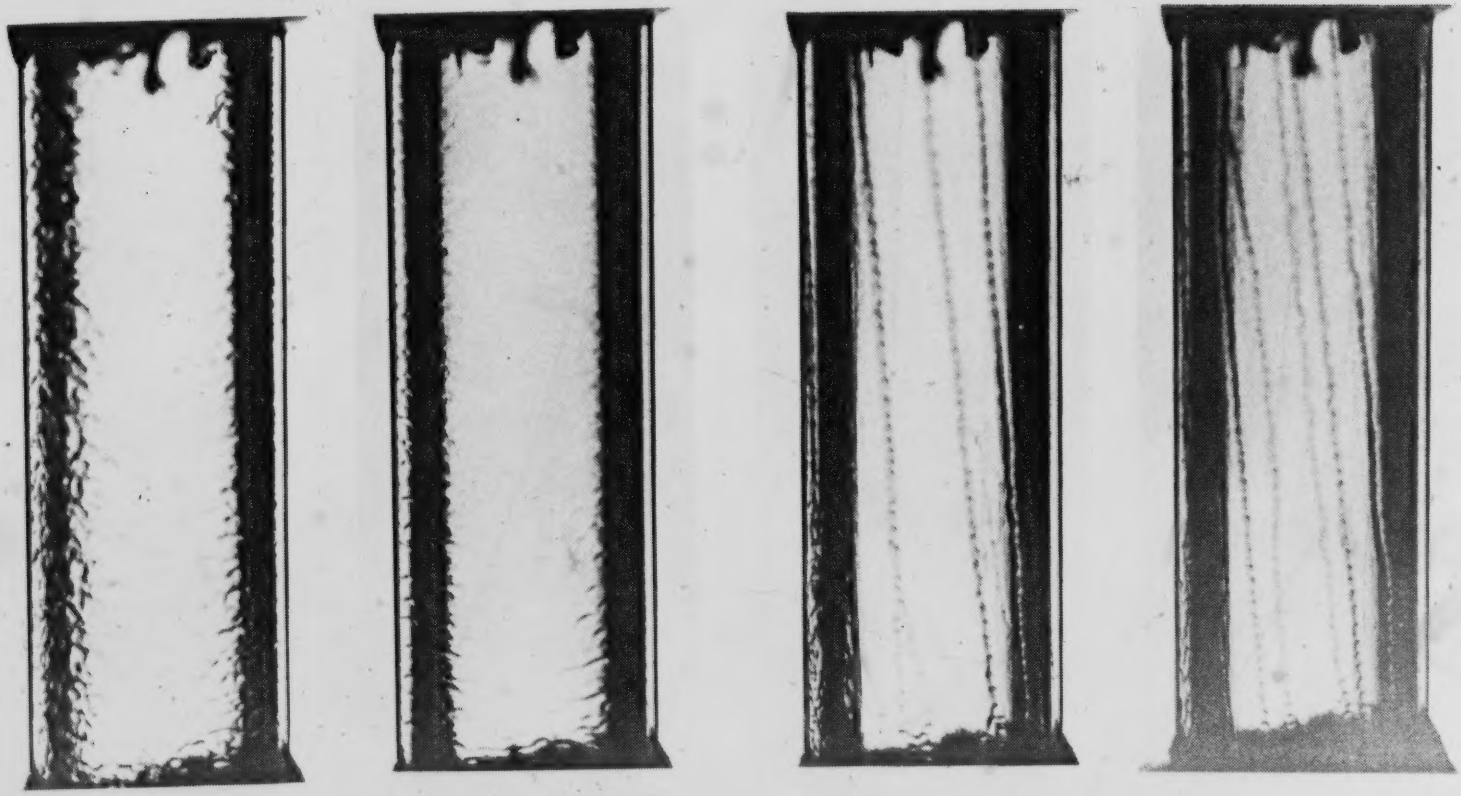

(e) (f) (g) (h)

Fig 4.39 continued

(a) 100% charge, T_h=55°C

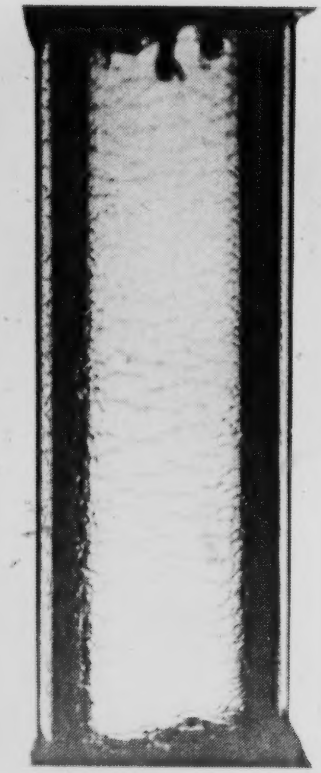

(b) 65% charge, T_h=85°C

Fig. 4.40 Effect of charge level and temperature on evaporator flow regimes with V_C=25 ml/s

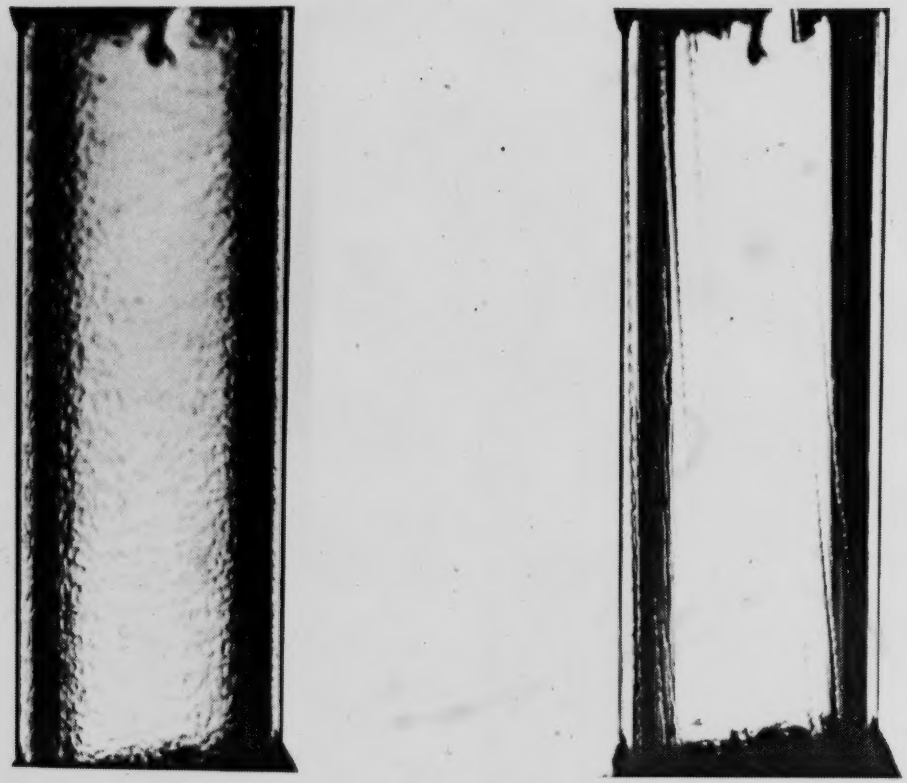

(a) V_C=25 ml/s (b) V_C=35 ml/s

Fig. 4.41 Effect of cooling water flow rate on evaporator exit flow with 20% charge level and 85°C heat source

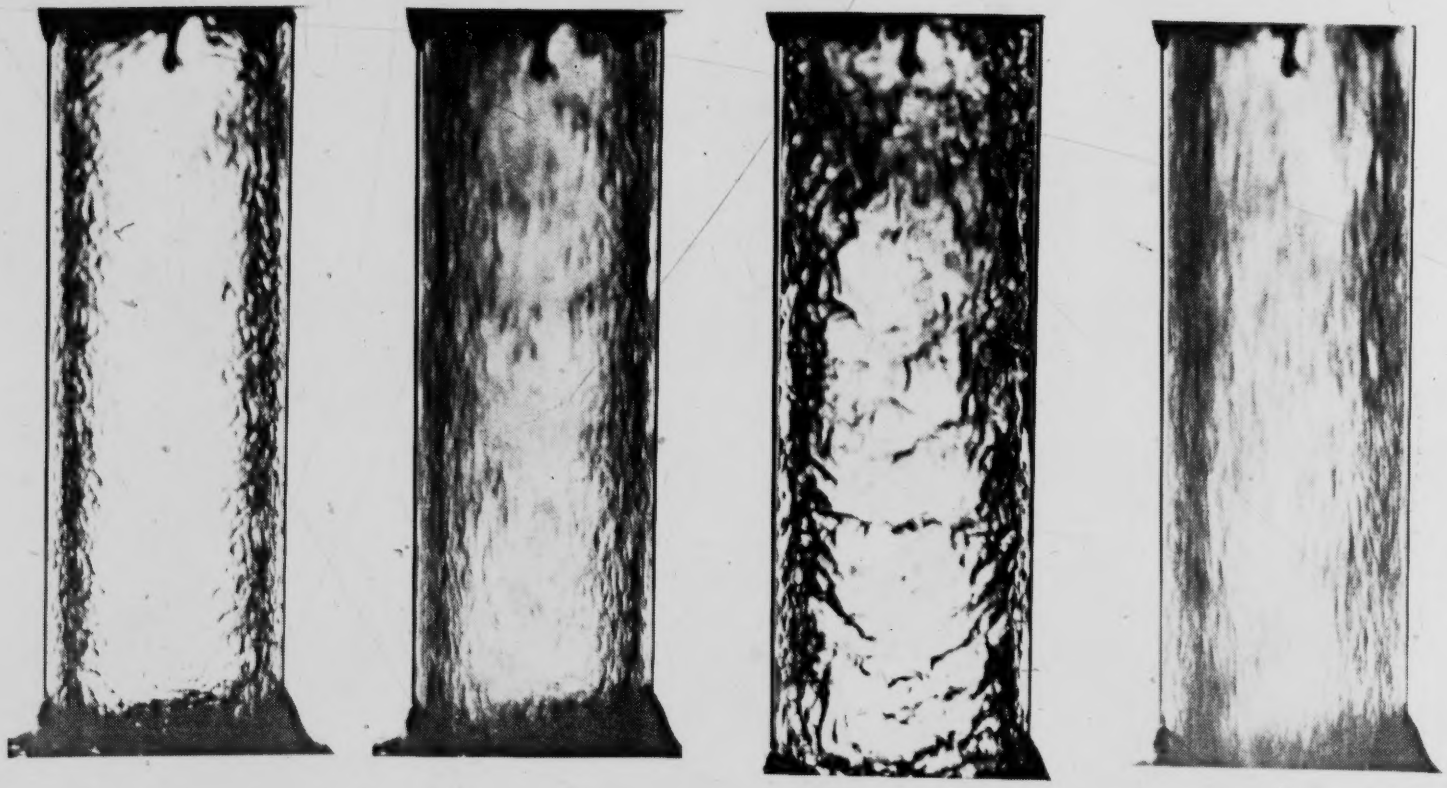

(a) 65% charge level

(b) 100% charge level

Fig. 4.42 Pulsing flow at evaporator exit with 55°C heat source and V_c =75 ml/s

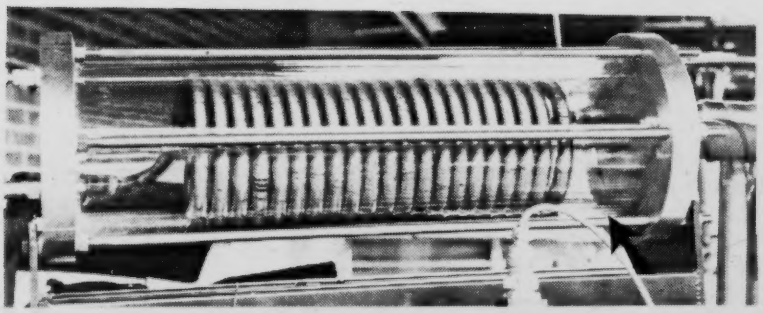

V_c =25 ml/s (a)

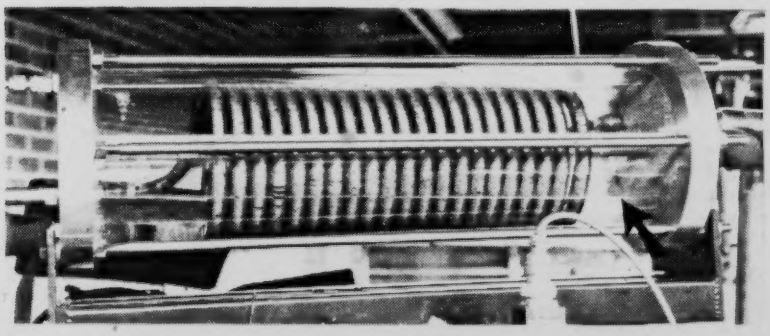

V_c =35 ml/s (b)

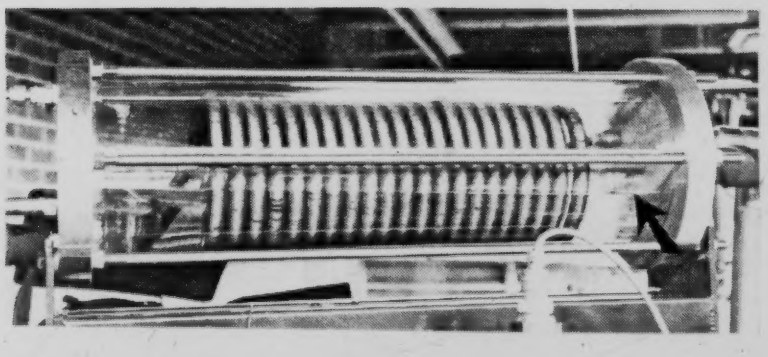

V_c =55 ml/s (c)

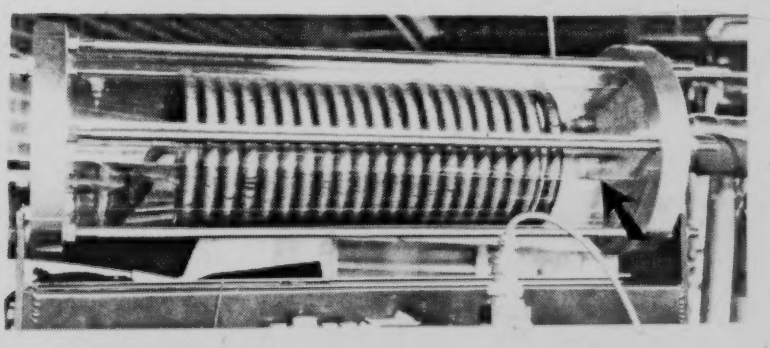

V_c =75 ml/s (d)

Fig. 4.43 Condenser flooding for 20% charge level and 85°C heat source

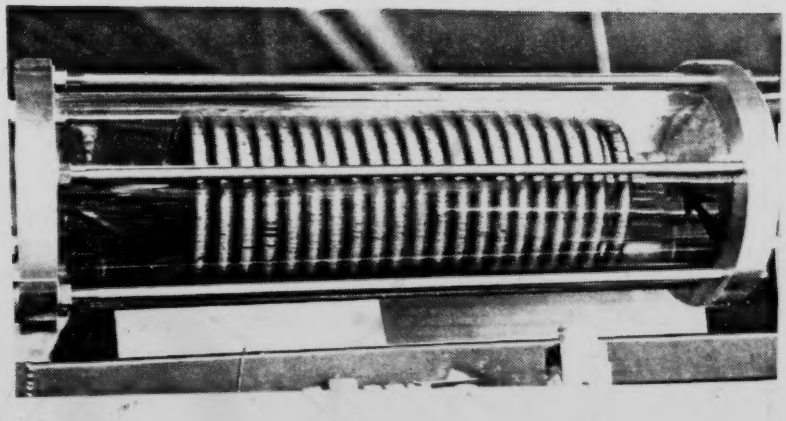

initial state (a)

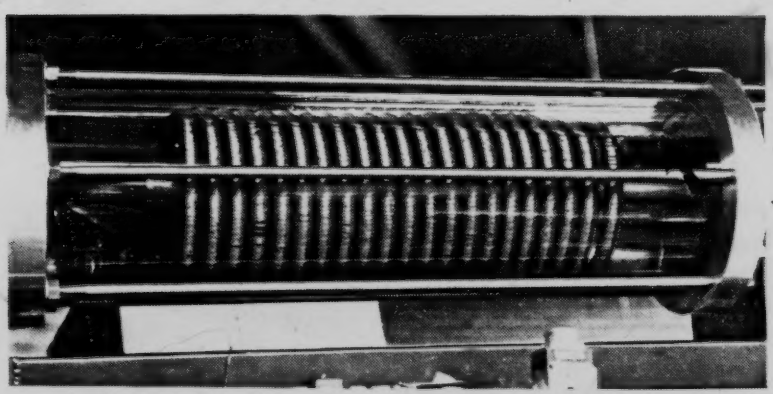

V_c =25 ml/s (b)

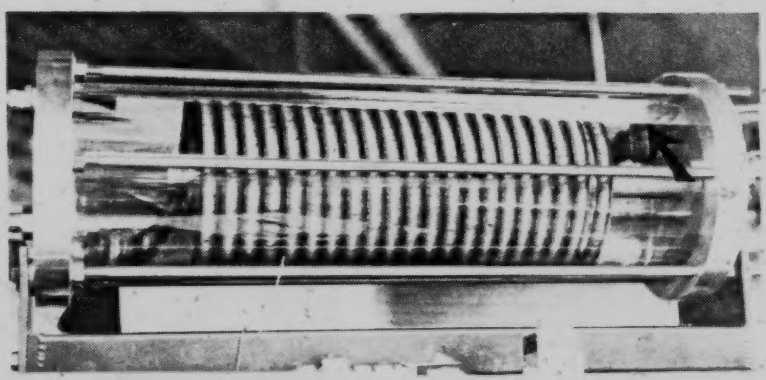

V_c =55 ml/s (c)

Fig. 4.44 Condenser flooding for 100% charge level and 85°C heat source

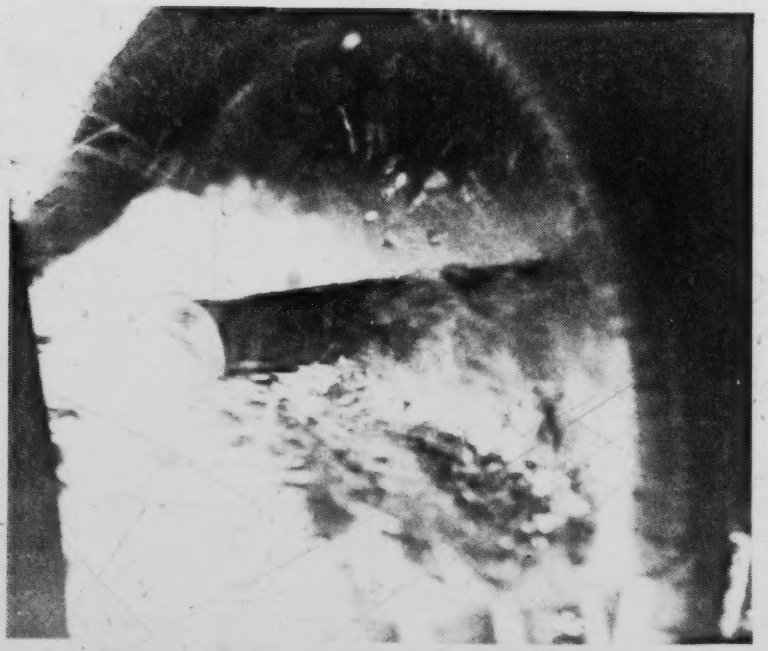

(a)

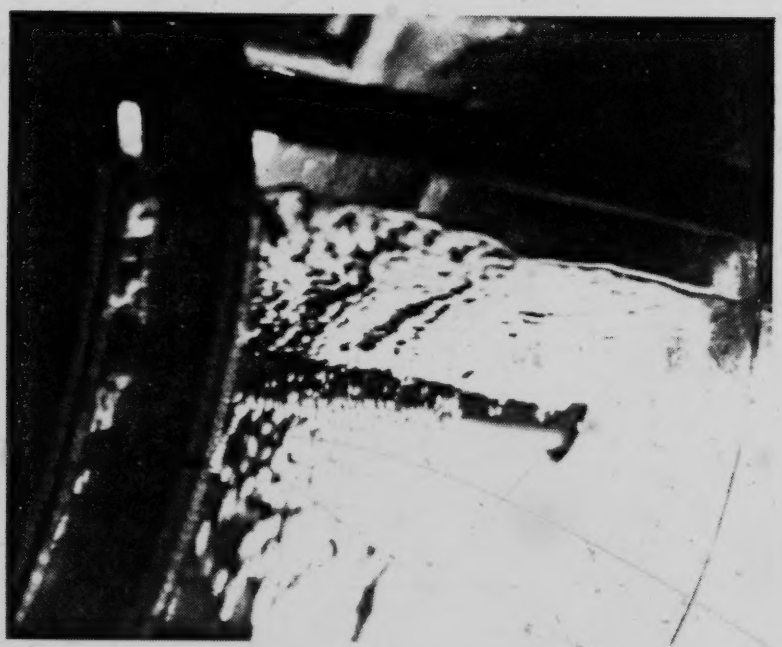

(b)

Fig. 4.45 Flooded condenser for 65% charge level, 85°C heat source, and V_C=75 ml/s

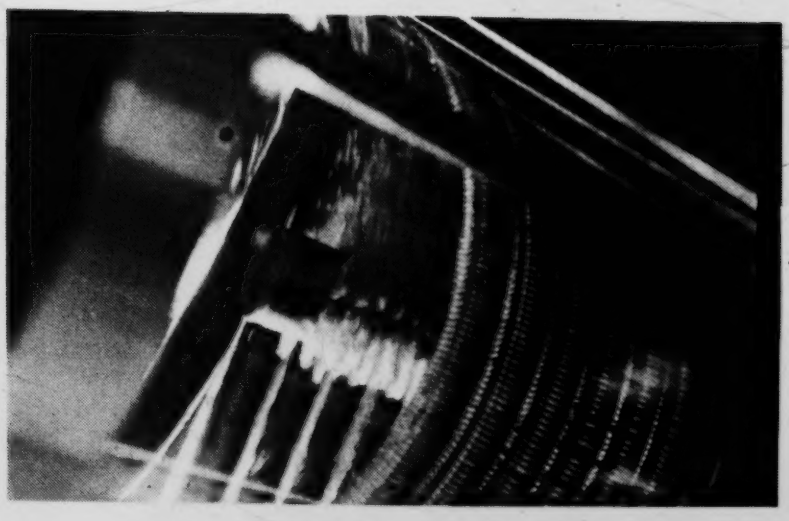

V_c=35 ml/s (a)

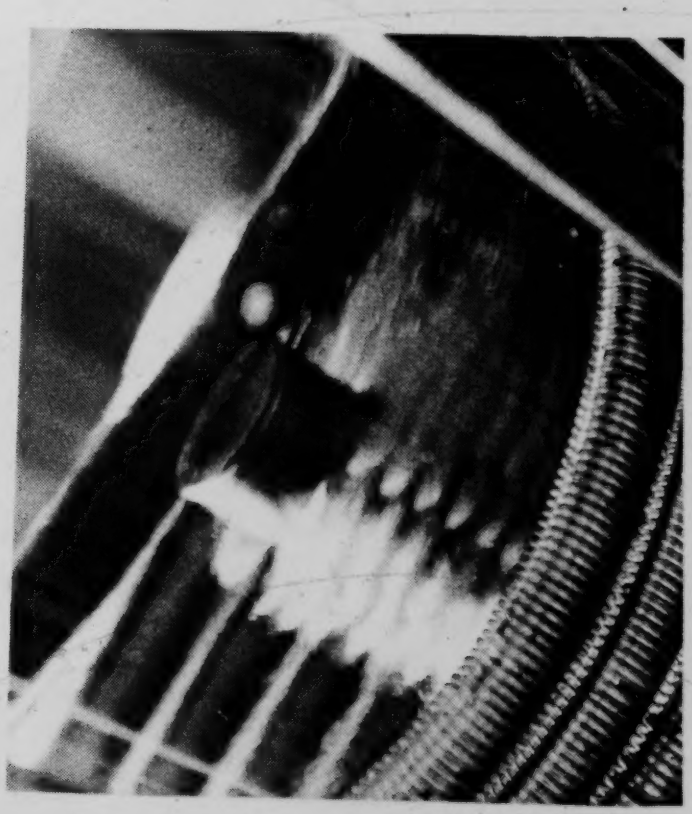

V_c=55 ml/s (b)

Fig. 4.46 Vapor injection into fully flooded condenser for 100% charge and 85°C heat source

5. Concluding Remarks

Three different working fluids were used to study the operating and heat transfer characteristics of a closed loop two-phase thermosyphon under the influence of various external parameters. The effects of system temperature difference, cooling water flow rate, initial liquid charge level, and liquid-vapor separator were examined for a low grade energy recovery situation (heat source <100°C).

The system was initially tested with liquid phase water as the working fluid to provide baseline data for future tests. External parameters which had a major effect on heat recovery were cooling water flow rate and system temperature difference. Increases in the uncontrolled variable of thermosyphon natural circulation rate were also found to improve the amount of heat transferred. The mass flow rate was found to increase with higher values of input heat flux which also corresponded to higher heat source temperature and cooling water flow rate.

The natural circulation in the primary loop set up a sympathetic link between the physically separated heat exchangers of the system. Forced flow eliminated this, and tests revealed that more heat could be transported with a pump in the system, but without an appreciable increase in thermodynamic efficiency. The single phase Nusselt number for the inner tube of the lower heat exchanger was found to be well correlated with an inverse Graetz parameter using a simple power relation.

The two-phase water system exhibited much higher mass flow rates than the single phase case, and heat recovery was improved. Parameters which contributed favourably to heat transport were high charge level, high heat source temperature, large cooling water flow rate, and the inclusion of a liquid-vapor separator in the riser line. Mass flow rates were found to increase with heat flux and vapor quality. The heat transfer processes in the evaporator and condenser were considered to be primarily single phase, enhanced by two-phase mixing with some additional latent heat transfer. The correlation of the evaporator tube Nusselt number with the inverse Graetz parameter for the low quality flow showed favourable results, indicating that future study is warranted. The condenser exhibited heat transfer coefficients far below those predicted by Nusselt theory.

The two-phase refrigerant R-113 system had a major advantage over the water charged arrangements in that self initiated natural circulation was rapid and occurred for all tests. The mechanism of heat transfer was primarily latent, as opposed to the sensible heating and cooling of the water filled loops. The total mass flow rate was found to decrease to a steady value and did not increase for higher heat flux.

Optimum efficiency was obtained when superheating of the flow at the evaporator exit was avoided, while at the same time maintaining high quality flow. Large cooling water flow rates and lower charge levels contributed to increased

vapor generation through a decrease in system pressure. The primary loop flow and pressure fluctuations were basically constant at 0.35-0.375 cycles/sec, and are believed to be the result of density wave type oscillations. Superheated vapor production resulted in a large variance of the system pressure signal which at times was physically evidenced by noise and shaking of the primary loop tubes. The convective boiling frictional component of pressure was found to decrease as superheated vapor was produced in the evaporator.

Flow visualization photographs of the shell side condensation revealed that liquid flooding was occurring, and was probably responsible for the low fin side heat transfer coefficients obtained. This could be avoided through better design of both the primary loop geometry and the condenser itself.

All three thermosyphon situations transported heat between the heating and cooling loops, with the Freon system having the best performance within the common range of operating parameters. Additional advantages of refrigerants are that they do not cause corrosion or scaling, and the type of refrigerant may be chosen to suit the desired heat source temperature range. They are however quite expensive, and the good performance of the two-phase water system suggests it to be an alternative for higher temperature operation. The single phase system performed reasonably well, but was not self starting for this particular

geometrical arrangement.

The two-phase closed loop thermosyphon is clearly suited to low grade heat recovery and transport as it is maintenance free, requires no pumps or power supplies, and will transfer heat between two independent and separated streams with a relatively low temperature difference. A current application of such a device may be found in phase change solar collector systems. It would also be suitable for gas to gas heat transfer, geothermal energy recovery, or heat recovery from contaminated waste gases or liquids.

The system tested could be improved, and one possibility would be the elimination of condenser flooding. Another unavoidable shortcoming was the flow restriction in the primary loop due to instrumentation. A similar system without large pressure drops to inhibit the thermosyphon flow would be expected to perform better. Better choice of heat exchangers for such a system would no doubt improve performance, as might the use of different working fluids. The interesting phenomena of flow and pressure oscillations in the primary loop deserve future study to further assess their physical mechanisms.

References

1. Veziroglu, T.N., ed., Alternative Energy Sources, Proceedings of the First-Fourth Miami International Conferences on Alternative Energy Sources, 1977-1981.

2. Wassel, A.T., Elghobashi, S.E., and Farr, J.L., "Mathematical Simulation of Ocean Thermal Energy Conversion Seawater Systems", J. Solar Engineering, Vol. 106, May 1984, pp. 198-205.

3. Mochida, Y., Kawano, S., Takahata, T., and Miyoshi, M., "Performance of the Heat Exchangers of a 100-kW (Gross) OTEC Plant", J. Solar Engineering, Vol. 106, May 1984, pp. 187-192.

4. Vandenberghe, D.G., and Vigrass, L.W., "Low-Grade Geothermal Energy: Feasibility and Demonstration at Regina, Canada", Alternative Energy Sources II, Vol. 5, 1981, pp. 2047-2070.

5. Bayley, F.J., and Lock, G.S.H., "Heat Transfer Characteristics of the Closed Thermosyphon", J. Heat Transfer 87, 1965, pp. 30-40.

6. Peace-Athabasca Delta Project Report, Intergovernmental Study Group, Dept. of the Environment, Queens Printer, Edmonton, 1972.

7. Lee, Y., and Mital, U., "A Two-Phase Closed Thermosyphon", Int. J. Heat Mass Transfer, Vol. 15, 1972, pp. 1695-1707.

8. Lee,Y., "Preservation of Permafrost by Means of Two-Phase Closed Thermosyphon", Annual Reports, DRB, 9511-96, University of Ottawa, 1969.

9. Bottum, E.W., "Refrigerant Charged Phase Change Solar Water and Space Heating Systems", ASHRAE Trans., Vol. 87(2), 1981, pp. 397-404.

10. Schreyer, J.M., "Residential Application of Refrigerant Charged Solar Collectors", Solar Energy, Vol.26, 1981, pp. 307-312.

11. Manasse, F.K., and O'Leary, J.A., "Heliophase Solar Hot Water Heating System", Proc. of the 1978 Annual Meeting, AS/ISES, Denver, Colorado, Vol. 2.2, 1978, pp. 36-40.

12. Al-Tamimi, A.I., Performance of a Flat-Plate Solar Collector in a Closed-Loop Thermosiphon Using

Refrigerant-11, Ph.D. Thesis, University of Michigan, 1972.

13. Lee, C.A., An Experimental Study of Refrigerant Charged Two-Phase Solar Collector Systems, M.Sc. Thesis, University of Alberta, 1983.

14. Kissner, F., "A Passive, Refrigerant-Driven, Solar Domestic Water Heating System -- The Ultimate in Efficiency and Freeze Protection for Cold Climate", Proc. of the National Conference on Solar Energy, SESCI, Montreal, Canada, 1981, pp. 201-205.

15. Cheng, K.C., Application of Boiling and Condensation Heat Transfer to Flat Plate Solar Collectors in Cold Region, Final Report, Alberta/Canada Energy Resources Research Fund, Contract U-79-9, 1982.

16. Cheng, K.C., Morioka, I., Ichimiya, K., and Sadler, G. W., "Experimental Study of a Two-Phase Thermosyphon System", Alternative Energy Sources IV, Vol. 1, 1982, pp. 151-170.

17. McDonald, T.W., Hwang, K.S., and DiCiccio, R., "Thermosyphon Loop Performance Characteristics: Part 1. Experimental Study", ASHRAE Trans. 83(2), 1977, pp. 250-258.

18. De Paz, J.F., On the Stability of a Free Convection Loop, Ph.D. Thesis, Purdue University, 1972.

19. El-Masri, M.A., and Bara, R.J., "Natural Circulation in a Long Vertical Loop", J. Thermal Engineering, Vol. 3, No. 2, 1983, pp. 32-44.

20. Fujii, T., Kato, Y., and Mihara, K., "Expressions of Transport and Thermodynamic Properties of Air, Steam, and Water", Report No. 66, Institute of Industrial Science, Kyushu University, Japan, 1972.

21. Van Wylen, G.J., and Sonntag, R.E., Fundamentals of Classical Thermodynamics, John Wiley and Sons, 2nd ed., 1976, pp. 99-100.

22. Holman, J.P., Heat Transfer, McGraw-Hill, 1981, pp. 447-449.

23. Ozisik, M.N., Basic Heat Transfer, McGraw-Hill, 1977, pp. 447-451.

24. General Electric Corporate Research and Development: Heat Transfer and Fluid Flow Data Books, "Forced Convection", Dec. 1980, p. 21.

25. Holman, J.P., Heat Transfer, McGraw-Hill, 1981, pp. 454-456.

26. Moran, M.J., Availibility Analysis: A Guide to Efficient Energy Use, Prentice-Hall, 1982, pp. 44-76 and 86.

27. McAdams, W.H., Heat Transmission, McGraw-Hill, 3rd ed., 1954, pp. 230-233.

28. Metais, B., and Eckert, E.R.G., "Forced, Mixed, and Free Convection Regimes", J. Heat Transfer, Ser. C, Vol. 86, 1964, p. 295.

29. Cheng, K.C., and Yuen, F.P., "Flow Visualization Studies on Secondary Flow Patterns in Curved Tubes and Isothermally Heated Horizontal Tubes", ASME paper 84-HT-62, 22nd ASME/AIChE National Heat Transfer Conference, Niagara Falls, New York, 1984.

30. Rohsenow, W.M., and Hartnett, J.P., Handbook of Heat Transfer, McGraw-Hill, 1973, 7-149.

31. Shah, M., "A New Correlation for Heat Transfer During Boiling Flow Through Pipes", ASHRAE Trans., Vol. 82, Part II, 1976, pp. 66-86.

32. Shrock, V.E., and Grossman, L.M., "Forced Convective Boiling in Tubes", Nuclear Science and Engineering, Vol. 12, 1962, pp. 474-481.

33. Beatty, K., and Katz, D.L., "Condensation of Vapors on Outside of Finned Tubes", Chemical Engineering Progress, Vol. 44, 1948, pp. 55-69.

34. Dupont of Canada, "Freon Refrigerants", Physical Properties Pamphlet, R11-371, FR-82.

35. Mastroianni, M.J., Stahl, R.F., and Sheldon, P.N., "Physical and Thermodynamic Properties of 1,1,2 - Trifluorotrichloroethane (R-113)", J. Chemical and Engineering Data, Vol. 23, No.2, 1978, pp.113-118.

36. ASHRAE Handbook 1981 Fundamentals, pp. 17.90-17.91.

37. Fujii, T., Nozu, S., and Honda, H., "Expressions of Thermodynamic and Transport Properties of Refrigerants R-11, R-12, R-22, and R-113", Institute of Industrial Science, Kyushu University, Japan, 1977.

38. Miller, I., and Freund, J.E., Probability and Statisitcs for Engineers, 2nd ed., Prentice-Hall, 1977, p. 151.

39. Chen, J.C., "Correlation for Boiling Heat Transfer to Saturated Fluids in Convective Flow", Industrial and

Engineering Chemistry, Process Design and Development, Vol. 5, No. 3, 1966, pp. 322-329.

40. Kandlikar, S.G., "An Improved Correlation for Predicting Two-Phase Flow Boiling Heat Transfer Coefficient in Horizontal and Vertical Tubes", Paper presented at the 21st National Heat Transfer Conference, Seattle, Wash., July 24-28, 1984.

41. Veziroglu, T.N., and Lee, S.S., "Instabilities in Boiling Upward Flows", Int. Symposium on Research on Co-Current Gas-Liquid Flow, 1968, pp. 303-345.

42. Kakac, S., and Veziroglu, T.N., "A Review of Two-Phase Flow Instabilities", Advances in Two-Phase Flow and Heat Transfer, Vol. II, Martinus Nijhoff Publishers, 1983, pp. 577-667.

43. Stenning, A.H., "Instabilities in the Flow of a Boiling Liquid", J. Basic Engineering, Trans. ASME, Series D, Vol. 86, 1964, pp. 213-217.

44. Veziroglu, T.N., and Lee, S.S., "Boiling Flow Instabilities in Parallel Channels", Proc Instn Mech Engrs, Vol. 184, Pt 3C, 1969-70, pp. 7-17.

45. Collier, J.G., Convective Boiling and Condensation, McGraw-Hill, 2nd ed., 1981, pp. 26-69

Appendix I

Sample Data Acquisition Program

```
THE FOLLOWING IS A DATA ACQUISTION PROGRAM
WRITTEN IN BASIC FOR AN HP-85 MICROCOMPUTER
AND HP-3497A DATA ACQUISTION CONTROL UNIT

THIS IS SPECIFIC TO THE PARTICULAR
EXPERIMENTAL SETUP AND TESTS DONE

10 DATA ACQUISITION PROGRAM FOR FREON R113 TESTS
20
30 DIM M(21),B(21),T(21),X(31),Z(5),C2$[100],D$[15],Z1(5)
40 DIM V1(100),V2(100),V3(100)
50 PRINTER IS 704,96
60 DEF FND9(T) = ((1+.0000087*T^1.85)*.001)^-1
70 DEF FNC9(T) = 4179+.000079*(T-10)^2.9
80 CLEAR
90 DISP "ENTER THE DATE AND TIME OF DAY EX: AUG 3/83,H,M,S"
100 INPUT D$,H,M,S
110 SETTIME H*3600+M*60+S,0
120 PRINT USING 130 ; D$,H,M,S
130 IMAGE /5X,"THE DATE IS ",15A,"TIME IS ",2D," HOURS,
",2D," MIN, AND ",2D," SEC"
140 FOR I=1 TO 31
150 X(I)=0
160 NEXT I
170 DISP "ENTER THE LAST STORAGE IDENTIFICATION NUMBER"
180 INPUT K
190
200 *********** LINEAR CALIBRATION DATA *************
210 DATA 19049.734,19563.643,19242.378,19462.731,
19161.669,20040.256,19094.625
220 DATA 19551.966,18931.699
230 DATA .683,.343,3.261,1.374,6.928,14.881,
6.4738,11.9882,11.197
240 DATA 3.475,6.957,19552.46
250 DATA 27.995,27.484,27.696,27.528,27.726,27.534,
27.957,27.442,28.007
260 DATA .094,.005,-.459,.019,-.054,1.044,-.2364,.9795,2.338
270 DATA -.255,-.207,29.179
280 *********** READ THE CALIBRATION DATA ************
290
300 FOR I=1 TO 21
310 READ M(I)
320 NEXT I
330 FOR I=1 TO 21
340 READ B(I)
350 NEXT I
360 CLEAR
370 DISP " PRESSURE TRANSDUCERS MUST BE ZEROED WITH NO FLOW
RATE, INPUT ANY LETTER TO COMMENCE"
380 INPUT N$
390 IF N$="Y" THEN 400
400 FOR I=1 TO 5
410 Z(I)=0
420 NEXT I
```

```
430
440 **** OBTAINING ZERO FLOW RATE READINGS FROM PT'S ****
450 CLEAR 709
460 FOR J=1 TO 50
470 FOR I=1 TO 5
480 OUTPUT 709 ;"AC"&VAL$(I+88);"VT3"
490 ENTER 709 ; A
500 Z(I)=Z(I)+A
510 NEXT I
520 NEXT J
530 FOR I=1 TO 5
540 Z(I)=Z(I)/50
550 Z1(I)=Z(I)*M(I+9)+B(I+9)
560 NEXT I
570 PRINT USING 580
580 IMAGE /5X,"INITIAL VOLTAGES AND PRESSURES"
590 FOR I=1 TO 5
600 PRINT USING 620 ; I,Z(I),Z1(I)
610 NEXT I
620 IMAGE 5X,2D,3X,2D.3D,3X,4D.3D
630 PRINT USING 640
640 IMAGE 2/
650 ON ERROR GOTO 2480
655 ********* PF KEY LABELLING ***********
660 ON KEY# 1,"MAN" GOTO 770
670 ON KEY# 2,"FLOW" GOTO 2410
680 ON KEY# 8,"STORE" GOTO 2560
690 ON KEY# 5,"RERUN" GOTO 890
700 ON KEY# 4,"PRESS" GOTO 2240
710 ON KEY# 3,"CHK" GOTO 2330
720 ON KEY# 7,"STAT" GOTO 2680
730 CLEAR
740 KEY LABEL
750 BEEP 50,1000
760 GOTO 760
770 CLEAR
780 DISP "ENTER THE BAROMETRIC PRESSURE IN kPA"
790 INPUT X(22)
800 DISP "ENTER THE NUMBER OF READINGS PER CHANNEL"
810 INPUT N5
820 DISP "ENTER THE REFERENCE PRESSURE IN in. Hg"
830 INPUT P3
840 DISP "ENTER THE APPROXIMATE SYSTEM PRESSURE IN in. Hg"
850 INPUT P4
860 DISP "ENTER THE CHARGE LEVEL IN %"
870 INPUT C4
880 K=K+1
890 PRINT USING 900 ; K
900 IMAGE //5X,"********* RUN NUMBER ",3D," ***********"
910 PRINT USING 920 ; N5
920 IMAGE /5X,3D," READINGS PER CHANNEL"
930 GOSUB 960
940 GOTO 1360
950
```

```
960 ***** D/A WITH N5 READINGS FOR EACH CHANNEL *****
970 CLEAR DISP "ENTER THE HEATING FLUID ROTAMETER READING"
980 INPUT H4
990 FOR I=1 TO 21
1000 T(I)=0
1010 NEXT I
1020 CLEAR 709
1030 FOR J=1 TO N5
1040 FOR I=1 TO 17
1050 OUTPUT 709 ;"AC"&VAL$(I+79);"VT3"
1060 ENTER 709 ; A
1070 T(I)=T(I)+A
1080 NEXT I
1090 OUTPUT 709 ;"AC71VT3"
1100 ENTER 709 ; A
1110 T(18)=T(18)+A
1120 OUTPUT 709 ;"AC67VT3"
1130 ENTER 709 ; A
1140 T(19)=T(19)+A
1150 OUTPUT 709 ;"AC66VT3"
1160 ENTER 709 ; A
1170 T(20)=T(20)+A
1180 OUTPUT 709 ;"AC09VT3"
1190 ENTER 709 ; A
1200 T(21)=T(21)+A
1210 NEXT J
1220 T1=TIME
1230
1240 ***** AVERAGE AND CONVERT TO CALIBRATED UNITS *****
1250 FOR I=1 TO 21
1260 T(I)=T(I)/N5
1270 T(15)=H4
1280 X(I)=T(I)*M(I)+B(I)
1290 NEXT I
1300
1310 ***** ADJUST PT READINGS TO ZERO REFERENCE *****
1320 FOR I=10 TO 14
1330 X(I)=X(I)-Z1(I-9)
1340 NEXT I
1350 RETURN
1360 Q1=X(15)*.000001*FND9(X(1))*(FNC9(X(1))/2+FNC9(X(5))/2)
*(X(1)-X(5)) HF HEAT TRANS
1370 Q2=X(18)*.000001*FND9(X(2))*(FNC9(X(2))/2+FNC9(X(6))/2)
*(X(2)-X(6)) CF HEAT TRANS
1380 H=IP(T1/3600)
1390 M=IP(FP(T1/3600)*60)
1400 S=T1-(H*3600+M*60)
1410 PRINT USING 1420 ; D$
1420 IMAGE /5X,"THE DATE IS ",10A
1430 PRINT USING 1440 ; X(22)
1440 IMAGE 5X,"BAROMETRIC PRESSURE = ",3D.3D," KILOPASCALS"
1450 PRINT USING 1460 ; P3
1460 IMAGE 5X,"REFERENCE PRESSURE IS ",2D.D," in. Hg VAC"
1470 PRINT USING 1480 ; P4
```

```
1480 IMAGE 5X,"INITIAL EVAPORATOR GAUGE PRESSURE ",2D.D,"
in. Hg VAC"
1490 PRINT USING 1500 ; C4
1500 IMAGE 5X,"CHARGE LEVEL ",3D," %"
1510 PRINT USING 1520 ; X(21)
1520 IMAGE 5X,"ROOM TEMP ",2D.D," DEG. C"
1530 PRINT USING 1540 ; T1,H,M,S
1540 IMAGE 5X,"TIME IS NOW ",5D," SECONDS OR ",2D," HOURS,
",2D," MINUTES,AND ",2D," SECONDS"
1550 GOSUB 1570
1560 GOTO 2010
1570 PRINT USING 1580
1580 IMAGE //5X"------ SYSTEM FLOW RATES CC/S -------"
1590 PRINT USING 1600 ; X(15)
1600 IMAGE /5X,"HEATING FLUID: ",3D.D
1610 PRINT USING 1620 ; X(17)
1620 IMAGE 5X,"WORKING FLUID THROUGH CONDENSER",3D.D
1630 PRINT USING 1640 ; X(16)
1640 IMAGE 5X,"WORKING FLUID THROUGH DOWNCOMER",3D.D
1650 PRINT USING 1660 ; X(18)
1660 IMAGE 5X,"CONDENSER COOLING FLUID: ",3D.D
1670 PRINT USING 1680
1680 IMAGE /5X,"------- SYSTEM PROPERTIES --------"
1690 PRINT USING 1700
1700 IMAGE /5X"EVAPORATOR HEATING FLUID"
1710 PRINT USING 1720 ; X(1),X(5),X(14)
1720 IMAGE " TEMP IN= ",2D.D," TEMP OUT= ",2D.D," DEG
C",4X," PRESSURE DROP= ",2D.2D," kPa"
1730 PRINT USING 1740
1740 IMAGE /,5X,"EVAPORATOR WORKING FLUID"
1750 PRINT USING 1760 ; X(4),X(7),X(11)
1760 IMAGE " TEMP IN=",2D.D," TEMP OUT= ",2D.D," DEG C",5X,"
PRESSURE DROP= ",2D.2D," kPa"
1770 PRINT USING 1780 ; X(19)
1780 IMAGE " EXIT GAUGE PRESS",4D.3D," kPa"
1790 PRINT USING 1800
1800 IMAGE /,5X,"CONDENSER COOLING FLUID"
1810 PRINT USING 1720 ; X(6),X(2),X(13)
1820 PRINT USING 1830
1830 IMAGE /,5X,"CONDENSER WORKING FLUID"
1840 PRINT USING 1760 ; X(3),X(8),X(10)
1850 PRINT USING 1860 ; X(20)
1860 IMAGE " INLET GAUGE PRESS ",4D.3D," kPa"
1870 PRINT USING 1880 ; X(9)
1880 IMAGE /,5X,"DOWNCOMER TEMP= ",2D.D," DEG C"
1890 PRINT USING 1900 ; X(12)
1900 IMAGE /,5X,"SYSTEM PRESSURE FLUCTUATION= ",2D.2D," kPa"
1910 QUALITY BASED ON MASS FLOW RATE
1920 IF X(16)<.5 THEN 1970
1930
Q3=X(17)*FND9(X(8))/(X(17)*FND9(X(8))+X(16)*FND9(X(9)))*100
1940 PRINT USING 1950 ; Q3
1950 IMAGE /5X,"QUALITY BASED ON FLOW RATE ",2D.D," %",/
1960 GOTO 1990
```

```
1970 PRINT USING 1980
1980 IMAGE /5X,"DOWNCOMER FLOW?"
1990 RETURN
2000
2010 PRINT USING 2020 ; Q1/1000
2020 IMAGE 5X,"RATE OF HEAT TRANSFER FROM HEATING
FLUID=",2D.2D," KILOWATTS"
2030 PRINT USING 2040 ; Q2/1000
2040 IMAGE 5X,"RATE OF HEAT EXTRACTION BY COOLING
FLUID=",2D.2D
2050 PRINT USING 2060
2060 IMAGE /5X,"------- SYSTEM ACQUISITION CHECK -------"
2070 PRINT USING 2080
2080 IMAGE /2X,"TC OUTPUT VOLTAGE",10X,"TEMP,DEG C"
2090 FOR I=1 TO 9
2100 PRINT USING 2120 ; T(I),X(I)
2110 NEXT I
2120 IMAGE 3X,2D.4D,22X,3D.D
2130 PRINT USING 2140
2140 IMAGE //2X,"PT OUTPUT VOLTAGE",10X,"PRESSURE DROP"
2150 FOR I=10 TO 14
2160 PRINT USING 2180 ; T(I),X(I)
2170 NEXT I
2180 IMAGE 3X,2D.3D,20X,3D.D,3X,"kPa"
2190 DISP "ENTER COMMENT"
2200 INPUT C2$
2210 GOTO 730
2220
2230 ***** ROUTINE TO CORRECT INITIAL PRESSURES *****
2240 DISP "TO BE USED FOR MANUAL INPUT OF INITIAL PRESSURES
OR RE-READING THE PRESSURES"
2250 DISP "FOR AUTOMATIC READING ENTER 'A', OTHERWISE
RETURN"
2260 INPUT N$
2270 IF N$="A" THEN 370
2280 DISP "ENTER THE INITIAL VOLTAGES AND PRESSURES ON TWO
SEPARATE LINES"
2290 INPUT Z(1),Z(2),Z(3),Z(4),Z(5)
2300 INPUT Z1(1),Z1(2),Z1(3),Z1(4),Z1(5)
2310 GOTO 570
2320
2330 ************ CHECK PROPERTIES ***************
2340 N5=5
2350 GOSUB 960
2360 GOSUB 1570
2370 PRINT USING 2380
2380 IMAGE 10/
2390 GOTO 740
2400
2410 ************** CHECK FLOW RATES ******************
2420 N5=1
2430 GOSUB 960
2440 DISP USING 2450 ; X(15),X(18),X(17),X(16)
2450 IMAGE /5X,"HF ",3D.D," CC/S",/5X,"CF ",3D.D,/5X,"WF
```

```
(COND) ",3D.D,/5X,"WF (DOWN) ";3D.D
2460 GOTO 740
2470
2480 ************* ERROR RECOVERY ****************
2490 FOR I=1 TO 5
2500 BEEP
2510 WAIT 200
2520 NEXT I
2530 CLEAR DISP "ERROR TYPE";ERRN;" OCCURRED ON LINE";ERRL
2540 GOTO 740
2550
2560 ************ STORE DATA ONTO TAPE ***************
2570 IF X(18)<10 THEN 2590
2580 GOTO 2620
2590 DISP USING 2600 ; X(18)
2600 IMAGE /,"WARNING CF FLOW=",2D.D," INPUT CORRECT VALUE"
2610 INPUT X(18)
2620 ASSIGN# 1 TO "DATA.F"
2630 PRINT# 1,K ; K,D$,H,C2$,X()
2640 ASSIGN# 1 TO *
2650 C2$=""
2660 GOTO 730
2670
2680 ************ STATISTICS **************
2690 CLEAR
2700 DISP "ENTER DOMINANT COND FREQ Hz, RMS OF TOTAL SIGNAL
V"
2710 INPUT X(23),A3
2720 DISP "ENTER DOMINANT DC FREQ ,RMS OF TOTAL SIGNAL"
2730 INPUT X(24),C3
2740 DISP "ENTER DOMINANT PRESS FREQ,RMS OF TOTAL SIGNAL"
2750 INPUT X(25),D3
2760 X(29)=A3*M(17)
2770 X(30)=C3*M(16)
2780 X(31)=D3*M(12)
2790 FOR I=1 TO 100
2800 V1(I)=0
2810 V2(I)=0
2820 V3(I)=0
2830 NEXT I
2840 CLEAR 709
2850 FOR I=1 TO 100
2860 OUTPUT 709 ;"AC96VT3"
2870 ENTER 709 ; V1(I)
2880 NEXT I
2890 FOR I=1 TO 100
2900 OUTPUT 709 ;"AC95VT3"
2910 ENTER 709 ; V2(I)
2920 NEXT I
2930 FOR I=1 TO 100
2940 OUTPUT 709 ;"AC91VT3"
2950 ENTER 709 ; V3(I)
2960 NEXT I
2970 A=0 C=0 D=0
```

```
2980 FOR I=1 TO 100
2990 A=A+V1(I)
3000 C=C+V2(I)
3010 D=D+V3(I)
3020 NEXT I
3030 A=A/100 C=C/100
3040 D=D/100
3050 A1=A*M(17)+B(17)
3060 C1=C*M(16)+B(16)
3070 D1=D*M(12)+B(12)
3080 PRINT USING 3090
3090 IMAGE //,17X,"COND",5X,"DC",5X,"PRESS"
3100 PRINT USING 3110 ; X(23),X(24),X(25)
3110 IMAGE /,5X,"DOM
FREQ",1X,2D.3D,3X,2D.3D,2X,2D.3D,3X,"Hz"
3120 PRINT USING 3130 ; X(29),X(30),X(31)
3130 IMAGE /5X,"TOTAL RMS",1X,2D.3D,2X,2D.3D,2X,4D.3D," USER
UNITS
3140 PRINT USING 3150 ; A1,C1,D1
3150 IMAGE /,5X,"MEAN VALUES ",2D.D,3X,2D.D,3X,4D.3D
3160 A2=0 C2=0 D2=0
3170 FOR I=1 TO 100
3180 A2=A2+(V1(I)-A)^2
3190 C2=C2+(V2(I)-C)^2
3200 D2=D2+(V3(I)-D)^2
3210 NEXT I
3220 A2=A2/99 C2=C2/99
3230 D2=D2/99
3240 X(26)=A2*M(17)
3250 X(27)=C2*M(16)
3260 X(28)=D2*M(12)
3270 PRINT USING 3280 ; X(26),X(27),X(28)
3280 IMAGE /5X,"VARIANCE",2X,2D.4D,2X,2D.4D,2X,2D.4D
3290 PRINT USING 3300
3300 IMAGE 2/
3310 PRINT USING 3340 ;
X(1),X(2),X(3),X(4),X(5),X(6),X(7),X(8),X(9),X(10)
3320 PRINT USING 3340 ;
X(11),X(12),X(13),X(14),X(15),X(16),X(17),X(18),X(19),X(20)
3330 PRINT USING 3340 ; X(21),X(22),X(23),X(24),X(25),X(26),
X(27),X(28),X(29),X(30),X(31)
3340 IMAGE 10(3D.3D)
3350 PRINT USING 3360
3360 IMAGE 5/
3370 GOTO 740
3380 END
```

Appendix II

Properties of Liquid Water

```
C     PROPERTIES OF LIQUID WATER

C     ARGUMENT OF EACH FUNCTION IS WATER
C     TEMPERATURE IN DEGREES CENTIGRADE

C     VALID RANGES MAY BE FOUND IN REF. [20]
C     OR CHECKED FROM TABLES


C     DENSITY, KG/(CU. M)
      FUNCTION WDENS(T)
      WDENS=((1+8.7E-6*T**1.85)*1.0E-3)**(-1)
      RETURN
      END


C     ABSOLUTE VISCOSITY, KG/(M S)
      FUNCTION WAVISC(T)
      WAVISC=2.4E-5*10.0**(251.0/(T+135.0))
      RETURN
      END


C     CONSTANT PRESSURE SPECIFIC HEAT, J/(KG K)
      FUNCTION WSPH(T)
      WSPH=4179.0+7.9E-5*(T-10.0)**2.9
      RETURN
      END


C     THERMAL CONDUCTIVITY, W/(M C)
      FUNCTION WCOND(T)
      WCOND=0.6881-4.0E-6*(135.0-T)**2.1
      RETURN
      END


C     COEFF. THERMAL EXPANSION, 1/K
      FUNCTION WBETA(T)
      A1=-0.06427E-3
      A2=8.5053E-6
      A3=-6.79E-8
      B1=A1+2.0*A2*T+3.0*A3*T**2
      B2=1+A1*T+A2*T**2+A3*T**3
      WBETA=B1*B2
      RETURN
      END
```

Appendix III

Properties of Refrigerant R-113

```
C   PROPERTIES OF FREON R-113

C   FUNCTION ARGUMENTS ARE TEMPERATURES
C   IN DEGREES CENTIGRADE
C   UNLESS OTHERWISE INDICATED

C   VALID RANGES MAY BE FOUND IN REF. [37]
C   OR CHECKED FROM TABLES


C   ******* LIQUID PHASE PROPERTIES *******


C     DENSITY, KG/(CU. M)
      FUNCTION FLDENS(T)
      SV=(0.617+6.47E-04*T**1.10)*1.0E-03
      FLDENS=1.0/SV
      RETURN
      END


C     LATENT HEAT OF VAPORIZATION, J/KG
      FUNCTION FLATE(T)
      FLATE=(1.611-3.10E-03*T)*1.0E+05
      RETURN
      END


C     CONSTANT PRESSURE SPECIFIC HEAT, J/(KG K)
      FUNCTION FLSPH(T)
      FLSPH=(0.929+1.03E-03*T)*1.0E+03
      RETURN
      END


C     ABSOLUTE VISCOSITY, KG/(M S)
      FUNCTION FLVISC(T)
      EX=503./(T+271)
      FLVISC=1.34E-05*10.**EX
      RETURN
      END


C     THERMAL CONDUCTIVITY, W/(M C)
      FUNCTION FLCOND(T)
      FLCOND=0.0802-2.03E-04*T
      RETURN
      END
```

```
C *******  VAPOR PHASE PROPERTIES  *******

C       ABSOLUTE VISCOSITY, KG/(M S)
        FUNCTION FVVISC(T)
        FVVISC=(0.920+3.0E-03*T)*1.0E-05
        RETURN
        END


C       SATURATED VAPOR DENSITY, KG/(CU. M)
C       EP = ABSOLUTE PRESSURE, KPA
        FUNCTION FSVDEN(T,EP)
        ERP=EP/3413.0
        ZS=(1.0+0.636*ERP**0.816)**(-1.0)
        FSVDEN=187.39*EP*1000.0/ZS/8314.0/(T+273.15)
        RETURN
        END
```